

**Growth-Induced Polarity Formation  
in Molecular Crystals:  
Analytical Theory and Monte Carlo  
Simulations**

Inauguraldissertation  
der Philosophisch-naturwissenschaftlichen Fakultät  
der Universität Bern

vorgelegt von

**Thomas Wüst**

von Oberriet-Montlingen (St. Gallen)

Leiter der Arbeit:

Prof. Dr. J. Hulliger

Departement für Chemie und Biochemie





**Growth-Induced Polarity Formation in  
Molecular Crystals:  
Analytical Theory and Monte Carlo  
Simulations**

Inauguraldissertation  
der Philosophisch-naturwissenschaftlichen Fakultät  
der Universität Bern

vorgelegt von  
**Thomas Wüst**  
von Oberriet-Montlingen (St. Gallen)

Leiter der Arbeit:  
Prof. Dr. J. Hulliger  
Departement für Chemie und Biochemie

Koreferent:  
Prof. Dr. H. Bebie  
Institut für Theoretische Physik

Von der Philosophisch-naturwissenschaftlichen Fakultät angenommen.

Bern, 1. Februar 2005

Der Dekan:  
Prof. Dr. P. Messerli



*For my parents and Claire*



# Acknowledgments

First of all, I thank Jürg Hulliger for having supervised my PhD thesis. I acknowledge his proposition to change from Zürich to Bern to join his group. In particular, I am indebted for the freedom he gave to me, both, to let me follow my own ideas as well as to choose the places (e.g. Ticino) in which I felt stimulated for working and thinking about my thesis.

Then, I would like to thank Hans Bebie for his kind willingness and interest to advice me and to be my co-referee, although being retired. During our many discussions, I appreciated very much his clear scientific view. His ability to classify into questions and answers even the most complex problems helped me a lot.

I would like to thank Claire Gervais for the fruitful collaboration, but especially for her never-ending patience and interest to listen to me and my scientific problems. Because I think that telling to somebody being involved in the topic is already a big step towards understanding. Thank You for the many scientific 'ballades'.

I would like to acknowledge Hans Peter Lüthi who gave me the opportunity to start my PhD at ETH Zürich, and to work with a perfect infrastructure, particularly, with the fastest computers of Switzerland. Furthermore, the several lectures and exercises I could give for his students, as well as the seminar talks given in the group of Prof. W. van Gunsteren gave me a good basis for presenting scientific subjects, also in English.

I thank Stefan Portmann for his expertise in any kind of computational issues. It was thanks to him that I had enough knowledge to fulfill any required computational task alone in Bern.

Finally, I would like to thank my family and Claire for being always present whenever I needed it.



# Contents

<b>Abstract</b>	<b>xiii</b>
<b>Zusammenfassung</b>	<b>xv</b>
<b>Publications</b>	<b>xvii</b>
<b>1 Introduction</b>	<b>1</b>
<b>2 How Symmetrical Molecules Can Induce Polarity: On the Paradox of Dilution</b>	<b>7</b>
2.1 Abstract . . . . .	7
2.2 Introduction . . . . .	7
2.3 Definitions and General Survey . . . . .	8
2.4 Monte Carlo Simulations . . . . .	12
2.5 Results . . . . .	14
2.6 Conclusion . . . . .	15
<b>3 Growth-Induced Polarity Formation in Solid Solutions of Or- ganic Molecules: Markov Mean-Field Model and Monte Carlo Simulations</b>	<b>21</b>
3.1 Abstract . . . . .	21
3.2 Introduction . . . . .	22
3.3 The Growth Model . . . . .	23
3.4 Mathematical Treatment . . . . .	27
3.4.1 Markov Mean-Field Description . . . . .	27
3.4.2 Monte Carlo Simulations . . . . .	29
3.5 Results . . . . .	31
3.5.1 Orientational Selectivity . . . . .	32
3.5.2 Miscibility . . . . .	34
3.5.3 Overview of Phenomena in $(X, X_{\text{net}})$ Space . . . . .	39
3.6 Discussion . . . . .	41

3.6.1	Comparison between MMF Description and Monte Carlo Simulations . . . . .	41
3.6.2	Applicability to Real Systems . . . . .	46
3.7	Conclusion . . . . .	46
3.8	Appendix A: Numerical Procedure for Markov Mean-Field Equations . . . . .	47
3.9	Appendix B: The Monte Carlo Algorithm . . . . .	49
<b>4</b>	<b>Growth-Induced Polarity Formation in Solid Solutions: Supplementary Material</b>	<b>51</b>
4.1	Influence of $X_{\text{gas}}$ , $T$ and Energy Range on $(X, X_{\text{net}})$ Density Distributions . . . . .	51
<b>5</b>	<b>Growth-Induced Polarity Formation in Solid Solutions of Two Polar Components: A Statistical Analysis</b>	<b>59</b>
5.1	Introduction . . . . .	59
5.2	Definitions and Symmetry Relations . . . . .	60
5.3	Results and Discussion . . . . .	63
5.3.1	$(X, X_{\text{net}})$ Density Distributions . . . . .	63
5.3.2	$X_{\text{net}}$ Distributions for Systems (a), (b) and (c) . . . . .	66
5.3.3	An Analytical Approach . . . . .	70
5.4	Conclusion . . . . .	74
<b>6</b>	<b>Influence of the Growth Mechanism on Macroscopic Polarity Formation</b>	<b>75</b>
6.1	Introduction . . . . .	75
6.2	The Growth Models and their Description by Monte Carlo Simulations . . . . .	78
6.2.1	The Five Growth Models . . . . .	78
6.2.2	Monte Carlo Simulations . . . . .	81
6.3	Results . . . . .	82
6.3.1	Polarity Formation . . . . .	83
6.3.2	Phase Transition . . . . .	84
6.4	Markov Mean-Field Approximation . . . . .	92
6.5	The Two-Layer Systems . . . . .	93
6.5.1	The Equivalent Two-Layer System for the Layer Growth Model (0) . . . . .	93
6.5.2	The Two-Layer Systems for Growth Models (i) - (iv) . . . . .	95
6.5.3	Comparisons of $X_{\text{net}}$ between Growth Models, Two- Layer Systems and Analytical Description . . . . .	98
6.6	Discussion . . . . .	103



6.7	Conclusion . . . . .	106
<b>7</b>	<b>The Program POLARITY</b>	<b>109</b>
7.1	The Input File . . . . .	109
7.2	The Output . . . . .	117
7.3	Outlook . . . . .	118
<b>8</b>	<b>Conclusion and Outlook</b>	<b>119</b>
	<b>Bibliography</b>	<b>130</b>
	<b>Curriculum Vitae</b>	<b>131</b>



# Abstract

This thesis is devoted to the theoretical investigation of growth-induced polarity formation in single- and two-component molecular crystals. In a first part, the evolution of polarity in solid solutions of polar (**H**) and non-polar (**G**) molecules, or polar **H** and **G** molecules was investigated applying a layer-by-layer growth model. This model is characterized by the assumption of thermal equilibrium formation of adlayers, with respect to the up and down orientation of the dipoles of **H** (and **G**) molecules and to an exchange of **H** and **G** molecules, taking longitudinal and lateral Ising-type nearest neighbor interactions into account. Previously attached layers are kept frozen. The asymptotic statistics of the model after many steps of growth was analyzed by means of a Markov mean-field approximation and Monte Carlo simulations. The investigation mainly focused on the interplay between orientational ordering (ratio between up and down) and miscibility of the two components in the solid, according to different sets of interaction energies. Native structures (**H**, **G**) were assumed centrosymmetric.

The influence of non-polar (**G**) molecules on polarity formation can be classified in three different behaviors: (i) Dilution of polarity in case they are non-selective with respect to the up and down orientation of polar (**H**) molecules. (ii) Enhancement of polarity due to a coupled effect of **H** and **G** molecules. (iii) Creation of polarity in case single-component systems of polar (**H**) molecules show no macroscopic polarity. For (ii) and (iii), polarity passes a maximum for non-zero concentrations of **G** molecules. Probabilities for the occurrence of possible configurations (polarity vs molar fraction of **G** molecules) were investigated by means of a statistical analysis choosing sets of interaction energies randomly within an assumed, but realistic range. High probabilities for significant vectorial alignment of **H** molecules are found for very low and very high fractions of **G** molecules, respectively, as well as for ordered **HG** compounds. Generally, longitudinal interactions mainly determine the formation of polarity, while lateral couplings influence miscibility between the two components.

In systems with two polar components, the notions of orientational selec-

tivity and miscibility still apply. However, here lateral interactions strongly influence both, miscibility as well as polarity formation. Potentiality to obtain macroscopic polarity was compared for three types of systems: Single-component systems of polar (H) molecules only, two-component systems of polar (H) and non-polar (G) molecules and two-component systems of two polar (H, G) molecules. The admixture of G molecules (non-polar or polar) to a polar H compound increases the probability to yield a high vectorial alignment of molecular dipoles.

In a second part, the influence of the growth mechanism on polarity formation for single-component systems of polar molecules was investigated. The layer-by-layer growth model was compared with four different growth processes (growth along steps, growth along kink sites, cluster growth, and random deposition) being characterized by a reduced lateral cooperativity between molecules during their attachment on the crystal surface. Even though the growth process can significantly influence polarity, in case growth proceeds in an ordered way, polarity formation remains mainly a thermodynamically driven process. In particular, the asymptotic statistics of ordered growth processes can be reasonably well described by corresponding two-layer systems in thermal equilibrium. Contrarily, local kinetic effects can determine polarity if molecules are attached in a random manner. However, for any of the investigated growth processes, the effect of a reduced lateral cooperativity between molecules may be compensated upon growth if longitudinal couplings are strong enough. In such cases, the local lateral environment can be represented by an effective lateral coordination number, whatever the assumed growth process.

# Zusammenfassung

Diese Arbeit ist der Untersuchung wachstumsinduzierter Polaritätsbildung in ein- und zweikomponentigen molekularen Kristallen gewidmet. In einem ersten Teil wurde die Entwicklung von Polarität in festen Lösungen von polaren (H) und unpolaren (G) Molekülen oder polaren H und G Molekülen untersucht unter Verwendung eines Schicht-Wachstumsmodell. Dieses Modell ist durch die Annahme charakterisiert, dass neu angelagerte Molekülschichten vollständig ins thermische Gleichgewicht relaxieren, sowohl in Bezug auf die nach oben/unten Ausrichtung der Dipole von H (und G) Molekülen, als auch auf den Austausch von H und G Molekülen, unter Berücksichtigung von longitudinalen und lateralen Wechselwirkungen mit nächsten Nachbarn vom Ising'schen Typ. Vorangehende Schichten bleiben eingefroren. Die asymptotische Statistik des Modells wurde mittels einer Markov mean-field Näherung und Monte Carlo Simulationen analysiert. Die Untersuchung konzentrierte sich hauptsächlich auf das Zusammenspiel zwischen Ausrichtungsordnung (Verhältnis Ausrichtung der Dipole nach oben/unten) und Mischbarkeit der beiden Komponenten im Festkörper, entsprechend verschiedenen Wechselwirkungsenergien. Es wurde angenommen, dass die ursprünglichen Strukturen (H, G) ein Symmetriezentrum haben.

Der Einfluss von unpolaren (G) Molekülen auf die Polaritätsbildung kann in drei verschiedene Verhalten eingeordnet werden: (i) Verminderung von Polarität im Falle, dass unpolare Moleküle nichtsektiv in Bezug auf die nach oben/unten Ausrichtung von polaren (H) Molekülen wirken. (ii) Steigerung der Polarität, wegen eines gekoppelten Effekts von H und G Molekülen. (iii) Schaffung von Polarität im Falle, dass einkomponentige Systeme von polaren (H) Molekülen keine makroskopische Polarität aufweisen. Für (ii) und (iii) tritt ein Maximum der Polarität für nichtverschwindende Konzentrationen von G Molekülen auf. Wahrscheinlichkeiten für das Auftreten möglicher Zusammensetzungen (Polarität vs molarer Anteil der G Moleküle) wurden mittels einer statistischen Analyse untersucht, bei der Wechselwirkungsenergien zufällig innerhalb eines angenommenen, jedoch realistischen Bereichs ausgewählt wurden. Hohe Wahrscheinlichkeiten für signifikante vektorielle

Ausrichtung von H Molekülen wurden für sehr kleine, beziehungsweise sehr grosse Anteile von G Molekülen gefunden, als auch für geordnete HG Strukturen. Im allgemeinen bestimmen longitudinale Wechselwirkungen hauptsächlich die Polaritätsbildung, während laterale Kopplungen die Mischbarkeit zwischen H und G Molekülen beeinflussen.

Die Vorstellungen von Orientierungsselektivität und Mischbarkeit sind auch in Systemen mit zwei polaren Komponenten gültig. Jedoch beeinflussen hier laterale Wechselwirkungen nebst der Mischbarkeit auch die Polaritätsbildung. Das Potential zur Bildung makroskopischer Polarität wurde für drei Typen von Systemen verglichen: Einkomponentige Systeme bestehend aus polaren (H) Molekülen, zweikomponentige Systeme aus polaren (H) und unpolaren (G) Molekülen und zweikomponentige Systeme aus zwei polaren (H,G) Molekülen. Die Beimischung von G Molekülen (unpolar oder polar) erhöht die Wahrscheinlichkeit zur Erzeugung einer hohen vektoriellen Ausrichtung der molekularen Dipole.

In einem zweiten Teil wurde der Einfluss des Wachstumsprozess auf die Polaritätsbildung für einkomponentige Systeme aus polaren Molekülen untersucht. Das Schichtwachstumsmodell wurde mit vier verschiedenen Wachstumsprozessen verglichen (Wachstum entlang Kanten, Wachstum entlang Knick-Stellen, Cluster Wachstum und zufällige Anlagerung), die sich durch eine reduzierte laterale Kooperativität zwischen Molekülen während ihrer Anlagerung auf der Kristalloberfläche auszeichnen. Obwohl der Wachstumsprozess die Polarität erheblich beeinflussen kann, im Falle, dass das Wachstum in einer geordneten Art und Weise verläuft, bleibt die Polaritätsbildung ein thermodynamisch geführter Prozess. Insbesondere kann die asymptotische Statistik geordneter Wachstumsprozesse ziemlich gut durch entsprechende Zwei-Schichtsysteme im thermodynamischen Gleichgewicht beschrieben werden. Im Gegensatz dazu können lokale kinetische Effekte die Polariätsbildung bestimmen, wenn Moleküle in einer zufälligen Art und Weise angelagert werden. Jedoch kann der Effekt der reduzierten lateralen Kooperativität zwischen Molekülen für irgendeinen der untersuchten Wachstumsprozesse durch hinreichend starke longitudinale Wechselwirkungen während des Wachstums kompensiert werden. In solchen Fällen ist es möglich die lokale laterale Umgebung durch eine effektive laterale Koordinationszahl zu beschreiben, unabhängig vom vorausgesetzten Wachstumsmodell.

# Publications

Chapter 2 and 3 are based on the following two publications:

- T. Wüst, C. Gervais and J. Hulliger. How symmetrical molecules can induce polarity: On the paradox of dilution, *Cryst. Growth Des.*, in press.
- T. Wüst and J. Hulliger. Growth-induced polarity formation in solid solutions of organic molecules: Markov mean-field model and Monte Carlo simulations, *J. Chem. Phys.*, in press.

Chapter 5 and 6 are intended for publication later.

Collaboration on other publications:

- C. Gervais, T. Wüst, N. R. Behrnd, G. Couderc and J. Hulliger. Impact of solid solution formation on polarity: Molecular modeling and experimental investigation of the system (4-chloro-4'-nitrostilbene)<sub>1-x</sub> – (4,4'-dinitrostilbene)<sub>x</sub>, in preparation.
- C. Gervais, T. Wüst, N. R. Behrnd, M. Wübbenhorst and J. Hulliger. Prediction of growth-induced polarity in centrosymmetric molecular crystals using force field methods, *Chem. Mater.*, in press.
- J. Hulliger, M. Losada, C. Gervais, T. Wüst and F. Budde. Effects of an external electrical field on the polarization of growing organic crystals: A theoretical study, *Chem. Phys. Lett.*, 377:340, 2003.
- H. I. Süss, T. Wüst, A. Sieber, R. Althaus, F. Budde, H. P. Lüthi, G. D. McManus, J. Rawson and J. Hulliger. Alignment of radicals into chains by a Markov mechanism for polarity formation, *CrystEngComm*, 4:432, 2002.

## International Meetings:

- *Monte Carlo simulation of orientational state of molecules at crystal surfaces: Macroscopic polarity formation.* 2. Workshop in Angewandte Simulation in der Kristallzüchtung. Deutsche Gesellschaft für Kristallwachstum und Kristallzüchtung. Memmelsdorf bei Bamberg, Germany. 10-11 October 2002.
- *Polarity formation in supramolecular materials*, poster. 6<sup>th</sup> World Congress of Theoretically Oriented Chemists (WATOC02). Lugano, Switzerland. 4-9 August 2002.
- Summerschool on Computational Quantum Chemistry. Milano, Italy. 24-28 July 2000.



# Chapter 1

## Introduction

The invention of the transistor in 1948 (Nobel prize in physics for W. Shockley, J. Bardeen and W. Brattain) set off the revolution in computer technology [14]. Nowadays, millions of transistors are arranged in integrated circuits and the ongoing miniaturization of these devices allows the design of even more complex and faster logical circuits. However, the transistor was not the first three terminal device being capable to amplify electrical signals or make an electrical switch. The vacuum tube triode preceded the transistor by nearly 50 years and fulfilled the same tasks, i. e. in that sense, the transistor was not a new functional device.

Why is the transistor such an important discovery? Because the functionality of the device (amplifier/switch) is *inherently* linked to the *properties* of the semiconducting *material* it is made of. While the vacuum tube triode consisted of a large and energy consuming apparatus, for the transistor an elegant combination of semiconductor p-n-junctions was sufficient to reach and overpass the same functionality, due to the unique properties of this material.

This example shows that the investigation and understanding of the physics of materials and the production of new materials with designed properties is of great importance and can have a large technological and also social impact. Besides, the study of physical properties of materials is a fascinating scientific field for itself as well as a rich source for new model systems in theoretical and computational physics.

Most of the research in material sciences is devoted to the investigation of solid-state bulk properties, such as ferromagnetism, ferroelectricity, superconductivity, luminescence and others [67].

However, particularly for molecular crystals, certain physical properties are strongly related to the *growth process*, due to different physical and chem-

ical environments or broken symmetries at growing surfaces compared to the bulk state [49, 86, 89, 90]. In this thesis, we investigate theoretically such a growth-induced property, namely *growth-induced polarity formation in molecular crystals*.

Experimentally, this type of phenomenon has been found in single-component crystals [51], solid solutions [52], host-guest systems of organic molecules [35, 41] as well as in living systems (tissue polarity) [37].

Beside growth-induced polarity formation, the only way to yield polarity with a high probability is to use enantiomerically pure dipolar building blocks. Crystallization in one of the 11 enantiomorphic groups gives high chances to obtain third-rank tensor properties such as piezoelectricity and second-order optical nonlinearity (being allowed only for 10 of the 11 point groups). However, growth-induced polarity has the advantage to be observed in a wider range of compounds (even non-chiral), which is of special interest when considering that polar and acentric materials have found applications in various real devices such as frequency doublers, amplitude modulators or pyroelectric sensors. Apart from these practical issues, conceptual investigation of the mechanism leading to polarity during crystal growth has shown to provide for the first time an explanation as to why all living tissue is pyroelectric [37].

Theoretically, growth-induced polarity formation has been described by the following model: A crystal built up from polar molecules is subjected to slow layer-by-layer growth. Molecules are attached to a face ( $hkl$ ) of a given seed crystal structure. Among the possible processes which can occur during the attachment of molecules on surface sites, only the *up* and *down* orientations of the molecular dipoles along the growth direction is considered. Adlayers relax to thermal equilibrium with respect to these two orientational states, while previously grown layers (substrate) are kept frozen. This is justified due to the large energy of activation for dipole reversals in the bulk for the types of molecules considered.

Grown as such, macroscopic polarity may evolve, (irrespective of the symmetry of the initial seed structure), because each layer forms some orientational disorder and grown-in orientational defects in the substrate influence the degree of disorder in the next adlayer. See [31, 30, 33, 78, 34, 42, 76, 4, 43, 39, 5, 40, 36, 38] (chronological order) for a complete overview of theoretical work on growth-induced polarity formation by means of this model.

Principally, this growth model makes reference to two concepts in related fields of statistical physics: The *solid-on-solid* (SOS) model which is widely applied to describe crystal growth processes [53, 15, 45, 27, 28, 88], and the *Ising* model well known in magnetism [44, 11, 12, 6, 71, 70, 72, 21, 69, 32].

With respect to SOS systems, the actual growth model shows the essential features to describe crystal growth, i. e. decomposition of the space into *nutrient* (gas or liquid phase), *interface* (surface layer) and *bulk* (solid phase), as well as the directionality of the growth. Besides, the solid state is described in a discrete manner, i. e. molecules are represented as building blocks occupying discrete sites on a periodic lattice and vacancies or overhangs are excluded. However, the main purpose of solid-on-solid models is to study the influence of kinetic effects on solid-state properties, such as surface diffusion or evaporation-deposition rates. In the present layer-by-layer growth model, these effects are not taken into account.

To the contrary, the surface layer is treated as in the two-dimensional Ising model. Polar molecules are represented by a *finite* number of degrees of freedom, which are in the present case, the *up* and *down* orientation of molecular dipoles. Further on, the surface layer is allowed to relax to thermal equilibrium with respect to these two orientational states, taking nearest neighbor interactions among molecules within the adlayer and with the substrate into account. That is, the statistics of orientational order is solely determined by the requirement of the global minimum of the free energy of an adlayer.

This layer-by-layer growth model has satisfactorily described polarity formation in single-component systems, (including host-guest systems, without interactions between host and guest components). However, growth-induced polar properties were also observed in two-component systems, such as solid solutions, and no theoretical model was available so far. In these systems, the interplay between growth-induced *polarity formation* and *miscibility* between the two components is of particular interest.

In this work, the growth model is extended to describe two-component systems, composed of polar and non-polar molecules (Chapters 2, 3 and 4), and two polar components (Chapter 5), respectively. In both cases, in addition to the two orientations of dipoles, the *chemical nature* of the molecules has to be taken into consideration for the occupation of a surface site. Specifically, the study focuses on the following issues:

- Characterization of fundamental behaviors of growth-induced polarity formation as a function of the composition of polar and non-polar species in the solid (Chapter 2).
- Influence of specific molecular interactions on growth-induced polarity formation and miscibility between the two components (Chapter 3).
- Overview of different types of structural order/disorder (e. g. ordered mixed structure, solid solution or non-miscible crystal) and their degree

of polarity by means of a statistical distribution analysis (Chapters 3, 4 and 5).

- Comparison of the phenomenology of macroscopic polarity formation between two-component systems of polar/non-polar and two polar components, respectively (Chapter 5).
- Prediction of the statistical potentiality to provide polarity for the three systems: (a) single-component crystals of polar molecules only, (b) crystals with polar/non-polar components, and (c) crystals with two polar components (Chapter 5).

Thermal equilibration of the surface layer implies slow growth conditions or, equivalently, some form of fast redistribution of molecules on the surface. Especially in case of molecular crystals, this requirement can not be fulfilled always. Geometrical constraints, sterical hindrances or reduced mobility of molecules in connection with kinetic effects lead to much more complex processes on the surface than being described by a layer-by-layer model.

In Chapter 6, a first attempt is made to take such effects into consideration, in order to study their influence on growth-induced polarity formation. Four different growth mechanisms for the attachment of molecules on surface sites are introduced and compared with the layer-by-layer growth model. These growth processes reflect particularly a *reduced cooperativity* between molecules during their attachment on a crystal surface, however, being still based on the original model. Two main points are addressed:

- Influence of the growth mechanism (and in particular the mobility of molecules on the surface) on growth-induced polarity formation.
- Dependence of the appearance of phase transitions on the growth process and, therefore, on the cooperativity between molecules on the surface.

It has been shown that the asymptotic statistics of the layer-by-layer growth model is equivalent to the canonical distribution of a specific two-layer system in thermodynamic equilibrium [5]. Motivated by this result, we additionally investigate to which extent it is possible to describe the non-equilibrium dynamics of the other growth models by similar equilibrium two-layer systems.

Monte Carlo (MC) simulations [9, 8, 66, 58] are widely used, both, in thermodynamic equilibrium statistical physics (like the Ising model [57]), as well as for the investigation of dynamic processes in crystal growth (kinetic Monte Carlo [28, 60, 46, 47]). A major strength of this method is the possibility to

treat only relevant degrees of freedom at certain time scales of a system.

An alternative to MC for the simulation of crystal growth is molecular dynamics (MD) [29, 59]. The time needed for numerical integration of Newton's laws can be kept in reasonable ranges by considering only most important degrees of freedom (e.g. molecules are treated as rigid) and by describing intermolecular interactions with a simple potential. However, in case of crystal growth, MD still faces a major problem in the choice of the integration time step [9]: It is required to be much less than the characteristic time of the fastest degree of freedom (optimization of the molecules attached on the surface), but it has to be sufficiently high to ensure the evolution of the system (approach and attachment of the molecules on the surface). This is principally for that reason that MC methods are preferentially employed for the simulation of crystal growth processes and therefore, are also chosen for the present study.

In this work, analytical descriptions are based on a mean-field approximation [11, 12]. In consideration of the complexity of models to be investigated, which are, nevertheless, idealized representations of processes compared to real systems, this level of theory is considered to be sufficient. To work out its validity is also part of this study.



## Chapter 2

# How Symmetrical Molecules Can Induce Polarity: On the Paradox of Dilution

### 2.1 Abstract

Monte Carlo simulations show that solid solution  $H_{1-X}G_X$  formation between dipolar (H) and symmetrical molecules (G) can yield a high degree of polar order, although both the structure of the dipolar and symmetrical component is assumed centrosymmetric. Previous studies have shown that polarity can evolve in a centric packing of dipolar molecules only if the difference in error probabilities for attaching the molecule in a faulted state 'up' or 'down' is not zero. This, however, is not necessary if a centrosymmetric growing seed of dipolar molecules is being *diluted* by symmetrical molecules. Here, polarity is arising from the presence of G molecules influencing the 'up' and 'down' states of dipolar H molecules. Most pronounced effects of polarity are predicted for molecules H and G undergoing a strong hydrogen-bond type interaction. As maxima of polarity can occur at relatively low values of  $X$  (molar fraction of symmetrical molecules), there is no need for finding systems undergoing solid solution formation over a wide range. Values of  $X \lesssim 0.3$  may be sufficient to yield an  $X_{\text{net}}$  (net polarity, molar fraction of aligned dipoles) of about 0.4 - 0.6.

### 2.2 Introduction

It sounds like a paradox, but Monte Carlo simulations and the Markov-chain theory of polarity generation [40] make it clear: Increasing the molar fraction

$X$  of a symmetrical molecule  $G$  forming a solid solution  $H_{1-X}G_X$  with the centrosymmetric lattice of a dipolar molecule  $H$  can induce polar properties (pyroelectricity) for the solid solution material ( $0 < X < 1$ ).

In case a solid solution  $H_{1-X}G_X$  is existing for the entire range of composition, a maximum of net polarity can be obtained (Fig. 2.1b and 2.1d) which corresponds to a concentration  $X$  of symmetrical  $G$  molecules inducing a significant dilution of  $H$ . The paradox refers to the fact that dilution of a centrosymmetric lattice by symmetrical molecules results in a vectorial physical property [67] being not allowed for the components  $H(s)$ ,  $G$  and also  $G(s)$  ( $s$  stands for solid state). Furthermore, the phenomenon is predicted for conditions which do not fulfill the general criterion established for growth-induced polarity formation in molecular crystals such as channel-type inclusion compounds [42, 43] or single component materials [40, 36]. For these cases, it is a necessary condition for polarity formation upon growth of a centrosymmetric seed crystal to have a *difference* in the attachment probabilities (dipole 'up' or 'down')  $P_{ii}$  and  $P_{jj}$  referring to distinct molecular fragments  $i$  and  $j$ , such as terminal functional groups ( $i = A = \text{acceptor}$ ,  $j = D = \text{donor}$ ) [40, 42]. The present study shows that polarity can form during the growth of a solid solution  $H_{1-X}G_X$  even if  $P_{AA} = P_{DD}$ .

The reason for this is simply that symmetrical  $G$  molecules give rise to orientational selection ('up' vs 'down') exceeded by dipolar species  $H$ . This orientational selectivity increases with the number of  $G$  molecules present in the solid solution. However, as  $X$  is increased, the available fraction ( $1 - X$ ) of dipoles  $H$  being aligned in the same direction is reduced. Consequently, a maximum of net polarity is expected somewhere in between  $X \approx 0.2 - 0.6$  (Fig. 2.1b and 2.1d).

In the following sections, we present a formal description of the system along with Monte Carlo simulations using assumed, but realistic molecular interaction energies for input parameters.

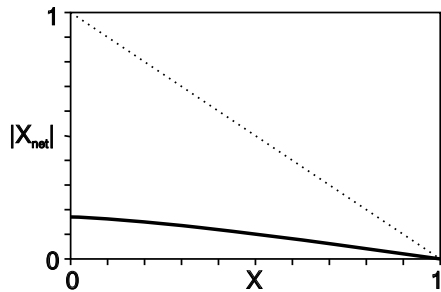
## 2.3 Definitions and General Survey

For any detailed introduction concerning a general discussion of growth-induced polarity formation and its experimental confirmation, we refer here to original work and reviews [40, 35]. A sur-view on literature reporting on effects of polarity in solid solutions is given in Ref. [52].

For a demonstration of basic phenomena we assume to have organic molecules featuring molecular interactions of the following type:

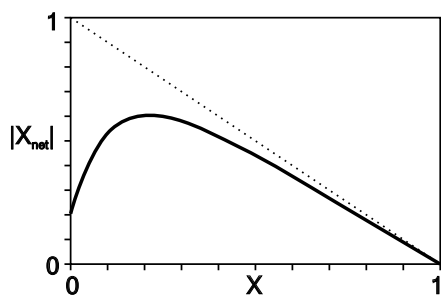
- (i) Interactions of dipolar molecules  $H$  described as  $A - \pi - D$  (two possible states for the dipole:  $\downarrow$  or  $\uparrow$ ):





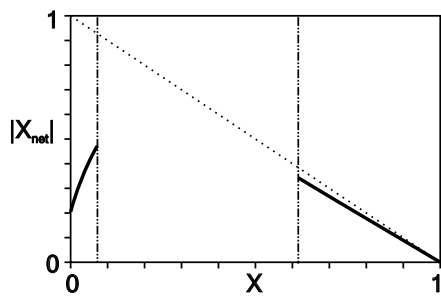
**a) Dilution of intrinsic polarity**

Polarity arises from H molecules only.  
G molecules are almost not selective for H species with respect to 'up' and 'down'.



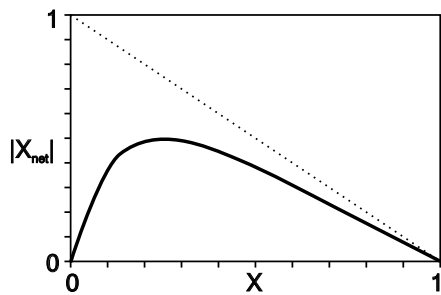
**b) Maximum of polarity**

Polarity arises from H and G molecules.



**c) Miscibility gap**

Polarity arises from H and G molecules.  
H and G molecules show demixing in the solid state.



**d) Polarity by dilution**

Polarity effected by G molecules only.  
H molecules are almost not selective with respect to 'up' and 'down'.

Dilution by symmetrical molecules G

**Figure 2.1:** Four representative cases showing the variation of polarity  $|X_{net}|$  with respect to the molar fraction  $X$  of symmetrical molecules G in solid solutions  $H_{1-X}G_X$  with polar molecules H.

$E_{AA}(-A \cdots A-)$ ,  $E_{DD}(-D \cdots D-)$ ,  $E_{AD}(-A \cdots D-)$ , where  $A/D$  are acceptor/donor fragments, respectively.

$E_p(\downarrow \cdots \downarrow)$ ,  $E_{ap}(\downarrow \cdots \uparrow)$ , where  $p/ap$  are parallel/antiparallel lateral interactions.

(ii) Interactions of symmetrical molecules  $G$  described as  $N - \pi - N$  (single state:  $| \rangle$ ), where  $N \equiv A$  or  $D$ :

$E_{NN}(-N \cdots N-)$ ,  $E_n(| \cdots |)$ , with  $n$  denoting the lateral interaction.

(iii) Interactions between dipolar and symmetrical molecules:

$E_{AN}(-A \cdots N-)$ ,  $E_{DN}(-D \cdots N-)$ ,  $E_m(\downarrow \cdots |, \uparrow \cdots |)$ , where  $m$  reads for mixed interactions.

We limit our discussion here to symmetrical molecules of the type  $A - \pi - A$ , ( $N \equiv A$ ). Therefore, it is assumed to have  $E_{NN} = E_{AN} = E_{AA}$  and  $E_{DN} = E_{AD}$ , whereas in general  $E_p \neq E_{ap} \neq E_m \neq E_n$ . To summarize, we will use the following energies and energy differences:

$$E_{AD} = E_{DN}, E_{DD}, E_{AA} = E_{AN} = E_{NN}, E_{ap}, E_p, E_m, E_n$$

and

$$\Delta E_A = E_{AA} - E_{AD}, \Delta E_D = E_{DD} - E_{AD}, \Delta E_{\perp} = E_p - E_{ap}.$$

A similar description holds for symmetrical molecules of the type  $D - \pi - D$ , ( $N \equiv D$ ).

Referring to the introduction, we consider only cases where  $\Delta E_{\perp} \geq 0$ , i. e. where molecules exceed either no lateral alignment (channel-type inclusion compounds) or are aligned in anti-parallel fashion (centrosymmetric single component structures).

As already extensively studied [40, 43, 36], a basic requirement for polarity formation in a *centric* structure of dipolar species is to have a difference of energy  $\Delta E_f = \Delta E_A - \Delta E_D$  being non zero. Considering that the preferred longitudinal interaction is  $-A \cdots D-$ ,  $\Delta E_f$  can be interpreted as the difference between the appearance of two types of defects, namely  $-A \cdots A-$  (probability of appearance  $P_{AA}$  driven by  $E_{AA}$ ) and  $-D \cdots D-$  (probability  $P_{DD}$  driven by  $E_{DD}$ ). Moreover, it has to be emphasized that these defects may arise only for differences  $\Delta E_A$  and  $\Delta E_D$  which are sufficiently small. This can be easily understood by the example of strong synthons  $-A \cdots D-$  leading to almost no creation of defects, even if  $\Delta E_f \neq 0$ . A real example is *p*-nitroaniline (centrosymmetric structure) featuring strong  $-\text{NH} \cdots \text{O}-$  interactions and showing almost no second harmonic generation effect for chemically very pure samples [48].

In case of solid solutions,  $\Delta E_f \neq 0$  is not anymore a necessary condition for polarity formation, because the deviation from 50 : 50 up/down can be effected by *symmetrical molecules*: For  $\Delta E_f = 0$ , polarity can arise if the difference in the probabilities between docking a molecule H 'up' ( $-A \cdots N-$ ) or 'down' ( $-D \cdots N-$ ) and a molecule G is sufficiently high. This corresponds to the energy difference  $E_{AN} - E_{DN}$ . As we limit the study to  $N \equiv A$ , here the difference is described by  $E_{AA} - E_{AD} = \Delta E_A$ .

The creation of polarity by symmetrical molecules G ( $\Delta E_A$ ) can interfere with that arising from the dipolar molecules ( $\Delta E_f$ ), leading thus to four cases represented in Fig. 2.1. On the vertical axis,  $X_{\text{net}} = X_A(\downarrow) - X_D(\uparrow)$  ( $X_A, X_D$ , molar fractions of H molecules in the solid with the acceptor- and donor-terminal oriented towards the nutrient, respectively) is a measure for net polarity [40]. On the horizontal axis, we have the molar fraction  $X$  of symmetrical molecules in the solid solution. The dotted line with derivative  $-1$  is the asymptotic limit for any of the curves in (a) to (d): All curves in the limes ( $\lim_{X \rightarrow 1} X_{\text{net}}$ ) are joining this line and no curve of  $X_{\text{net}}$  can surpass it at any  $X$ . The four cases presented in Fig. 2.1 can be interpreted as follows:

- (a) In many centrosymmetric crystal structures, dipolar molecules pack into sites where on average the molecular orientation is 50 : 50%. In such structures there is obviously no strong  $\Delta E_{\perp}$  responsible for an anti-parallel alignment, nor are there strong synthon interactions to form e. g. polar chains. However, already a small  $\Delta E_f$  can introduce a significant polarity for  $X = 0$  [40]. Because of the absence of a strong synthon interaction  $-A \cdots D-$ , the insertion of symmetrical molecules will essentially give rise to a *dilution, i. e. reduction of the intrinsic polarity*. In terms of energy, absence of selectivity effected by symmetrical molecules G can be explained by  $E_{AN} - E_{DN} = \Delta E_A \approx 0$ . Recently, this was demonstrated for 4-chloro-4'-nitro-stilbene, forming a solid solution with 4,4'-dinitrostilbene over the entire range of composition [52].
- (b) In that case, polarity arises from H but also G molecules. Because of  $\Delta E_A \neq \Delta E_D$  ( $\Delta E_f \neq 0$ ) there is an *intrinsic polarity* at  $X = 0$ . Moreover, the non-zero difference between  $E_{AN}$  and  $E_{DN}$  ( $\Delta E_A \neq 0$ ) enhances the selectivity for 'up' vs 'down', leading to a *maximum of polarity for  $X > 0$* . This case corresponds to molecules exhibiting moderately strong  $-A \cdots D-$  interactions, i. e.  $\Delta E_A$  and  $\Delta E_D$  are sufficiently small to give rise to polarity, but  $\Delta E_A$  is sufficiently high to give selectivity in the mixed interactions, (remind that  $\Delta E_A = E_{AN} - E_{DN}$  is responsible of polarity induced by G molecules).

- (c) There is a *miscibility gap*, because of two different structures for  $\mathbf{H}(s)$  and  $\mathbf{G}(s)$ . At both ends of the horizontal axis polarity increases due to the effect of  $\Delta E_f$  and  $\Delta E_A$ . Preliminary results for 4-cyano-4'-ethynyl-stilbene ( $\mathbf{H}$ ) and 4,4'-dicyano-stilbene ( $\mathbf{G}$ ) showed such kind of behavior.
- (d) This is the case of special interest, because *polarity is effected only by  $\mathbf{G}$  molecules*. The curve starts at both sides with *zero* polarity and passes through a maximum, just because of the effect of  $E_{AN}$  vs  $E_{DN}$  ( $\Delta E_A \neq 0$ ). This case is typical either for strong  $-A \cdots D-$  interactions, or for molecules presenting no significant difference between  $-A \cdots A-$  and  $-D \cdots D-$ . In the first case, a highly negative  $E_{AD}$  prevents the formation of any kind of defects between dipolar molecules, (so that  $X_{\text{net}}$  is zero at  $X = 0$ ), but provides a high selectivity for  $\mathbf{H}$  molecules effected by  $\mathbf{G}$  entities with respect to 'up' vs 'down'. In the second case, no polarity may arise at  $X = 0$  because of  $\Delta E_f = 0$ .

The influence of the strength of a  $-A \cdots D-$  interaction on polarity formation in solid solutions is summarized in Table 2.1: For a symmetrical molecule of type  $A-\pi-A$ , (assuming that the interactions  $-A \cdots A-$  and  $-D \cdots D-$  are weak), tuning of polarity in solid solutions is possible just by modifying the interaction strength  $-A \cdots D-$ . Indeed, this interaction is responsible for  $\Delta E_A = E_{AN} - E_{DN}$ , and therefore responsible for a modification of polarity by symmetrical molecules  $\mathbf{G}$ . It has to be noted that the same kind of results can be obtained for  $\mathbf{G}$  molecules of the type  $-D \cdots D-$ .

In the next sections we illustrate basic phenomena for case d) by use of Monte Carlo simulations and an analytical stochastic theory.

## 2.4 Monte Carlo Simulations

For Monte Carlo simulations [66] we consider the following model: Starting from a substrate layer, the growth of crystals is described by the attachment of entire layers of molecules one after another. Each layer consists of a square lattice with lattice sites being occupied either by a  $\mathbf{H}$  molecule, oriented 'down' or 'up' (with respect to the growth direction), or by a symmetrical molecule  $\mathbf{G}$ . Therefore, a site can be in one of three possible states (down, up, neutral), while empty sites are not allowed. The molecules of the uppermost layer are subjected to thermal relaxation with respect to (i) the orientation of the dipole in case of the  $\mathbf{H}$  molecules, (ii) an exchange of a  $\mathbf{H}$  molecule with a  $\mathbf{G}$  molecule and vice versa. Thermalization of molecules at

**Table 2.1:** Influence of the strength of an  $-A \cdots D-$  interaction on the resulting polarity ( $X_{\text{net}}$ ) for solid solutions between a dipolar molecule H ( $A - \pi - D$ ) and a symmetrical molecule G of the type  $A - \pi - A$ . The first two lines refer to conditions for having  $X_{\text{net}} \neq 0$  at  $X = 0$ . The fourth line indicates selectivity effected by G molecules between 'up' and 'down'. The last line refers to representative cases shown in Fig. 2.1.

$-A \cdots D-$ interaction	weak	moderate	strong	moderate to strong
$\Delta E_f = \Delta E_A - \Delta E_D$	$\Delta E_f \neq 0$	$\Delta E_f \neq 0$	$\Delta E_f \neq 0$	$\Delta E_f = 0$
Creation of defects	high $E_{AD} \approx E_{AA}, E_{DD}$	moderate $E_{AD} < E_{AA}, E_{DD}$	low $E_{AD} \ll E_{AA}, E_{DD}$	moderate to low
Polarity at $X = 0$	yes	yes	almost no	no
Selectivity effected by G molecules	no $E_{DN} \approx E_{AN}$	yes $E_{DN} < E_{AN}$	yes $E_{DN} \ll E_{AN}$	yes
Corresponding Figure	2.1a dilution	2.1b maximum	2.1d polarity by dilution	

defined sites is effected by taking into account four nearest neighbor interactions to molecules within the layer and the longitudinal interaction with the corresponding molecule of the previous layer. As crystal growth is assumed to take place near equilibrium (slow growth rate), the chemical potentials of the two molecules are considered to be equal in the solid and in the gas phase, i. e.  $\mu_H^{\text{solid}} = \mu_H^{\text{gas}}$  and  $\mu_G^{\text{solid}} = \mu_G^{\text{gas}}$ . The chemical potentials of the gas phase are given by those of a mixture of two ideal gases with the molar fractions  $1 - X_{\text{gas}}$  for the H molecules and  $X_{\text{gas}}$  for the G molecules, respectively, (see [92] for further details). After equilibration, the state of the surface layer is frozen and a subsequent layer is attached, defining the new surface layer for undergoing thermalization. This process is repeated until a stationary state (concerning polarity) is reached by a subsequent addition of layers. For the thermalization of a layer, the following single molecule flip/exchange was applied by using a modified Metropolis algorithm:

1. A lattice site is selected randomly.
2. Given the *actual* state of this site, a *trial* state is defined by choosing one of the two other possible states randomly (i. e. with equal probability of 0.5).
3. The acceptance ratio  $r$  between these two states is calculated:

$$r = e^{(\Delta\mu - E_{\text{trial}} + E_{\text{actual}})/k_B T}, \quad \Delta\mu = \mu_{\text{trial}} - \mu_{\text{actual}},$$

where  $k_B$  is the Boltzmann constant and  $T$  the temperature of the system.  $E_{\text{trial}}$  and  $E_{\text{actual}}$  are the energies of the two states. Note that the chemical potential of H molecules is the same for both dipole orientations.

4. If  $r \geq 1$ , the *trial* state is accepted, otherwise it is taken with probability  $r$ .
5. Steps 1 - 4 are repeated until thermal equilibrium is reached.

As we are interested in the polar properties of as grown crystals and not in details of the process itself, thermodynamical arguments are sufficient for the simulation and therefore no *kinetic* aspects were included here.

In addition to Monte Carlo simulations, an analytical description for the system has been undertaken in terms of a Markov mean-field process for the three different states (down, up, neutral). For a detailed description of the analytical theory and a thorough discussion comparing the two approaches, see Ref. [92].

## 2.5 Results

For an illustration of the theoretical discussion given above we show the influence of (i) the longitudinal energy difference  $\Delta E_A = \Delta E_D$ , (see Fig. 2.2 and 2.3), and (ii) the lateral energy difference  $\Delta E_{\perp}$ , (see Fig. 2.4 and 2.5) on the formation of polarity ( $X_{\text{net}}$ ). All energies are given in kJ/mol. For the entire analysis the following interaction energies were kept constant:

$$E_{AA} = E_{DD} = E_{AN} = E_{NN} = -2,$$

$$E_{ap} = -2,$$

$$E_m = -2, E_n = -3.$$

Note that the condition  $E_{AA} = E_{DD}$  leads to zero polarity at  $X = 0$  as explained above ( $\Delta E_f = 0$ ). Sufficiently negative values for  $E_m$  and  $E_n$  ensure formation of a solid solution at least for a small range of  $X$ .

In case (i), the series  $E_{AD} = E_{DN} = -10, -8, -6$  was chosen with  $E_p = -1$ , leading to the following energy differences:  $\Delta E_A = \Delta E_D = 8, 6, 4$  and  $\Delta E_{\perp} = 1$  (Fig. 2.2,2.3).

In case (ii), the series  $E_p = -1, 0, 1$  was chosen with  $E_{AD} = E_{DN} = -10$ , resulting in  $\Delta E_{\perp} = 1, 2, 3$  and  $\Delta E_A = \Delta E_D = 8$  (Fig. 2.4,2.5). The temperature was set to  $T = 300$  K.

Calculations were done with the Monte Carlo method (lattice size:  $100 \times 100$ ; single layer equilibration time: 1000 Monte Carlo steps per lattice site on average; growth equilibration time: 50 layers; measurement interval: one layer;

measurement range: 200 layers; see [92] for details) and the Markov mean-field model presented in [92].

The variation of  $X_{\text{net}}$  with respect to the concentration  $X$  of symmetrical molecules **G** is shown in Fig. 2.2 and 2.4. Starting by  $X_{\text{net}} = 0$  and  $X = 0$ , polarity is formed by the inclusion of symmetrical molecules **G**, passing a maximum within  $0 < X < 1$ , decreasing and approaching a gradient of -1 in the limit  $X \rightarrow 1$ . As expected, a larger value for the energy difference  $\Delta E_A = E_{AN} - E_{DN}$  enhances the selectivity between 'up' and 'down' states for the polar molecules **H** and, therefore, leads to a higher maximum  $X_{\text{net}}$  (Fig. 2.2). On the other hand, larger values of  $\Delta E_{\perp}$  stabilize the centric orientational state of the crystal (because  $E_{ap} \ll E_p$ ) and consequently weaken the effect of polarity formation (Fig. 2.4).

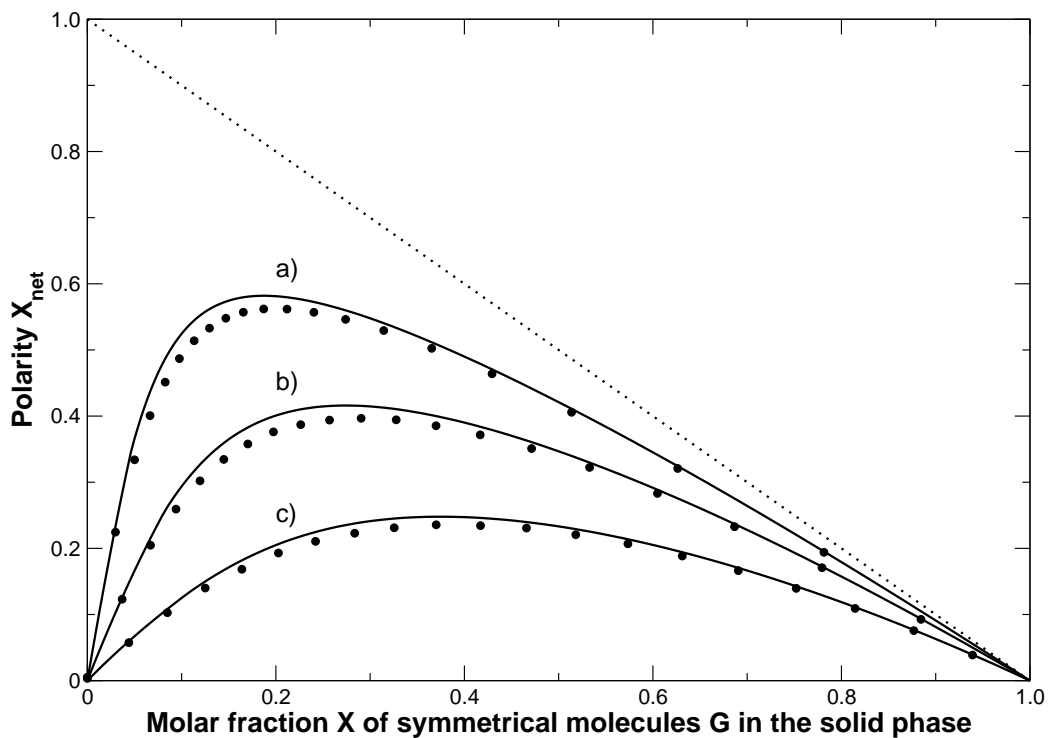
In both cases, Monte Carlo simulations and the analytical stochastic approach [92] are in very good agreement. As shown in Fig. 2.6, snapshots of Monte Carlo simulations for three different values of  $X_{\text{gas}}$  indicate that symmetrical molecules **G** are randomly distributed within the layer, showing virtually no tendency for clustering. Given this condition, the system can be described satisfactorily by a mean-field approach.

Because chemical potentials were taken into account in both models (Monte Carlo simulations and analytical theory), the fractions of **H** and **G** molecules in the solid phase can differ from those in the gas phase. This effect is shown in Fig. 2.3 and 2.5, which represent the distribution between the molar fractions of the symmetrical molecules **G** in the two phases, ( $X_{\text{gas}}$  vs  $X$ ). Further insight to the systems can be gained by looking up supplementary material.

## 2.6 Conclusion

The effectiveness of the concept *Growth and Design* is made evident by Monte Carlo simulations which show for the first time that polarity in solid solutions can be *tuned* for a wide range of  $X_{\text{net}}$ . These calculations are considered a base for the search of real molecules. Fortunately, maximum net polarity is obtained for a system with relatively low  $X$  as the limiting asymptote in Fig. 2.1 features a negative derivative. This makes it much more probable for finding real systems, because dipolar and symmetrical molecules do in general not crystallize in isomorphous structures. Therefore, a miscibility gap (Fig. 2.1c) is likely to encounter. This may not work out to a problem if  $X$  can be kept sufficiently low, as high  $X_{\text{net}}$  values may be reached before a miscibility gap is limiting further increase.

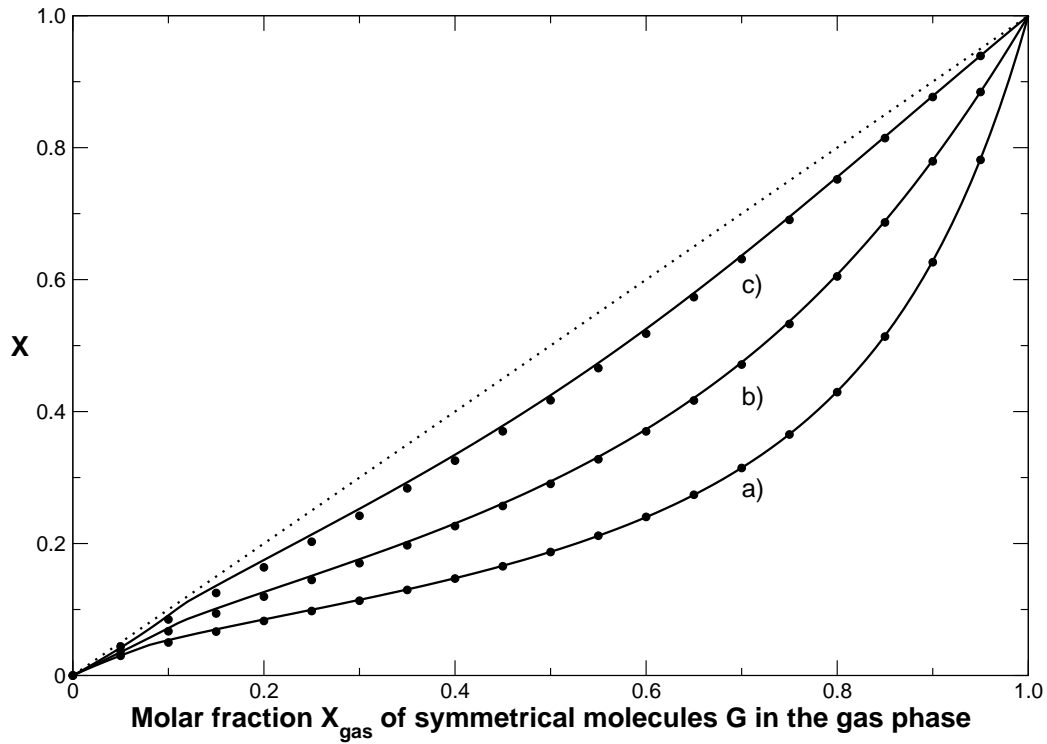
Calculations support the idea that in the case of polarity tuning by solid solutions, the interaction  $E_{AD}$  is most important (Table 2.1): Best molecules



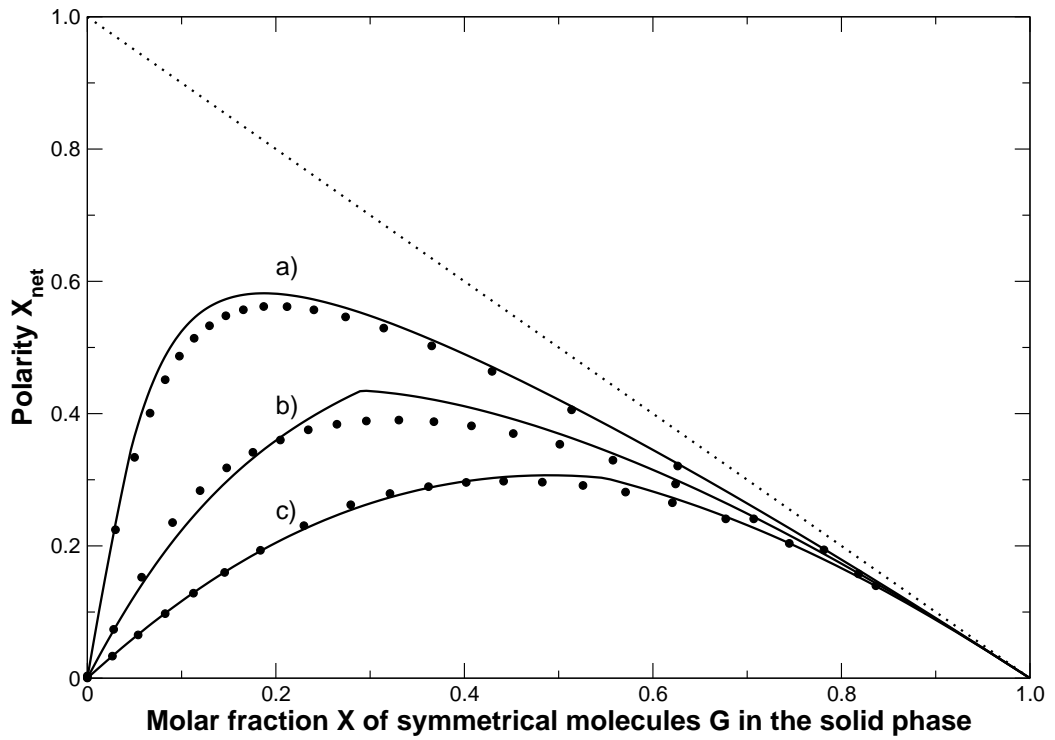
**Figure 2.2:** Polarity  $X_{\text{net}}$  vs dilution  $X$  by symmetrical molecules  $G$  in the solid state. Longitudinal energy differences  $\Delta E_A = \Delta E_D$ : 8, 6, 4 [kJ/mol], a) - c).  $\Delta E_{\perp} = 1$  kJ/mol,  $T = 300$  K. *Points:* Monte Carlo simulations. *Lines:* Markov mean-field model [92]. Error bars for results of the Monte Carlo simulations are too small to be shown here. Dotted line: Asymptotic limit for  $X_{\text{net}}$  vs  $X$ .

feature low energies  $|E_{AA}|$ ,  $|E_{DD}|$  and a largest possible  $E_{ND} < 0$  ( $N \equiv A$ ). Consequently, dipolar molecules which can undergo hydrogen bridging are most interesting for being tested. Experiments along these lines are in progress. Preliminary results for *p*-nitroaniline and other centrosymmetric structures of  $H$  molecules support present theoretical findings.

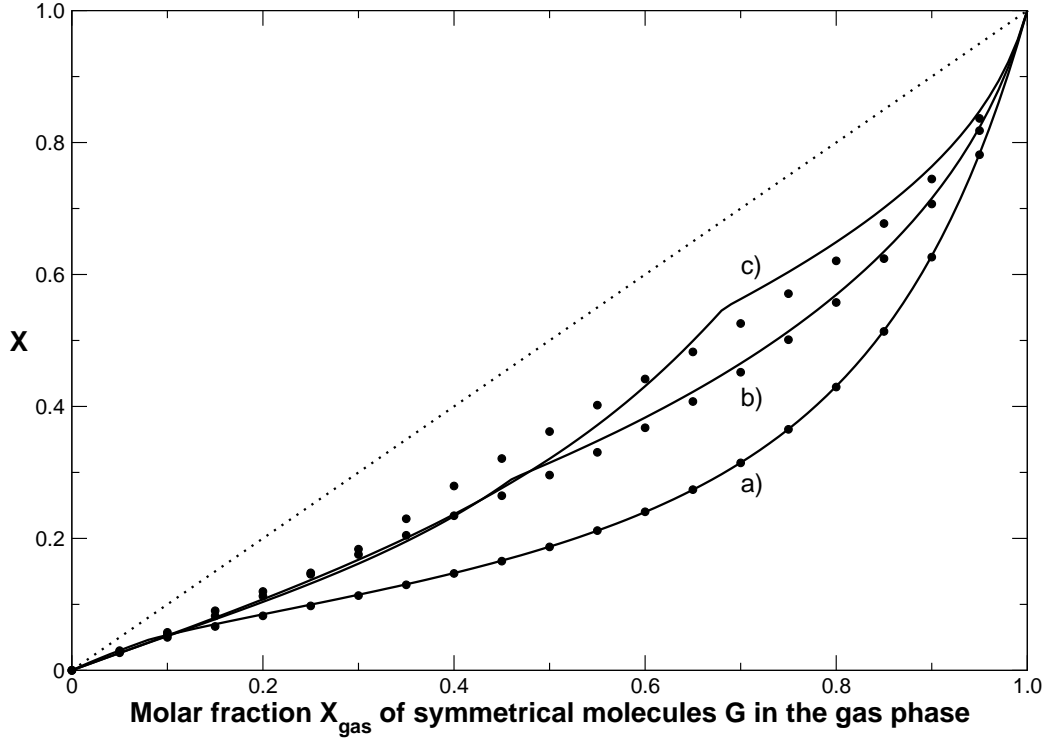




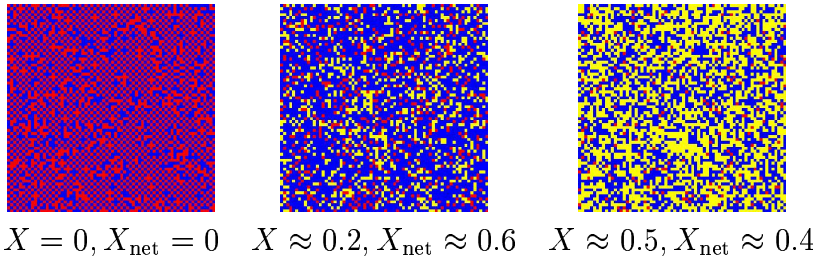
**Figure 2.3:** Molar fraction  $X$  of symmetrical molecules  $G$  in the solid phase vs  $X_{\text{gas}}$  of symmetrical molecules  $G$  in the gas phase. Longitudinal energy differences  $\Delta E_A = \Delta E_D$ : 8, 6, 4 [kJ/mol], a) - c).  $\Delta E_{\perp} = 1$  kJ/mol,  $T = 300$  K. *Points*: Monte Carlo simulations. *Lines*: Markov mean-field model [92]. Note that the Monte Carlo points are uniformly distributed over the  $X$  axis. Dotted line: Distribution coefficient of one.



**Figure 2.4:** Polarity  $X_{\text{net}}$  vs dilution  $X$  by symmetrical molecules  $G$  in the solid state. Lateral energy differences  $\Delta E_{\perp}$ : 1, 2, 3 [kJ/mol], a) - c).  $\Delta E_A = \Delta E_D = 8$  kJ/mol,  $T = 300$  K. *Points*: Monte Carlo simulations. *Lines*: Markov mean-field model [92]. Error bars for results of the Monte Carlo simulations are too small to be shown here. Dotted line: Asymptotic limit for  $X_{\text{net}}$  vs  $X$ .



**Figure 2.5:** Molar fraction  $X$  of symmetrical molecules  $G$  in the solid phase vs  $X_{\text{gas}}$  of symmetrical molecules  $G$  in the gas phase. Lateral energy differences  $\Delta E_{\perp}$ : 1, 2, 3 [kJ/mol], a) - c).  $\Delta E_A = \Delta E_D = 8$  kJ/mol,  $T = 300$  K. *Points*: Monte Carlo simulations. *Lines*: Markov mean-field model [92]. Note that the Monte Carlo points are uniformly distributed over the  $X$  axis. Dotted line: Distribution coefficient of one.



**Figure 2.6:** Snapshots of Monte Carlo simulations for three different cases of  $X_{\text{gas}}$  (0, 0.53, 0.85) [92]. Energies [kJ/mol]:  $E_{AD} = -10$ ,  $E_{AA} = E_{DD} = -2$ ,  $E_p = -1$ ,  $E_{ap} = -2$ ,  $E_n = -3$ ,  $E_m = -2$ . Temperature: 300 K. *Blue*: Polar molecules  $H$  in state 'down'. *Red*: Polar molecules  $H$  in state 'up'. *Yellow*: Symmetrical molecules  $G$ . Lattice size:  $70 \times 70$ . Snapshots taken after 100 layers of growth.



## Chapter 3

# Growth-Induced Polarity Formation in Solid Solutions of Organic Molecules: Markov Mean-Field Model and Monte Carlo Simulations

### 3.1 Abstract

A layer-by-layer growth model is presented for the theoretical investigation of growth-induced polarity formation in solid solutions  $H_{1-X}G_X$  of polar (H) and non-polar (G) molecules ( $X$ : molar fraction of G molecules in the solid,  $0 < X < 1$ ). The model is characterized by the assumption of thermal equilibrium formation of adlayers, with respect to the up and down orientation of the dipoles of H molecules and to an exchange of H and G molecules, while previously attached layers are kept frozen. The model is analyzed by means of a Markov mean-field description and Monte Carlo simulations. In solid solutions, polarity results from a combined effect of orientational selectivity by H and G molecules with respect to the alignment of the dipoles of H molecules and miscibility between the two components. Even though both native structures (H,G) may be centrosymmetric, polarity can arise just from the admixture of G molecules in the H crystal upon growth. An overview of possible phenomena is given by random selection of molecular interaction energies within an assumed but realistic energy range. The analytical approach describes sufficiently basic phenomena and is in good agreement with simulations. High probabilities for significant vectorial alignment of H molecules

are found for low ( $X \leq 0.2$ ) and high ( $X \geq 0.8$ ) fractions of G molecules, respectively, as well as for ordered HG compounds ( $X = 0.5$ ).

## 3.2 Introduction

Symmetry lowering at the surface of as grown sectors of molecular crystals can cause the appearance of physical properties which may not be allowed by the symmetry group of the bulk. In case these properties get kinetic stabilization, *growth-induced* property formation is a true alternative to nucleation.

In a series of theoretical and experimental papers we have investigated the evolvment of a vectorial property (e. g. pyroelectricity) driven by a Markov process of orientational alignment of polar molecules being attached to slowly growing crystal faces ( $hkl$ ) [40, 39, 5, 78]. Because of ergodicity, property formation by a Markov process does not depend on the seeding state. In that sense, growth-induced polarity formation is possible even for a seed being centrosymmetric.

In this work we investigate growth-induced polarity formation in *two-component crystals* of organic molecules. Previous studies have demonstrated experimentally the appearance or modification of physical properties due to symmetry reduction by the admixture of guest molecules into a host crystal upon growth (second-order nonlinear optical effects) [49, 86, 89, 90]. However, no formal and quantitative theoretical investigation on polarity formation in molecular solid solutions was ever published. We describe a growth model showing that significant vectorial alignment can be obtained for a *centrosymmetric* host lattice (h) of polar molecules (H) which undergoes solid solution formation  $H_{1-X}G_X$  by the inclusion of non-polar guest molecules (G), crystallizing in a centrosymmetric structure (g), ( $X$  being the molar fraction of G molecules in the solid solution,  $0 < X < 1$ ).

The model to be investigated is defined as follows: A two-component crystal built up of polar (H) and non-polar (G) molecules is subjected to a slow layer-by-layer growth. Among the possible processes which can occur during the attachment of molecules on surface sites, only two are considered: (i) The up or down orientation ( $\downarrow, \uparrow$ ) of the dipole moment of H molecules, and (ii) the exchange of H and G molecules. Thermal equilibration with respect to processes (i) and (ii) takes place only for the adlayer taking into account longitudinal and lateral Ising-type nearest neighbor interactions, while the substrate layer itself (i. e. the layer attached in the previous step) is kept frozen. This is justified by the large energy of activation for dipole reversals (H) or exchanges (H,G) in the bulk for molecular crystals considered here. In

the limit of slow growth, it is assumed that thermodynamic arguments reasonably well apply, i. e. kinetic effects are not required for polarity formation. The evolution of the system is investigated by means of a Markov mean-field description and Monte Carlo simulations, describing the orientational order of vectors representing H molecules in the asymptotic limit of many attached layers. In this model, polarity formation is analyzed along with solid solution formation, where novelty is focusing on a combined effect: Non-polar molecules (G) can effect vectorial ordering of polar molecules (H) as a result of growth. By random selection of molecular interaction energies constrained within realistic intervals, an overview of possible phenomena is given which may be or have been observed for real solid solutions  $H_{1-x}G_x$  [52].

In recognition of previous work on organic solid solutions and binary alloys, the present analysis focusing on a quantitative prediction of polarity phenomena has no precedent in literature [65, 93, 73, 87, 16, 64, 74, 63].

### 3.3 The Growth Model

The building blocks of the two-component system are organic molecules of the following type: Host (H) molecules  $A - \pi - D$ , ( $A$ : electronic acceptor terminal;  $D$ : electronic donor terminal;  $\pi$ : delocalized  $\pi$ -electron system connecting  $A$  and  $D$ ), carrying a dipole moment  $\mu_{el}$  pointing from  $A$  to  $D$ ; guest (G) molecules  $N - \pi - N$ , ( $N$ : functional group, either  $A$  or  $D$ ), featuring no dipole moment.

Crystal growth is considered from the gas phase at constant temperature  $T$  and pressure  $P$ . For a sufficiently low pressure, the work for a change of volume can be neglected, i. e.  $P\Delta V \approx 0$ . The molar fractions of the host (H) and guest (G) components in the gas are given as  $1 - X_{\text{gas}}$  and  $X_{\text{gas}}$ , respectively ( $0 \leq X_{\text{gas}} \leq 1$ ) and chemical potentials are specified by  $\mu_H^{\text{gas}}$  and  $\mu_G^{\text{gas}}$ . For a number of molecules in the surrounding gas being much larger than in the growing crystal, the gas phase is considered a *reservoir*, leaving molar fractions and chemical potentials unchanged ( $X_{\text{gas}}$ ,  $\mu_H^{\text{gas}}$ ,  $\mu_G^{\text{gas}}$  are constant). It is assumed that the crystal grows layer-by-layer from any seeding state, with molecules being arranged on a 2D square lattice. Empty or multiply occupied sites are not allowed. For the particular type of molecules involved (elongated principal axis), only one degree of freedom for the attachment of admolecules on a surface site is taken into account: Polar molecules can be attached either parallel ( $\uparrow$ ) or anti-parallel ( $\downarrow$ ) with respect to the projection of their dipole moment onto the growth direction, pointing their donor ( $D$ ) or acceptor ( $A$ ) terminal toward the nutrient, respectively. *Macroscopic polarity formation originates from an unequal ratio of these two orientational*

*states of H molecules.* For non-polar molecules a sole attachment possibility ( $|$ ) is indicated by the molecular terminal ( $N$ ). Consequently, the occupation of a lattice site is uniquely characterized by one of the states  $\{A, D, N\}$ .

The growth model is based on the following main assumptions: (i) The growth of the crystal proceeds layer-by-layer, i. e. a new layer is formed after the preceding layer is completed. (ii) The surface layer is subjected to thermal relaxation with respect to the orientational state ( $\uparrow, \downarrow$ ) of H molecules and to the exchange of H with G molecules and vice versa, i. e. in terms of the three states  $\{A, D, N\}$ . Thermal relaxation of the surface layer takes place after all the molecules are attached. (iii) Formerly grown layers are kept frozen when a new layer is attached. This may be justified due to the high activation energy for a  $180^\circ$  reorientation (H) or exchange (H,G) of molecules in the bulk for elongated prolate-type molecules. (iv) Crystal growth takes place near thermal equilibrium, i. e. the time for the growth of a layer is larger than the surface layer relaxation time.

Thermal relaxation of an admolecule on a surface site is effected by taking into account nearest neighbor interactions with molecules of the same layer (lateral) and the interaction with the molecule in the previously attached *substrate layer* on the corresponding site (longitudinal). The interaction energies depend on the type (H,G) and the directional state (H) of the two molecules involved. Laterally, isotropic interactions are assumed. Considering H and G molecules with similar shapes and crystallizing in identical crystal structures, one set of interaction energies is sufficient in this model and defined as follows:

1. Interactions between H molecules:  
 Longitudinal:  $E_{AA}$  ( $-A \cdots A-$ ),  $E_{DD}$  ( $-D \cdots D-$ ),  
 $E_{AD}$  ( $-A \cdots D-$ ,  $-D \cdots A-$ ).  
 Lateral:  $E_p$  ( $\downarrow \cdots \downarrow, \uparrow \cdots \uparrow$ ),  $E_{ap}$  ( $\downarrow \cdots \uparrow, \uparrow \cdots \downarrow$ ), where  $p, ap$  stands for parallel and anti-parallel, respectively.
2. Interactions between G molecules:  
 Longitudinal:  $E_{NN}$  ( $-N \cdots N-$ ).  
 Lateral:  $E_n$  ( $|\cdots|$ ), with  $n$  denoting neutral.
3. Interactions between H and G molecules:  
 Longitudinal:  $E_{NA}$  ( $-N \cdots A-$ ,  $-A \cdots N-$ ),  
 $E_{ND}$  ( $-N \cdots D-$ ,  $-D \cdots N-$ ).  
 Lateral:  $E_m$  ( $\downarrow \cdots |, \uparrow \cdots |$ ), where  $m$  reads for mixed.

For an illustration of the growth model with corresponding interaction energies, see Fig. 3.1.



Given the assumption of crystal growth taking place near thermal equilibrium, we are allowed to set  $\mu_H = \mu_H^{\text{gas}}$  and  $\mu_G = \mu_G^{\text{gas}}$ , where  $\mu_H$  and  $\mu_G$  are the chemical potentials of H and G molecules in the adlayer, respectively. The chemical potential is the same for both orientations ( $\uparrow, \downarrow$ ) of the H molecules in the solid.

The chemical potentials of the two components in the gas phase are approximated by those of a mixture of two ideal gases with molar fractions  $1 - X_{\text{gas}}$  (H) and  $X_{\text{gas}}$  (G) [50]. Being interested in solid solutions of components with a similar structural shape, we set  $m_H = m_G \equiv m$ , where  $m_H$  and  $m_G$  are the masses of H and G molecules, respectively. With these approximations it is

$$\mu_H = \mu_H^{\text{gas}} = \mu_0 + k_B T \ln(1 - X_{\text{gas}}) \quad (3.1a)$$

and

$$\mu_G = \mu_G^{\text{gas}} = \mu_0 + k_B T \ln X_{\text{gas}} \quad (3.1b)$$

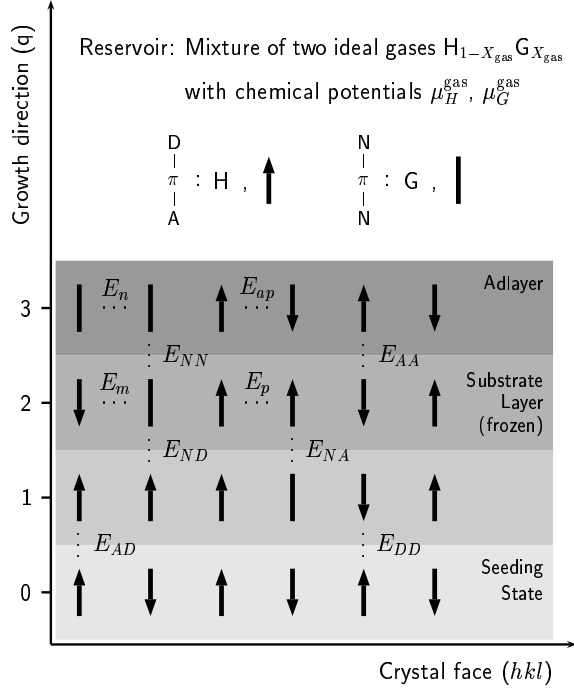
where

$$\mu_0 = k_B T \ln \left( \frac{P}{k_B T} \left( \frac{h^2}{2\pi m k_B T} \right)^{3/2} \right) \quad (3.1c)$$

is a system parameter,  $k_B$  is the Boltzmann constant and  $h$  is the Planck constant.

In view of a growth-induced process, keeping the previously attached layers frozen, we describe a state showing a minimal free energy  $F$  *only* for the surface layer, but not for the bulk. Therefore, the growth process leads to a metastable bulk state, being justified only if re-orientational flips or exchanges of molecules are not taking place after the attachment of subsequent layers. Moreover, as we assume that polarity formation in the solid solution arises from the orientational states ( $\uparrow, \downarrow$ ) of H molecules only, thermodynamical arguments are considered sufficient for describing the growth process and no kinetic aspects are taken into account here.

The growth process has reached stationarity, if the molar fractions of sites being in states  $\{A, D, N\}$  become approximately the same for all subsequently attached layers differing only within the range of thermal fluctuations. In this work the main analysis is focusing on this regime. Two macroscopic quantities are defined for this asymptotic state: (i) The molar fraction of G molecules  $X$  in the solid ( $0 \leq X \leq 1$ ). (ii) The net polarity  $X_{\text{net}}$  given by the difference between the molar fractions of H molecules, oriented downwards ( $\downarrow$ ) and upwards ( $\uparrow$ ) ( $-1 \leq X_{\text{net}} \leq 1$ ). Physical quantities having their origin in polar properties of the molecules are proportional to  $X_{\text{net}}$ , (e.g. the electrical polarization  $P_s$  in a particular growth sector).



**Figure 3.1:** Schematic illustration of the layer-by-layer growth for solid solutions  $H_{1-X}G_X$  of polar (H) and non-polar (G) molecules ( $0 < X < 1$ ).  $X_{\text{gas}}$  is the molar fraction of G molecules in the gas. Arrows refer to projections of the dipole moments of H molecules with respect to the growth direction ( $q$ ). Adlayers are in thermal and diffusive contact with the surrounding gas (reservoir), while previously attached layers are kept frozen.  $E_{AD}, E_{AA}, E_{DD}, E_{NA}, E_{ND}, E_{NN}$  and  $E_p, E_{ap}, E_m, E_n$  correspond to nearest neighbor molecular interaction energies between adjacent layers (longitudinal) and within layers (lateral), respectively.

The layer-by-layer growth, the square lattice symmetry and the present set of energies are sufficient for an investigation of the principal properties of growth-induced polarity formation in solid solutions. However, crystal structures generally require a more detailed description in terms of lattice symmetries, interaction energies and growth process. For example, non-isotropic interactions in connection with crystal growth along steps or kinks should be considered. Furthermore, the contributions of different crystal faces ( $hkl$ ) must be taken into account separately for a quantitative prediction of macroscopic polarity. In this respect, the growth model presented along this work attempts to work out *fundamental phenomena* based on a thorough reduction, however, being aware of the complexity of real systems [26].

## 3.4 Mathematical Treatment

The present growth model for solid solutions is described in terms of a Markov process. In that frame it is an extension of the Markov mean-field model applied previously to single-component crystals [40]. Complementary to an analytical theory, Monte Carlo simulations were performed.

### 3.4.1 Markov Mean-Field Description

Originally, the description of the layer-by-layer growth as a Markov process was applied to investigate the evolution of polarity in channel-type inclusion compounds [43, 31, 30], where H molecules form isolated 1D chains without lateral influence on polarity formation. The successive attachment of admolecules, where the attachment probabilities only depend on the *longitudinal* interaction with the molecule on the corresponding site in the substrate layer, represents a stochastic process fulfilling the criterion of a homogeneous Markov chain with constant transition probabilities [13].

By taking into account the influence of lateral interactions on the attachment probabilities, the system does not correspond to a Markov process, since the occupation of a site by an admolecule depends both, on the interaction with the substrate molecule *and* on the interactions with the neighboring admolecules. However, if we consider the lateral neighborhood of the *substrate* layer, instead of that of the *actual* layer, the Markov property is met again. This is justified because we account for lateral interactions only within a mean-field approximation: Here it is assumed that in the limit of a large number of attached layers, the fractions of sites being in states  $\{A, D, N\}$  in two successive layers are the same within statistical deviations. Indeed, the equivalence of these fractions is exactly the condition for the asymptotic state of the system.

The Markov chain is defined by the sequence  $\{S_q\}$  of admolecules being attached on a given lattice site in successive layers  $q = 1, 2, \dots, \infty$  starting from a seeding state ( $q = 0$ ).  $S_q$  takes values from the set  $\{A, D, N\}$ , referring to the attachment of a H molecule oriented downwards ( $\downarrow$ ), a H molecule oriented upwards ( $\uparrow$ ), or a G molecule, respectively. The probabilities for  $S_q = i$  with  $i \in \{A, D, N\}$  in layer  $q$  correspond to the molar fractions of sites being in state  $\{A, D, N\}$  in this layer. They are denoted by  $X_A^q$ ,  $X_D^q$  and  $X_N^q$ , respectively.

Given the particular geometrical conditions in the present model, (square lattice, nearest lateral neighbors), *two* Markov chains have to be considered for an adequate description: One for sites belonging to the sublattice (*I*) with  $x + y = \text{even}$  ( $x, y$ : lattice coordinates) and one for the sublattice (*II*)

with  $x + y = \text{odd}$  [40]. Separate Markov processes and molar fractions  $X_i^{g,q}$ ,  $i \in \{A, D, N\}$ , are necessary to account for the two sublattices  $g = I, II$ . The evolution of the two Markov chains ( $g = I, II$ ) is expressed by the matrix equations

$$\begin{pmatrix} X_A^{g,q+1} \\ X_D^{g,q+1} \\ X_N^{g,q+1} \end{pmatrix} = \begin{pmatrix} P_{AD}^g & P_{DD}^g & P_{ND}^g \\ P_{AA}^g & P_{DA}^g & P_{NA}^g \\ P_{AN}^g & P_{DN}^g & P_{NN}^g \end{pmatrix} \begin{pmatrix} X_A^{g,q} \\ X_D^{g,q} \\ X_N^{g,q} \end{pmatrix}, \quad (3.2)$$

where  $(X_A^{g,q}, X_D^{g,q}, X_N^{g,q})$  and  $(X_A^{g,q+1}, X_D^{g,q+1}, X_N^{g,q+1})$  are the molar fractions of sites  $\{A, D, N\}$  in the substrate layer ( $q$ ) and adlayer ( $q+1$ ), respectively ( $q = 0, 1, 2, \dots, \infty$ ). For each  $q \geq 0$  holds

$$X_A^{g,q} + X_D^{g,q} + X_N^{g,q} = 1, \quad g = I, II. \quad (3.3)$$

$P_{s's}^g$  is the transition probability that an admolecule, (specified by its molecular terminal  $s \in \{D, A, N\}$  oriented toward the substrate), will be attached onto a molecule of the substrate layer, (specified by its molecular terminal  $s' \in \{A, D, N\}$  oriented toward the nutrient), belonging to a site of sublattice  $g$ . This notation arises from the fact, that the probability is directly influenced by the longitudinal interaction energy between the two terminals  $s$  and  $s'$ . Based on the assumption of *thermal equilibrium* formation of an adlayer, the transition probabilities  $P_{s's}^g$  are given by normalized Gibbs factors

$$P_{s's}^g = \frac{1}{Z_{s'}} e^{\beta(\mu_s - f_{s's}^g)}, \quad (3.4a)$$

with

$$Z_{s'} = \sum_s^{\{A,D,N\}} e^{\beta(\mu_s - f_{s's}^g)}, \quad s' \in \{A, D, N\}, \quad (3.4b)$$

being the normalization factor, ( $\beta = 1/k_B T$ ).  $\mu_s$  refers to the chemical potential of a H molecule, if  $s \in \{A, D\}$ , otherwise to that of a G molecule ( $s = N$ ). Note that transition probabilities  $P_{s's}^g$  depend on the molar fractions  $X_i^{g,q}$ ,  $i \in \{A, D, N\}$  in the substrate layer ( $q$ ) because of the energy terms  $f_{s's}^g$  defined in Table 3.1.

Given the particular expressions for the chemical potentials, see Eqs. (3.1), Eq. (3.4) simplifies to

$$P_{s's}^g = \frac{1}{Z_{s'}} x_s e^{-\beta f_{s's}^g}, \quad (3.5a)$$

with

$$Z_{s'} = \sum_s^{\{A,D,N\}} x_s e^{-\beta f_{s's}^g}, \quad s' \in \{A, D, N\}, \quad (3.5b)$$

and  $x_s = 1 - X_{\text{gas}}$ , if  $s \in \{A, D\}$ , otherwise  $x_s = X_{\text{gas}}$  ( $s = N$ ).

In view of the Markov chain description, the condition that the growth process has reached a stationary state, is expressed by

$$\begin{pmatrix} X_A^g \\ X_D^g \\ X_N^g \end{pmatrix} = \begin{pmatrix} P_{AD}^g & P_{DD}^g & P_{ND}^g \\ P_{AA}^g & P_{DA}^g & P_{NA}^g \\ P_{AN}^g & P_{DN}^g & P_{NN}^g \end{pmatrix} \begin{pmatrix} X_A^g \\ X_D^g \\ X_N^g \end{pmatrix}, \quad (3.6)$$

i. e. equal molar fractions in the substrate layer and the adlayer, for the two sublattices  $g = I, II$  separately. Eq. (3.6) sets up a system of coupled non-linear equations for the *stationary* molar fractions  $X_A^I, X_A^{II}, X_D^I, X_D^{II}, X_N^I, X_N^{II}$ . For details on the numerical solution, including an efficient criterion in order to find only physical solutions, see Appendix 3.8.

Given the molar fractions in the stationary state, the macroscopic quantities  $X$  and  $X_{\text{net}}$  are obtained as follows:

$$X = 1 - \left( \frac{X_A^I + X_A^{II}}{2} + \frac{X_D^I + X_D^{II}}{2} \right), \quad (3.7)$$

$$X_{\text{net}} = \frac{X_A^I + X_A^{II}}{2} - \frac{X_D^I + X_D^{II}}{2}. \quad (3.8)$$

The present analytical description reproduces the case of polarity formation in single-component crystals, if  $X_{\text{gas}} = 0$  [40].

### 3.4.2 Monte Carlo Simulations

The Monte Carlo procedure consists in a successive attachment and thermal equilibration of adlayers, starting from a seed layer. Given that each lattice site is in one of the states  $\{A, D, N\}$ , an adlayer can take up  $3^{N_L}$  possible configurations, where  $N_L$  is the number of lattice sites in a layer. At thermal equilibrium, the probability  $p_\nu$  to find an adlayer in configuration  $\nu$ , with  $N_H$  H molecules,  $N_L - N_H$  G molecules and energy  $E_\nu$ , is given by the Gibbs factor

$$p_\nu = \frac{1}{\mathcal{Z}} e^{\beta(N_H \mu_H + (N_L - N_H) \mu_G - E_\nu)}. \quad (3.9a)$$

$\mathcal{Z}$  is the grand canonical partition function

$$\mathcal{Z} = \sum_{N_H=0}^{N_L} \sum_{\lambda} e^{\beta(N_H \mu_H + (N_L - N_H) \mu_G - E_\lambda)}, \quad (3.9b)$$

the second sum going over all configurations  $\lambda$  with  $N_H$  kept constant. Energies  $E_\lambda$  include nearest neighbor interactions within the adlayer and with

**Table 3.1:** Interaction energies  $f_{s's}^g$  for the attachment of an admolecule (specified by its molecular terminal  $s$  oriented toward the substrate) onto a substrate molecule (specified by its molecular terminal  $s'$  oriented toward the nutrient) consisting of two parts: (i) Longitudinal energy  $E_{s's}$  with  $s, s' \in \{A, D, N\}$ , and (ii) lateral mean-field estimate, depending on the sublattice  $g$  to which the molecules belong. The molar fractions  $X_{s'}^g$  refer to those of the substrate layer ( $g$ ).  $z_{\perp}$  is the coordination number, being 4 for a square lattice.

Sublattice	Terminal		Energy term $f_{s's}^g$
$g$	$s'$	$s$	
$I$	$A$	$D$	$E_{AD} + z_{\perp}(X_A^{II}E_p + X_D^{II}E_{ap} + X_N^{II}E_m)$
$I$	$A$	$A$	$E_{AA} + z_{\perp}(X_A^{II}E_{ap} + X_D^{II}E_p + X_N^{II}E_m)$
$I$	$A$	$N$	$E_{NA} + z_{\perp}(X_A^{II}E_m + X_D^{II}E_m + X_N^{II}E_n)$
$I$	$D$	$D$	$E_{DD} + z_{\perp}(X_A^{II}E_p + X_D^{II}E_{ap} + X_N^{II}E_m)$
$I$	$D$	$A$	$E_{AD} + z_{\perp}(X_A^{II}E_{ap} + X_D^{II}E_p + X_N^{II}E_m)$
$I$	$D$	$N$	$E_{ND} + z_{\perp}(X_A^{II}E_m + X_D^{II}E_m + X_N^{II}E_n)$
$I$	$N$	$D$	$E_{ND} + z_{\perp}(X_A^{II}E_p + X_D^{II}E_{ap} + X_N^{II}E_m)$
$I$	$N$	$A$	$E_{NA} + z_{\perp}(X_A^{II}E_{ap} + X_D^{II}E_p + X_N^{II}E_m)$
$I$	$N$	$N$	$E_{NN} + z_{\perp}(X_A^{II}E_m + X_D^{II}E_m + X_N^{II}E_n)$

Sublattice	Terminal		Energy term $f_{s's}^g$
$g$	$s'$	$s$	
$II$	$A$	$D$	$E_{AD} + z_{\perp}(X_A^IE_p + X_D^IE_{ap} + X_N^IE_m)$
$II$	$A$	$A$	$E_{AA} + z_{\perp}(X_A^IE_{ap} + X_D^IE_p + X_N^IE_m)$
$II$	$A$	$N$	$E_{NA} + z_{\perp}(X_A^IE_m + X_D^IE_m + X_N^IE_n)$
$II$	$D$	$D$	$E_{DD} + z_{\perp}(X_A^IE_p + X_D^IE_{ap} + X_N^IE_m)$
$II$	$D$	$A$	$E_{AD} + z_{\perp}(X_A^IE_{ap} + X_D^IE_p + X_N^IE_m)$
$II$	$D$	$N$	$E_{ND} + z_{\perp}(X_A^IE_m + X_D^IE_m + X_N^IE_n)$
$II$	$N$	$D$	$E_{ND} + z_{\perp}(X_A^IE_p + X_D^IE_{ap} + X_N^IE_m)$
$II$	$N$	$A$	$E_{NA} + z_{\perp}(X_A^IE_{ap} + X_D^IE_p + X_N^IE_m)$
$II$	$N$	$N$	$E_{NN} + z_{\perp}(X_A^IE_m + X_D^IE_m + X_N^IE_n)$

the substrate layer. Given Eqs. (3.1) for the chemical potentials  $\mu_H$  and  $\mu_G$ , Eqs. (3.9) can be written as

$$p_\nu = \frac{1}{\mathcal{Z}'} (1 - X_{\text{gas}})^{N_H} X_{\text{gas}}^{N_L - N_H} e^{-\beta E_\nu}, \quad (3.10a)$$

with

$$\mathcal{Z}' = \sum_{N_H=0}^{N_L} \sum_{\lambda} (1 - X_{\text{gas}})^{N_H} X_{\text{gas}}^{N_L - N_H} e^{-\beta E_\lambda}. \quad (3.10b)$$

Thermal equilibration of adlayers is achieved by means of a Metropolis algorithm, taking into account single molecule flips and exchanges [66, 58]. For details, see Appendix 3.9.

### 3.5 Results

Two factors determine growth-induced polarity formation in solid solutions  $\text{H}_{1-X}\text{G}_X$ : (i) *orientational selectivity* of H molecules with respect to a downward ( $\downarrow$ ) or upward ( $\uparrow$ ) orientation and (ii) *miscibility* between H and G molecules. For each factor, the characteristic behaviors were analyzed and the driving forces in terms of interaction energies responsible for this behavior were determined. Both, the Markov mean-field (MMF) description and Monte Carlo simulations (MCS) were applied, so that a comparison between the two approaches was possible.

Throughout the analysis we restrict ourselves to G molecules of the types  $A - \pi - A$  ( $N \equiv A$ ) or  $D - \pi - D$  ( $N \equiv D$ ), since many known examples are of these types [26]. In order to reduce the number of independent interaction energies, the following assumptions are made concerning longitudinal interaction energies involving G molecules:

$$E_{NA} = E_{NN} = E_{AA}, \quad (3.11a)$$

$$E_{ND} = E_{AD}, \quad (3.11b)$$

for  $N \equiv A$  and

$$E_{NA} = E_{AD}, \quad (3.12a)$$

$$E_{ND} = E_{NN} = E_{DD}, \quad (3.12b)$$

for  $N \equiv D$ . All energies were chosen within an assumed but realistic energy range of  $-10 \dots 2$  kJ/mol.

For the reason of clarity, the description made use of *single* energies so far. However, given the particular mathematical form of the Markov mean-field

model as well as the Monte Carlo procedure, the system is determined only by *differences* among longitudinal energies and lateral energies, independently. Therefore, without loss of generality, the following energy differences are introduced:

$$\Delta E_A = E_{AA} - E_{AD}, \quad (3.13a)$$

$$\Delta E_D = E_{DD} - E_{AD}, \quad (3.13b)$$

$$\Delta E_p = E_p - E_{ap}, \quad (3.13c)$$

$$\Delta E_m = E_m - E_{ap}, \quad (3.13d)$$

$$\Delta E_n = E_n - E_{ap}. \quad (3.13e)$$

These five energy differences, temperature  $T$  and the value of  $X_{\text{gas}}$  define the *complete set* of input parameters for the analysis. The longitudinal energy differences  $\Delta E_A$  and  $\Delta E_D$  are restricted to positive values only, because of a generally higher stability for  $-A \cdots D-$  interactions as compared to  $-A \cdots A-$  and  $-D \cdots D-$  for the type of molecules considered here. Being interested in formation of polarity (and not in diminution of polarity in polar crystals), crystal growth is only considered for *centrosymmetric* packings of H molecules, where  $\Delta E_p > 0$  [40]. Note that energy differences in Eqs. (3.13) are subject to the constraint that single energies stay within the range of  $-10 \dots 2$  kJ/mol.

### 3.5.1 Orientational Selectivity

In single-component crystals of H molecules, polarity arises if there is a non-zero difference between the attachment probabilities  $P_{AA}$  ( $-A \cdots A-$ ) and  $P_{DD}$  ( $-D \cdots D-$ ) [40]. In solid solutions  $\text{H}_{1-X}\text{G}_X$ , additionally to this selectivity of H molecules *by* H molecules, polarity may arise from the difference of attachment probabilities  $P_{NA}$  ( $-N \cdots A-$ ) and  $P_{ND}$  ( $-N \cdots D-$ ) when docking H molecules with the acceptor (A) or donor (D) terminals onto G molecules, respectively. In terms of interaction energies, orientational selectivity is determined as follows:

(i) Interactions between H and H molecules:  $\Delta E_A$ ,  $\Delta E_D$  and  $\Delta E_p$ . Known from studies on single-component crystals of H molecules, a necessary condition for polarity formation upon growth of a centric face ( $\Delta E_p > 0$ ) is to have a non-zero energy difference between  $\Delta E_A$  and  $\Delta E_D$ , i.e.  $\Delta E_f \equiv \Delta E_A - \Delta E_D \neq 0$  [40, 39, 43]. Oppositely, an increase of  $\Delta E_p$  tends to stabilize the centric packing of H molecules and consequently lowers the effect of polarity formation. Therefore, this energy difference is not considered a driving force of polarity formation.

(ii) Interactions between H and G molecules:  $E_{NA} - E_{ND}$ . A non-zero value



results in different attachment probabilities for H molecules being docked with the acceptor ( $A$ ) or donor ( $D$ ) terminals onto G molecules (terminal  $N$ ), respectively, and therefore in the formation of polarity. With Eqs. (3.11) and (3.12) this energy difference corresponds to  $\Delta E_A$  in case of  $N \equiv A$  and  $-\Delta E_D$  in case of  $N \equiv D$ . Due to the relations concerning longitudinal energy differences imposed by Eqs. (3.11) and (3.12), it follows that only *one* type of G molecules ( $N \equiv A, D$ ) has to be considered, since the two cases are equivalent (only differing in the sign of  $X_{\text{net}}$ ) if the values of  $E_{AA}$  and  $E_{DD}$  are interchanged. Here, exclusively  $N \equiv A$  is chosen.

The energy differences  $\Delta E_m$  and  $\Delta E_n$  have no direct influence on the orientational state of H molecules. However, being the determining factors for the miscibility between H and G molecules, they have a strong *indirect* impact on polarity, which is discussed below. For the moment, these energy differences are chosen so that solid solutions can form over the whole range of  $0 < X < 1$ .

According to the values of the two driving forces of polarity formation,  $\Delta E_f$  and  $\Delta E_A$ , i. e. (i) and (ii), respectively, three principally different situations occur with respect to the relation  $X_{\text{net}}$  vs  $X$  (for the variation of  $X$ , the value of  $X_{\text{gas}}$  passes continuously the range  $[0, 1]$ , while all other input parameters are kept constant):

- (i) *Dilution of intrinsic polarity*: Selectivity by H molecules only, i. e.  $\Delta E_A \approx 0$  and  $\Delta E_f < 0$ .  $X_{\text{net}}(X = 0) < 0$ . The maximum of absolute polarity is obtained at  $X = 0$ , i. e. for a single-component crystal of H molecules. Insertion of G molecules in the solid solution  $\text{H}_{1-X}\text{G}_X$  results just in a reduction of the total fraction  $1 - X$  of H molecules and therefore in a lowering of polarity.  $|X_{\text{net}}|$  decreases monotonically to zero for  $X \rightarrow 1$  (see Fig. 3.2).
- (ii) *Coupled effect on polarity*: Selectivity by H and G molecules, i. e.  $\Delta E_A > 0$  and  $\Delta E_f \neq 0$ .  $X_{\text{net}}(X = 0) \neq 0$ . G molecules increase the effect of polarity formation in the solid solution  $\text{H}_{1-X}\text{G}_X$ . However, as  $X \rightarrow 1$ , the available fraction  $1 - X$  of H molecules is reduced and consequently  $X_{\text{net}}$  passes a maximum between  $0 < X < 1$ . If  $\Delta E_f < 0$ , inversion of polarity from negative to positive values takes place between  $0 < X < 1$  (see Fig. 3.3).
- (iii) *Creation of polarity*: Selectivity by G molecules only, i. e.  $\Delta E_A > 0$  and  $\Delta E_f \approx 0$ .  $X_{\text{net}}(X = 0) \approx 0$ . A single-component crystal of H molecules features no polar properties. Only inclusion of G molecules in the solid solution  $\text{H}_{1-X}\text{G}_X$  results in polarity formation. Similarly to (ii), a maximum of  $X_{\text{net}}$  is obtained between  $0 < X < 1$  (see Fig. 3.4). This case is

of particular interest, since polarity formation, and therefore breaking of the centric crystal symmetry, is effected *only* by centrosymmetric molecules [91].

Clearly, for  $\Delta E_A \approx 0$  and  $\Delta E_f \approx 0$ , no polarity results at all. In cases (ii) and (iii), where orientational selectivity is effected by G molecules,  $X_{\text{net}}$  always passes a maximum value  $\max X_{\text{net}} > 0$  within  $0 < X < 1$ . This can be seen by examining the derivatives of the curves at the boundaries of  $X$ : At  $X = 1$ , it holds  $-1 \leq dX_{\text{net}}/dX < 0$ , because insertion of polar molecules (H) into a crystal of non-polar molecules (G) always increases  $|X_{\text{net}}|$ . As  $\Delta E_A > 0$ , H molecules are favorably attached onto G molecules with the acceptor (A) terminal oriented toward the nutrient, i. e.  $X_{\text{net}}$  increases in positive direction. At  $X = 0$ ,  $dX_{\text{net}}/dX > 0$ , since G molecules favor donor (D) sites and, in turn, cause H molecules to attach onto them, preferably with the acceptor (A) terminal oriented toward the nutrient ( $\Delta E_A > 0$ ). These considerations are only valid for  $\Delta E_p > 0$ , where the effect of orientational selectivity is larger than that of dilution for small concentrations of G molecules. For all situations,  $|X_{\text{net}}| \leq 1 - X$  holds for any value of  $X$ .

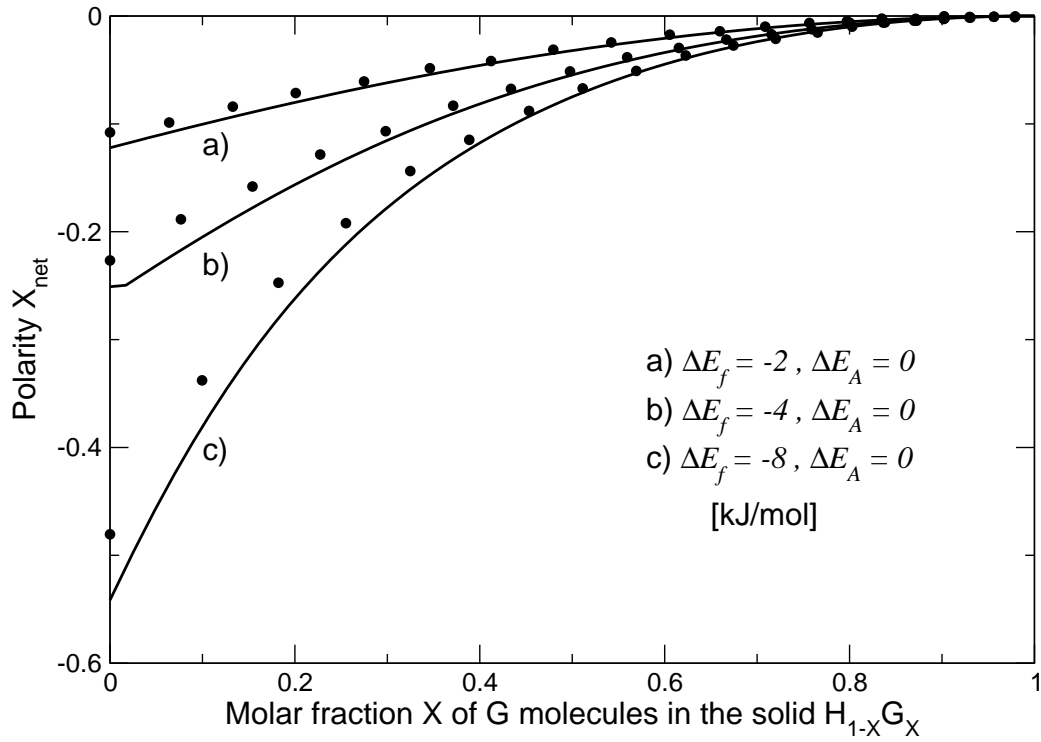
### 3.5.2 Miscibility

The total extent of polarity in the solid solution  $\text{H}_{1-X}\text{G}_X$  scales with the molar fraction  $(1 - X)$  of H molecules. Furthermore, the distribution of H and G molecules on the lattice, i. e. their pattern in space, has an influence on polarity formation, mainly with respect to the effect of the lateral energy difference  $\Delta E_p$ . Therefore, *miscibility* between H and G molecules in the solid has a large impact on polarity formation.

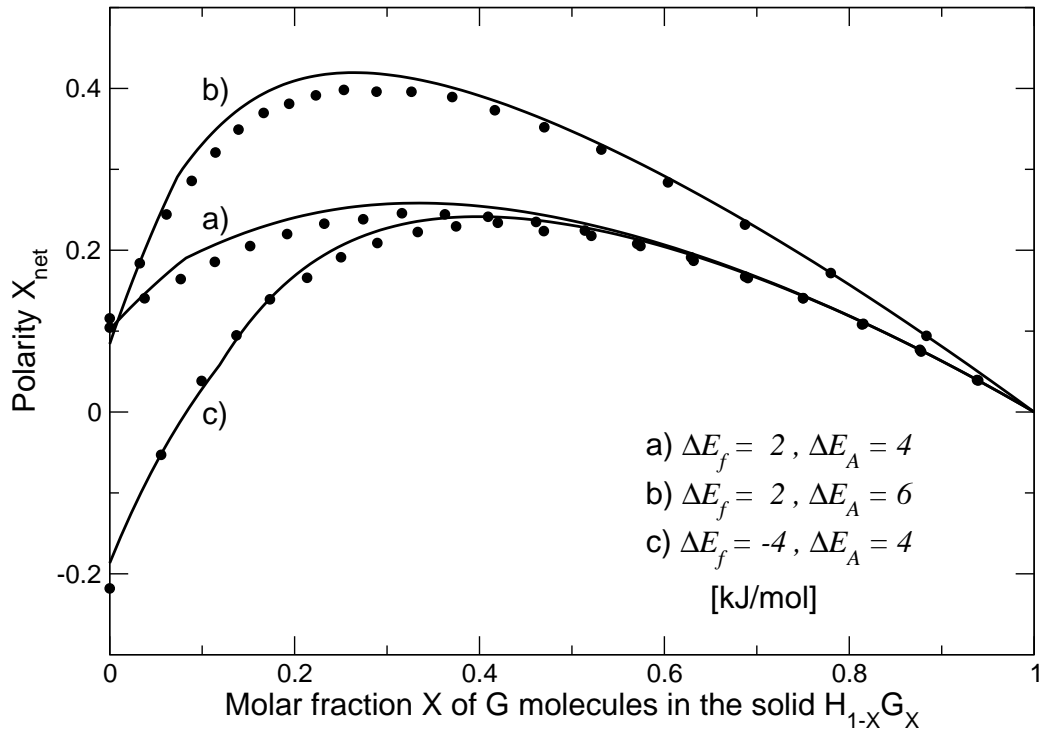
In the present model, miscibility is primarily determined by the lateral energy differences  $\Delta E_m$  and  $\Delta E_n$  relative to  $\Delta E_p$ . Besides, it is also effected by longitudinal energies, but as  $z_{\perp} = 4$ , (while there exists only one neighbor per molecule in longitudinal direction), they have a small influence on miscibility compared to lateral energies.

Externally, the molar fractions in the solid ( $X$ ) can be influenced by changing the available fractions of H and G molecules in the gas, i. e.  $X_{\text{gas}}$ .  $X_{\text{gas}}$  is the only variable parameter effecting the value of  $X$ , without having another impact on the system (contrary to the temperature  $T$ ). Therefore, miscibility and its consequence on polarity was investigated in dependence on  $X_{\text{gas}}$  for given sets of interaction energies and constant  $T$ . Four different cases were identified:

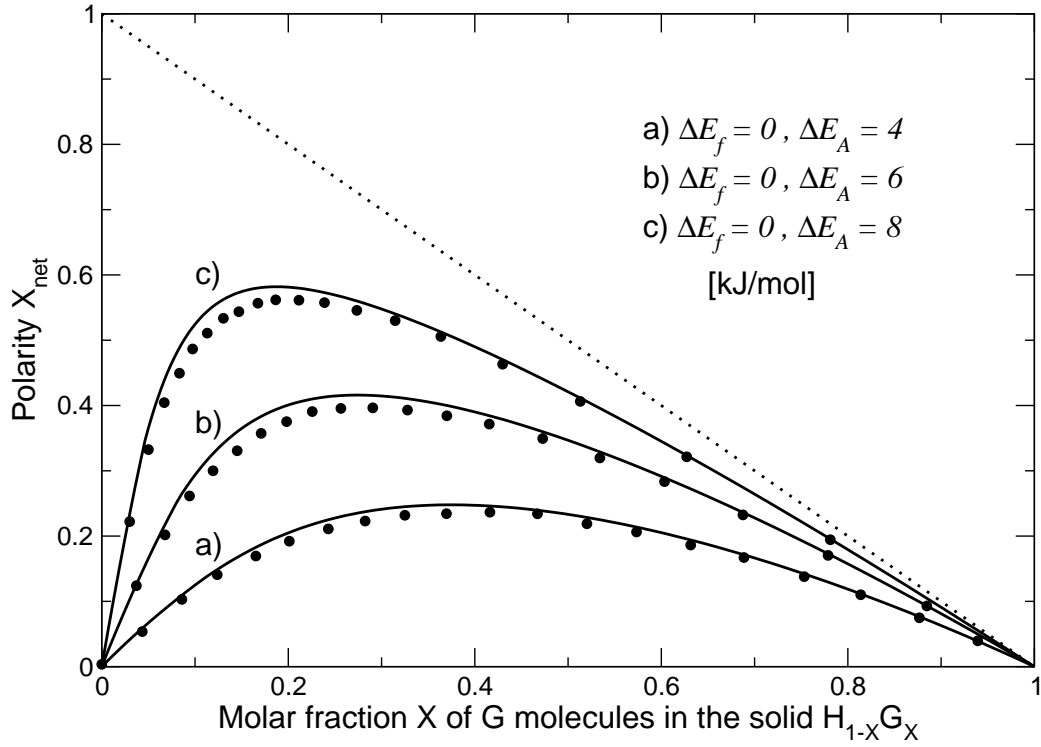
- (i) *Full miscibility*: Solid solution formation over the entire range of  $0 < X < 1$ . That is, principally any value of  $X$  can be obtained by varying



**Figure 3.2:** *Dilution of intrinsic polarity.* Polarity  $X_{\text{net}}$  vs molar fraction  $X$  of non-polar (G) molecules in the solid solution  $H_{1-X}G_X$ .  $\Delta E_p = 1$ ,  $\Delta E_m = 0$ ,  $\Delta E_n = -1$  [kJ/mol],  $T = 300$  K. *Lines:* Markov mean-field model (a possible kink in the curves indicates a phase transition, see text). *Dots:* Monte Carlo simulations (error bars are too small to be shown here: all standard deviations  $\sigma_X, \sigma_{X_{\text{net}}} < 0.003$ ).



**Figure 3.3:** *Coupled effect on polarity.* Polarity  $X_{\text{net}}$  vs molar fraction  $X$  of non-polar (G) molecules in the solid solution  $\text{H}_{1-X}\text{G}_X$ .  $\Delta E_p = 1, \Delta E_m = 0, \Delta E_n = -1$  [kJ/mol],  $T = 300$  K. *Lines:* Markov mean-field model (a possible kink in the curves indicates a phase transition, see text). *Dots:* Monte Carlo simulations (error bars are too small to be shown here: all standard deviations  $\sigma_X, \sigma_{X_{\text{net}}} < 0.003$ ).



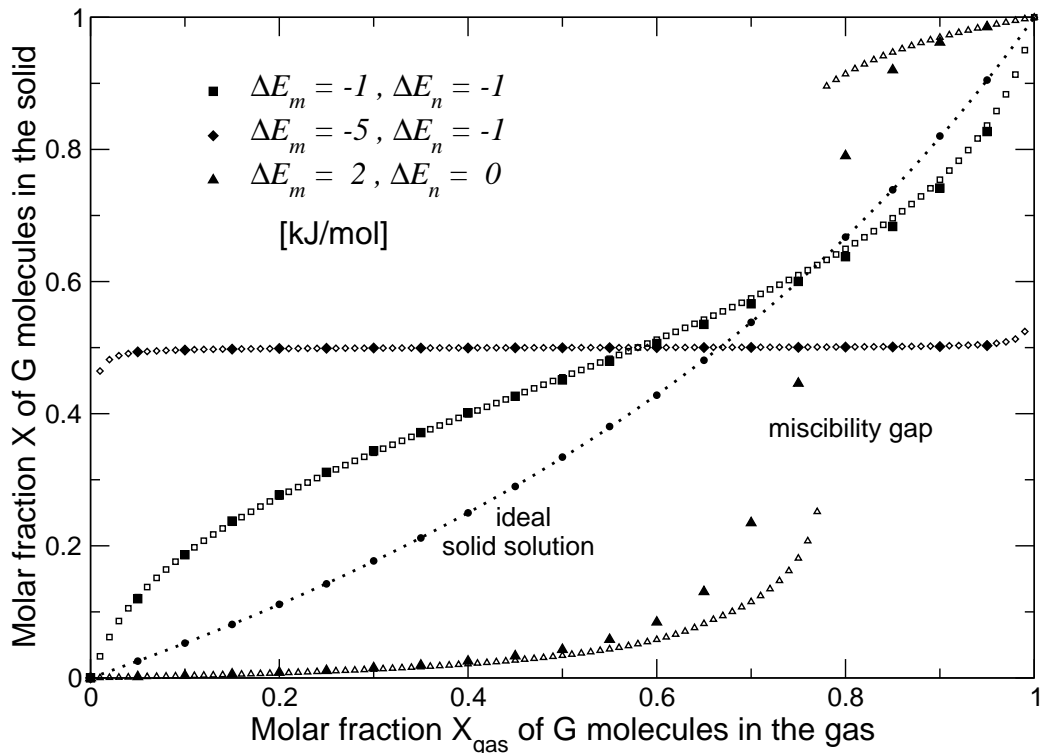
**Figure 3.4:** *Creation of polarity.* Polarity  $X_{\text{net}}$  vs molar fraction  $X$  of non-polar (G) molecules in the solid solution  $\text{H}_{1-X}\text{G}_X$ .  $\Delta E_p = 1$ ,  $\Delta E_m = 0$ ,  $\Delta E_n = -1$  [kJ/mol],  $T = 300$  K. *Lines:* Markov mean-field model. *Dots:* Monte Carlo simulations (error bars are too small to be shown here: all standard deviations  $\sigma_X, \sigma_{X_{\text{net}}} < 0.003$ ). *Dotted line:* Asymptotic limit for  $X_{\text{net}}$  vs  $X$ , no curve can pass this line.

$X_{\text{gas}}$  correspondingly, though  $X$  vs  $X_{\text{gas}}$  curves may deviate considerably from that of an ideal solid solution. Values of  $\Delta E_p$ ,  $\Delta E_m$  and  $\Delta E_n$  must be balanced to each other and are consequently relatively small. Concerning polarity, any situation discussed above may occur. See images (h) and (i) in Table 3.2.

- (ii) *Partial miscibility*: At least one forbidden region (miscibility gap) exists in the range of  $0 < X < 1$  for which no solid solution  $\text{H}_{1-X}\text{G}_X$  is formed. Mostly, insertion of G molecules in H crystals and vice versa takes place up to certain percentage (see images (j) - (n) in Table 3.2). Miscibility gaps appear for a wide range of combinations between lateral interaction energies, therefore no clear tendency was seen. Generally, solid solutions with a very large  $\max |X_{\text{net}}|$  at small  $X$  are only partial miscible due to a high orientational selectivity by G molecules. For the tuning of polarity, situations are of special interest, where  $X_{\text{net}}$  depends linearly on  $X$ , i. e.  $X_{\text{net}} \approx X$  ( $0 < X < 0.5$ ) or  $X_{\text{net}} \approx 1 - X$  ( $0.5 < X < 1$ ), see images (k) and (l) in Table 3.2, respectively.
- (iii) *No miscibility*: No solid solution formation for any value of  $0 < X_{\text{gas}} < 1$ . Apart from a small percentage of impurities, H and G molecules form just single-component crystals. Nearly pure H crystals are obtained if  $\Delta E_m > 0$  and  $\Delta E_n \gg 0$ . Polarity arises mainly due to orientational selectivity by H molecules (see images (a) - (e) in Table 3.2). G crystals (with  $X_{\text{net}} \approx 0$ ) are obtained if  $\Delta E_m < 0$  and  $\Delta E_n \ll 0$  (see image (f) in Table 3.2).
- (iv) *Intermediate compound*: Formation of an ordered structure of H and G molecules with constant  $X$  and  $X_{\text{net}}$  values for the entire range of  $0 < X_{\text{gas}} < 1$ . Due to symmetry constraints (square lattice with isotropic lateral nearest neighbor interactions), a checkerboard-like pattern of H and G molecules with  $X = 0.5$  and  $-0.5 \leq X_{\text{net}} \leq 0.5$  is the only kind of intermediate compound which can arise in the present model. Necessary condition is  $\Delta E_m \ll 0$  (see image (g) in Table 3.2). Large  $|X_{\text{net}}|$  values may be obtained even for relatively large  $\Delta E_p$ , since H molecules are almost entirely surrounded by G molecules within a layer.

Typical examples of  $X$  vs  $X_{\text{gas}}$  curves for the cases (i), (ii) and (iv), respectively, are shown in Fig. 3.5. For comparison, a curve for an ideal solid solution is given by setting all energies equal to zero.

It has to be emphasized that the purpose of the present model is to describe polarity formation in solid solutions  $\text{H}_{1-X}\text{G}_X$ . Herein, miscibility between H and G molecules plays an important role. In this respect, cases (i) - (iv)



**Figure 3.5:** Miscibility in solid solutions  $H_{1-X}G_X$ . Molar fraction  $X$  in the solid vs molar fraction  $X_{\text{gas}}$  in the gas of non-polar (G) molecules.  $0 \leq X_{\text{gas}} \leq 1$ , uniformly distributed.  $\Delta E_A = 4$ ,  $\Delta E_D = 2$ ,  $\Delta E_p = 1$  [kJ/mol],  $T = 300$  K.  $\blacksquare$  Full solid solution.  $\blacklozenge$  Intermediate compound.  $\blacktriangle$  Partial solid solution. *Non-filled symbols:* Markov mean-field model. *Filled symbols:* Monte Carlo simulations (error bars are too small to be shown here: all standard deviations  $\sigma_X < 0.009$ ).

above show qualitative behaviors of miscibility influencing polarity. However, in consideration of the limitations of the model (e.g. the same packing for H and G molecules with a minimal set of interaction energies) as well as the formation of a metastable bulk state, it is not intended to give an accurate measure of miscibility in solid solutions here.

### 3.5.3 Overview of Phenomena in $(X, X_{\text{net}})$ Space

Accurate values of molecular interaction energies are principally accessible by means of quantum chemical or classical force-field methods [82]. For a quantitative analysis of polarity formation in a specific system these calculations are prerequisite [26, 83].

However, in order to provide a qualitative insight of possible evolutions of polarity formation in arbitrary systems of H and G molecules, (underlying

the conditions of the present growth model), the following probabilistic approach was applied: 50 000 sets of interaction energies were picked out randomly within the range of  $-10 \dots 2$  kJ/mol. For each set a Markov mean-field calculation and a complete Monte Carlo simulation were performed with  $T = 300$  K and  $X_{\text{gas}} = 0.25$ . The obtained  $(X, X_{\text{net}})$  values were represented in 2D histogram plots, see Fig. 3.6 (upper). The histograms show the density distribution of  $(X, X_{\text{net}})$  results for the given energy range. From a statistical point of view, these plots allow to make predictions on polarity formation for any system, even though real energies are not known. Furthermore, they show the interplay between orientational selectivity by H and G molecules and miscibility between the two components, and provide a general comparison between the MMF description and MCS.

Since  $N \equiv A$ , the majority of  $(X, X_{\text{net}})$  values lay on the *positive* half plane ( $X_{\text{net}} \geq 0$ ). High densities occur for  $X$  values around 0, 0.5 and 1, respectively (see below). On the positive half plane, the density distribution is enclosed by the requirement  $X_{\text{net}} \leq 1 - X$ , while the border line on the negative half plane resembles the dilution cases of Fig. 3.2. Higher densities are observed below the diagonal  $X_{\text{net}} = X$  than above it ( $X_{\text{net}} \geq 0$ ), because for the majority of situations the centrosymmetric packing of H molecules is retained (strong influence of  $\Delta E_p > 0$ ) and polarity arises only due to inclusion of G molecules occupying preferably  $D$ -sites (see cases (k) and (n) in Table 3.2). In these cases, it holds  $X_{\text{net}} \leq X$ .

About 18 % of  $(X, X_{\text{net}})$  values have a net polarity  $|X_{\text{net}}| > 0.2$ , about 40 % of that percentage belongs to *intermediate compounds* ( $0.49 < X < 0.51$ ). Only 1.5 % of the energy sets have led to situations with  $|X_{\text{net}}| > 0.5$ . The reason for these relatively small percentages is the strong lowering effect of  $\Delta E_p$ . Nevertheless, for  $X \leq 0.2$  and  $X \geq 0.8$  high densities are observed featuring considerable polarity formation ( $0 \leq X_{\text{net}} \leq 0.2$ ). Therefore, in order to obtain polarity, there is no need for finding systems undergoing solid solution formation over the entire range of  $X$ .

Fig. 3.6 (lower) shows the distribution of  $\Delta E_m$  and  $\Delta E_n$  values (from the above energy sets) corresponding mainly to (A) H crystals with little inclusions of G, (B) and (D) solid solutions, (C) intermediate compounds, (E) G crystals with little inclusions of H. In  $(\Delta E_m, \Delta E_n)$  space these characteristic cases of miscibility between H and G molecules are manifested by separated regions with little overlap. The regions (B) and (D), where solid solutions may be formed, appear as relatively small strips compared to (A), (C) and (E). This explains the high densities in  $(X, X_{\text{net}})$  space for  $X$  values around 0, 0.5 and 1, respectively. Additionally, total percentages of  $(X, X_{\text{net}})$  values in these regions are given. The lower percentage of single-component crystals of G molecules than that of H molecules arises mainly due to  $\Delta E_A > 0$ . With



the given energy range ( $-10 \dots 2$  kJ/mol) solid solutions may form for about 35 % of the situations.

MMF calculations using the same energy sets and temperature but  $X_{\text{gas}}$  values of 0.5 and 0.75 have shown no significant differences, neither for  $(X, X_{\text{net}})$  density distributions nor for regions (A) - (E) in  $(\Delta E_m, \Delta E_n)$  space. That is, systems are mainly determined by interaction energies, while the influence of  $X_{\text{gas}}$  (and chemical potentials) is marginal here.

Increasing the energy range (MMF calculations with ranges up to  $-50 \dots 10$  kJ/mol were performed) has the effect that differences in the density distribution in  $(X, X_{\text{net}})$  space become even larger, i. e. very high densities for  $X$  values around 0, 0.5 and 1, respectively, and also along the diagonals ( $X_{\text{net}} \approx X$  and  $X_{\text{net}} \approx 1 - X$ , respectively), but very low densities in between. However, while regions (A) - (E) in  $(\Delta E_m, \Delta E_n)$  space expand with increasing energy range, their separating lines stay unchanged. Therefore, the subdivision in  $(\Delta E_m, \Delta E_n)$  space represents a *general property of the present model* and shows that solid solutions are only formed within a narrow band of  $\Delta E_m$  and  $\Delta E_n$  values.

Table 3.2 shows snapshots of grown layers from Monte Carlo simulations. These images are considered representative because (i) selection is based on Fig. 3.6, (ii) they cover most characteristic patterns arising in this model, (iii) concerning  $X_{\text{net}}$  vs  $X$  relations, Monte Carlo simulations and Markov mean-field description are in agreement for the chosen energy sets.

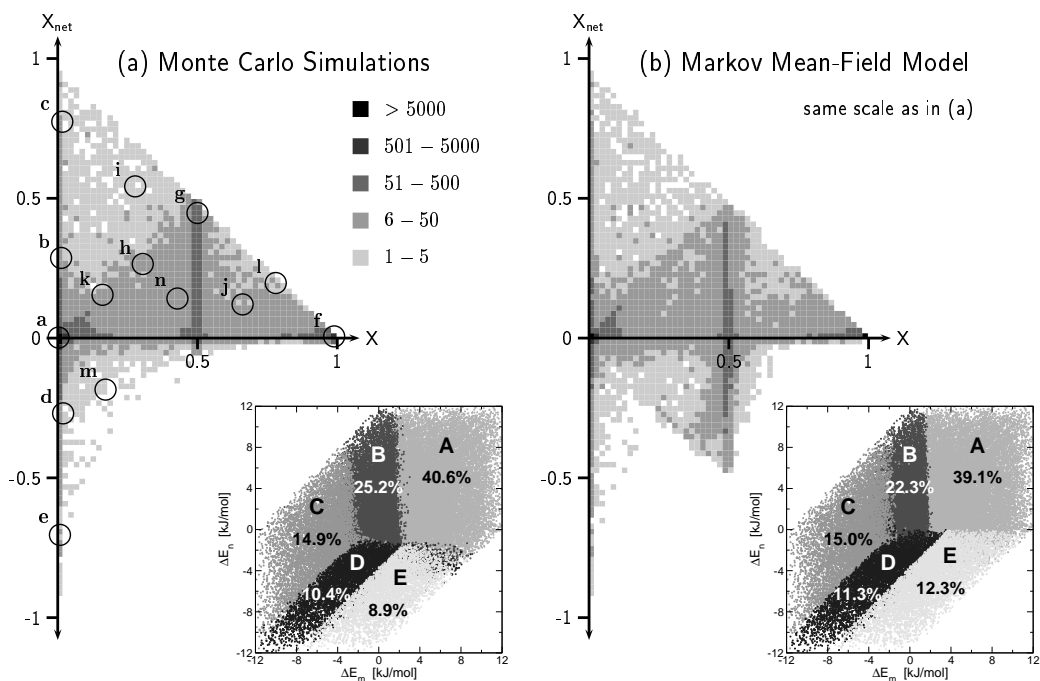
## 3.6 Discussion

### 3.6.1 Comparison between MMF Description and Monte Carlo Simulations

For results of MCS in Fig. 3.2 - 3.6, the following simulation parameters were used:  $\tau_L = 1000$ ,  $\tau_G = 50$ ,  $\tau_S = 200$  and  $s_L = 32 \times 32$  (for definitions, see Appendix 3.9).

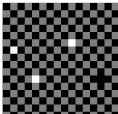

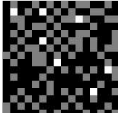

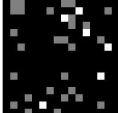



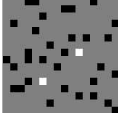

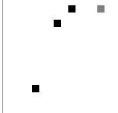
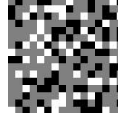


In case of Fig. 3.2, 3.3, 3.4 and 3.5, simulations with longer equilibration or sampling times as well as larger lattice sizes resulted in nearly the same average values for  $X$  and  $X_{\text{net}}$ , differing only by smaller standard deviations. That is, for these sets of interaction energies the chosen time scales are sufficient, especially with respect to stationarity of the growth process, and finite size effects are negligible.

In case of the 2D histogram (Fig. 3.6), proving validity of the simulation parameters for each energy set was not feasible. However, for test runs with 500 energy sets using different simulation parameters, less than 7 % of cor-



**Figure 3.6:** *Upper figures:* 2D histograms showing density distributions of  $(X, X_{\text{net}})$  results for 50 000 randomly chosen sets of interaction energies in the range of  $-10 \dots 2$  kJ/mol ( $T = 300$  K,  $X_{\text{gas}} = 0.25$ ). Resolution for both axis: 0.02. The number of energy sets is considered sufficient for representative density distributions, because similar results were obtained for smaller sets. For (a), centers of circles (with corresponding letters) locate the 14 representative MCS snapshots presented in Table 3.2. *Lower figures:* Distribution of  $\Delta E_m$  and  $\Delta E_n$  values (from the same energy sets) corresponding to  $X$  values in the ranges: (A)  $0 \leq X < 0.02$ , (B)  $0.02 \leq X < 0.49$ , (C)  $0.49 < X < 0.51$ , (D)  $0.51 \leq X \leq 0.98$ , (E)  $0.98 < X \leq 1$ , and total percentages of  $(X, X_{\text{net}})$  values in regions (A) - (E).

**Table 3.2:** Representative snapshots of crystal layers from Monte Carlo simulations after  $\approx 250$  growth steps ( $T = 300$  K,  $X_{\text{gas}} = 0.25$ ,  $\tau_L = 5\,000$ ,  $s_L = 16 \times 16$ ). (a) - (e) Single-component crystals of H molecules with minor inclusion of G molecules,  $X \approx 0$ . (f) Single-component crystal of G molecules with minor inclusion of H molecules,  $X \approx 1$ . (g) Intermediate compound,  $X = 0.5$ . (h), (i) Full range solid solutions,  $0 < X < 1$ . (j) - (n) Cases of partial miscibility. *Black*: H molecules with acceptor (A) terminal oriented toward the nutrient ( $\downarrow$ ). *Gray*: H molecules with donor (D) terminal oriented toward the nutrient ( $\uparrow$ ). *White*: G molecules ( $N \equiv A$ ). Numbers in parentheses:  $\Delta E_A$ ,  $\Delta E_D$ ,  $\Delta E_p$ ,  $\Delta E_m$ ,  $\Delta E_n$ , for corresponding cases [kJ/mol].

(a)		Centric packing of H; only few orientational defects; little selectivity by H, G; $X_{\text{net}} \approx 0$ ; (3.2/0.3/4.3/2.6/5.1)	(h)		Almost random distribution of H and G; selectivity by G; $X_{\text{net}}$ passes a maximum ( $> 0$ ); (5.4/5.7/1.8/-0.8/-1.0)
(b)		Partial breaking of centric packing of H; many orientational defects; selectivity by H, G; $X_{\text{net}} > 0$ ; (5.1/0.7/0.9/1.6/11.2)	(i)		Clusters of G; strong selectivity by G; $X_{\text{net}}$ passes a maximum ( $\gg 0$ ); (8.1/4.5/1.0/-0.5/-3.9)
(c)		Almost polar packing of H; strong selectivity by G; $X_{\text{net}} \gg 0$ ; (9.3/1.6/0.4/0.5/4.8)	(j)		Coexistence of different solid phases near a miscibility gap: Clusters of H (centric packing) and G; $X_{\text{net}} \geq 0$ ; (6.2/2.9/4.9/0.2/-2.9)
(d)		Partial breaking of centric packing of H; many orientational defects; selectivity by H only; $X_{\text{net}} < 0$ ; (1.1/5.6/0.9/2.0/3.9)	(k)		Centric packing of H with G occupying donor (D) sites; strong selectivity by G; $X_{\text{net}} \approx X$ , $0 < X < 0.5$ ; (10.4/4.8/8.7/-0.2/1.2)
(e)		Almost polar packing of H; strong selectivity by H only; $X_{\text{net}} \ll 0$ ; (1.4/9.2/0.4/2.6/4.2)	(l)		Strong selectivity by G; $X_{\text{net}} \approx 1 - X$ , $0.5 < X < 1$ ; (8.5/1.7/1.7/-3.5/-6.8)
(f)		$X_{\text{net}} \approx 0$ ; (3.2/2.1/0.5/-6.5/-10.9)	(m)		Dilution case: Random distribution of G; selectivity by H only; $X_{\text{net}} < 0$ ; (0.8/5.4/0.6/0.0/2.3)
(g)		Checkerboard-like pattern of H and G; selectivity by H, G; $0 \leq X_{\text{net}} \leq 0.5$ ; (7.8/1.6/3.5/-6.2/-3.0)	(n)		Clusters of H( $\downarrow$ )/H( $\uparrow$ ), H( $\downarrow$ )/G and H( $\uparrow$ )/G (centric patterns); $X_{\text{net}} \geq 0$ ; (2.2/1.8/4.5/-1.4/0.7)

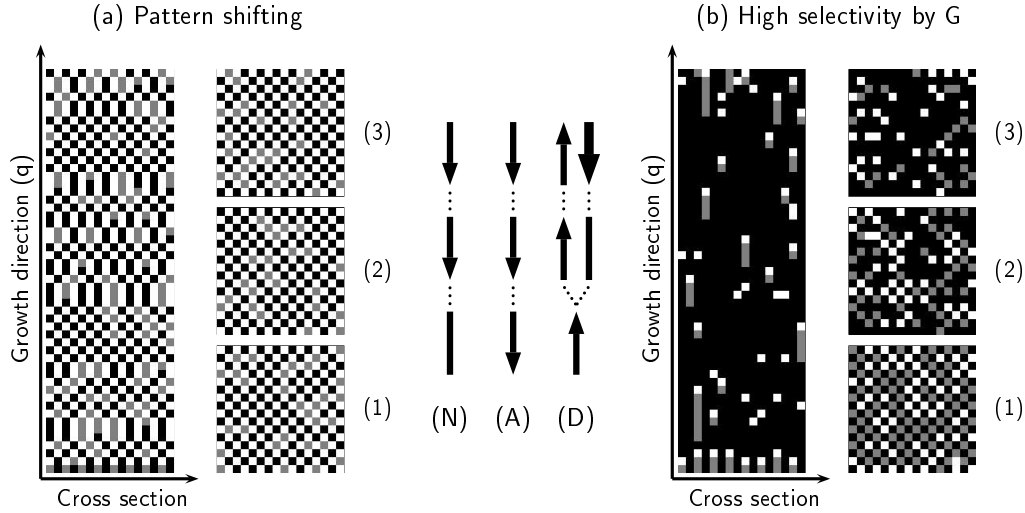
responding  $(X, X_{\text{net}})$  values deviated more than  $\pm 0.02$  from each other. For a difference of  $\pm 0.04$  the percentage became less than 1%. In consideration of the large differences in the density distribution (logarithmic scale), these deviations are negligible for the purpose of an overview.

In Fig. 3.2, 3.3 and 3.4 the agreement between results from the MMF description and MCS is good. Generally, the analytical approach slightly overestimates  $|X_{\text{net}}|$ . The reason for this tendency lays in the fact that the lateral neighborhood of growing layers (especially  $\Delta E_p$ , which lowers the effect of polarity formation) is only taken into account within a mean-field correction. In situations where G molecules are not distributed homogeneously on the lattice (vast majority), this can lead to an underestimate of the local impact of  $\Delta E_p$  and therefore to too large  $|X_{\text{net}}|$ .

For the description of miscibility, large deviations between results from the MMF description and MCS may occur, if components H, G are partially miscible (see Fig. 3.5). In general, the MMF model sharply separates regions characterized by a miscibility gap. In contrast, different solid phases can coexist in MCS by the formation of clusters (see case (j) in Table 3.2), and therefore, measurements of  $X$  merely represent average values of molar fractions of the different phases. Consequently, no clearly distinct regions in  $X$  vs  $X_{\text{gas}}$  curves may be expected in the case of simulations.

In  $X_{\text{net}}$  curves from MMF calculations a kink may be observed, e. g. Fig. 3.3 a) and b). It indicates a continuous phase transition from a disordered to an antiferromagnetic ordered distribution of H molecules, where the mean polarizations of the two sublattices  $g = I, II$  assume different values spontaneously. It has been observed already in the growth model of single-component crystals of polar molecules only [40, 5]. In the present system, this phase transition also becomes manifest with a variation of  $X_{\text{gas}}$ . A singularity in  $X_{\text{net}}$  is not observed in MCS, however, the phase transition can be clearly identified by the difference of sublattice polarizations or by fluctuation properties, e. g. a sharp peak in the specific heat, see Chapter 6.

Comparing the histograms (Fig. 3.6 upper) of the MMF model and MCS, generally similar density distributions are observed with high densities for  $X$  values around 0, 0.5 and 1, respectively. However, for the MMF description, regions with negative  $X_{\text{net}}$  values arise (with increasing densities, the closer  $X$  to 0.5) which are not manifest in case of MCS. This is an artifact of the analytical approach, having its origin in the requirement that at the stationary state, molar fractions in the substrate layer and the adlayer must be the same for each sublattice  $g = I, II$  separately. This condition is not always met, e. g. for situations, where G molecules shift continuously between the two sublattices upon growth (see Fig. 3.7a).



**Figure 3.7:** (a) and (b): Cross sections of 50 layers grown from centric seeds of H molecules and layers  $q = 1, 2, 3$  from Monte Carlo simulations of solid solutions  $H_{1-x}G_x$  ( $T = 300$  K,  $X_{\text{gas}} = 0.5$ ,  $\tau_L = 5000$ ,  $s_L = 16 \times 16$ ). *Black:* H molecules with acceptor (A) terminal oriented toward the nutrient ( $\downarrow$ ). *Gray:* H molecules with donor (D) terminal oriented toward the nutrient ( $\uparrow$ ). *White:* G molecules ( $N \equiv A$ ). (a) Continuing shift of near checkerboard-like HG pattern on sublattices  $g = I, II$  for subsequent attached layers, caused by the minimization of longitudinal energy contributions. As a consequence, H molecules will always be oriented favorably downwards (i.e.  $X_{\text{net}} \geq 0$ ) in case of MCS. Such an evolution can not be described by the MMF model.  $\Delta E_A = 3.4$ ,  $\Delta E_D = 6.6$ ,  $\Delta E_p = 2.9$ ,  $\Delta E_m = -6.7$ ,  $\Delta E_n = 2.6$  [kJ/mol]. (b) Graded inclusion of G molecules with a high orientational selectivity can result in  $X_{\text{net}} \approx 1$ .  $\Delta E_A = 12$ ,  $\Delta E_D = 10$ ,  $\Delta E_p = 1$ ,  $\Delta E_m = 0$ ,  $\Delta E_n = 1$  [kJ/mol]. *Center:* Favored attachment of molecules (H or G) and orientational state ( $\downarrow, \uparrow$  in case of H) along single Markov chains for sites  $\{N, A, D\}$  without taking into account lateral interactions. Upon growth, a change of preferred orientation of H molecules from a D-site may occur so that H molecules will be mostly oriented downwards ( $\downarrow$ ) in the course of the growth process.

### 3.6.2 Applicability to Real Systems

Since polar (H) and non-polar (G) molecules generally do not crystallize in isomorphous structures, (thus likely not forming full range solid solutions), practically, interest lays in solid solutions  $\text{H}_{1-X}\text{G}_X$  leading to large  $|X_{\text{net}}|$  values at *low molar fractions  $X$  of G molecules*. As shown in this study, this may arise under the following conditions: (i) Large  $|\Delta E_A|$  or  $|\Delta E_D|$  values ensuring a high selectivity by G molecules, (ii) low  $\Delta E_p$  values, (iii) appropriate  $\Delta E_m$  and  $\Delta E_n$  values allowing at least a small miscibility between the two components (see Fig. 3.7b).

Besides, large negative values of  $\Delta E_m$  (case (g) in Table 3.2) may yield large values of  $|X_{\text{net}}|$ , due to an effect of shielding between H molecules in lateral direction even for a relatively large  $\Delta E_p$ .

The present model may provide a qualitative filter for selecting molecules fulfilling the above requirements, given calculated molecular interaction energies from the literature [22, 23, 24].

A preliminary application of the present model to the system 4-chloro-4'-nitrostilbene/4,4'-dinitrostilbene (CNS/DNS) has shown a qualitative agreement with experiments, both, concerning polarity formation and miscibility (full range solid solution showing dilution of polarity) [52]. However, due to more complex conditions with respect to crystal structure and interaction energies in real systems, quantitative prediction can not be expected. For instance, in CNS/DNS the distinction between longitudinal and lateral neighbors is not straightforward. For more accurate calculations of  $X_{\text{net}}$ , the model may be adapted to each system individually.

## 3.7 Conclusion

The present model represents a sufficient formal description for studying phenomena related to growth-induced polarity formation in solid solutions  $\text{H}_{1-X}\text{G}_X$  of polar (H) and non-polar (G) molecules.

The Markov mean-field approach well describes basic features of the model and is generally in good agreement with Monte Carlo simulations. However, in cases of large local correlations as well as for a detailed insight to structural properties of crystals, Monte Carlo simulations are necessary (see Fig. 3.7a). In combination, the two methods provide an efficient predictive tool for a qualitative estimate of  $X$  and  $X_{\text{net}}$ , and can serve as a filter for searching interesting systems.

For the particular case of  $\Delta E_p > 0$  considered here, *longitudinal energies are mainly inducing polarity, whereas lateral energies determine the structure of*

*solid solutions or ordered compounds.*

Fig. 3.6 (upper) and Table 3.2 make clear that in the present model significant vectorial alignment of H molecules (i. e. large  $X_{\text{net}}$ ) may be obtained for (i) ordered structures HG ( $X \approx 0.5$ ), and (ii) solid solutions with  $X \leq 0.2$  or  $X \geq 0.8$ , respectively. Since many real systems  $\text{H}_{1-X}\text{G}_X$  represent cases of limited miscibility, (ii) is of special importance showing the high potential of two-component molecular crystals to feature growth-induced polar properties. Of particular interest are cases which can acquire nearly  $X_{\text{net}} \approx 1$ , because of a graded inclusion of G molecules which effectively align H molecules (see Fig. 3.7b).

With respect to real crystal structures, further developments of the growth model may include different crystal packings, next-nearest neighbor interactions (several attached layers taken into account) or more degrees of freedom for H and G molecules. While these advancements could only be described partially by means of an analytical theory, their realization is considered straightforward in case of Monte Carlo simulations. In any case, such refinements may result in improvements concerning quantitative predictions of  $X$  and  $X_{\text{net}}$  for real systems. However, the analysis has demonstrated that basic characteristics of growth-induced phenomena of polarity formation in solid solutions can be described completely by the present model.

### 3.8 Appendix A: Numerical Procedure for Markov Mean-Field Equations

Eq. (3.6) specifies a system of six coupled nonlinear equations for the variables  $X_A^g$ ,  $X_D^g$  and  $X_N^g$ , with  $g = I, II$ . Given the normalization condition, Eq. (3.3), the set reduces to four independent equations and variables, e. g.  $X_A^g$ ,  $X_D^g$ , which are required to be solved numerically. It must hold  $0 \leq X_i^g \leq 1$ , with  $g = I, II$  and  $i \in \{A, D, N\}$ , for any solutions.

Two principal difficulties arise in the numerical treatment of the Markov mean-field process at the stationary state for a given set of input parameters: (i) The number of solutions is *a priori* unknown. (ii) Generally, only one solution is physically reasonable in terms of a minimal free energy  $F$ . Therefore, the following procedure was applied:

1. A “pool” of initial guess vectors  $\mathbf{x}_i$ ,  $i = 1 - 7$ , for the unknown variables  $\{X_A^I, X_A^{II}, X_D^I, X_D^{II}\}$  is specified, covering basic patterns of the solution space: Polar cases:  $(0, 0, 0, 0)$ ,  $(1, 1, 0, 0)$ ,  $(0, 0, 1, 1)$ ; centric cases:  $(1, 0, 0, 1)$ ,  $(1, 0, 0, 0)$ ,  $(0, 0, 1, 0)$ ; mixed case:  $(\frac{1}{2}, \frac{1}{2}, \frac{1}{2}, \frac{1}{2})$ . The set could be extended, however it turned out to be sufficient, since cal-

culations with larger sets of starting vectors did not reveal additional solutions of the system.

2. Eq. (3.6) is solved numerically with Newton's method [80, 75], using successively  $\mathbf{x}_i$ ,  $i = 1 - 7$ , for an initial guess. Maximal 20 iterations are performed for each trial vector.
3. From the set of obtained numerical solutions, i. e. trials which have converged, an energy criterion is applied in order to find the physical solution.

The energy criterion consists in (i) calculating the mean-field free energy per molecule [50],  $\bar{F} = \bar{U} - TS$ , and (ii) choosing the numerical solution with *lowest*  $\bar{F}$ .  $\bar{U}$  and  $S$  are the internal energy (mean-field) and mixing entropy per molecule, respectively. Due to similar molecular frames and a given common crystal structure, single-component entropy terms for H and G molecules are considered the same and therefore contributing only by an additive constant to  $\bar{F}$ . At the stationary state of the growth process, molar fractions  $X_A^g$ ,  $X_D^g$  and  $X_N^g$ , with  $g = I, II$ , in successive layers are the same. Therefore, the mean internal energy  $\bar{U}^g$  per molecule belonging to a site of sublattice  $g$  is given as

$$\bar{U}^g = X_A^g \bar{u}_A^g + X_D^g \bar{u}_D^g + X_N^g \bar{u}_N^g, \quad (3.14)$$

with ( $g' = II$  if  $g = I$  and vice versa)

$$\bar{u}_A^g = X_A^g E_{AD} + X_D^g E_{DD} + X_N^g E_{ND} + \frac{z_{\perp}}{2} (X_A^{g'} E_p + X_D^{g'} E_{ap} + X_N^{g'} E_m), \quad (3.15a)$$

$$\bar{u}_D^g = X_A^g E_{AA} + X_D^g E_{DA} + X_N^g E_{NA} + \frac{z_{\perp}}{2} (X_A^{g'} E_{ap} + X_D^{g'} E_p + X_N^{g'} E_m), \quad (3.15b)$$

$$\bar{u}_N^g = X_A^g E_{AN} + X_D^g E_{DN} + X_N^g E_{NN} + \frac{z_{\perp}}{2} (X_A^{g'} E_m + X_D^{g'} E_m + X_N^{g'} E_n). \quad (3.15c)$$

The mixing entropy  $S^g$  per molecule belonging to a site of sublattice  $g$  is given as

$$S^g = -k_B (X_A^g \ln X_A^g + X_D^g \ln X_D^g + X_N^g \ln X_N^g). \quad (3.16)$$

Finally, the mean free energy per molecule is

$$\bar{F} = \frac{1}{2} \sum_g^{\{I, II\}} \bar{U}^g - TS^g. \quad (3.17)$$



Generally, differences in  $\bar{F}$  between distinct numerical solutions are large enough (relative to corresponding energy parameters), so that physical solutions are determined unambiguously with this energy criterion.

The described procedure provides an efficient way to find physical solutions for a wide range of interaction energies and temperatures as well as  $0 \leq X_{\text{gas}} \leq 1$ . Furthermore, it allows for a self-running generation of plots such as Fig. 3.6b. Nevertheless, it has to be noted, that there is neither guarantee for finding the solution with lowest mean free energy  $\bar{F}$ , nor any one at all. However, from the 50 000 randomly chosen interaction energies for Fig. 3.6, the procedure did not find any solutions only for about 0.15 %.

### 3.9 Appendix B: The Monte Carlo Algorithm

The Monte Carlo algorithm has “single-spin-flip” dynamics with respect to orientational flips of H molecules and exchanges of H and G molecules. It is described by the following main steps:

1. A lattice site is selected randomly.
2. Given the *actual* state  $\{A, D, N\}$  of this site, a *trial* step is defined by choosing one of the two other states randomly, with equal probabilities of  $\frac{1}{2}$ .
3. The acceptance ratio  $r$  between these two adlayer configurations is calculated by Eq. (3.18). The *trial* step is accepted, i. e. the *actual* state of the chosen site is replaced by the *trial* state, if  $r \geq 1$ . Otherwise, it is accepted with probability  $r$ . If rejected, the *actual* state is kept.
4. Steps 1 - 3 are repeated until thermal equilibrium is reached, i. e. the adlayer has come to a stationary state, where physical quantities fluctuating only around steady average values.

The acceptance ratio  $r$  is given by

$$r = \frac{p_{\text{trial}}}{p_{\text{actual}}} = e^{\beta(\Delta\mu - \Delta E)}, \quad (3.18)$$

where  $p_{\text{trial}}$ ,  $p_{\text{actual}}$  denote the equilibrium probabilities of the *trial* and *actual* adlayer configurations and  $\Delta\mu$ ,  $\Delta E$  the chemical potential and energy differences between them, respectively. Since the two configurations only differ by the state of one lattice site, it follows that  $\Delta\mu = \mu_{\text{trial}} - \mu_{\text{actual}}$ , with  $\mu_{\text{trial}}$

and  $\mu_{\text{actual}}$  being the chemical potentials of the corresponding molecules on this site, see Eqs. (3.9). With Eqs. (3.10), we obtain for  $0 < X_{\text{gas}} < 1$  that

$$e^{\beta\Delta\mu} = 1, \quad \frac{X_{\text{gas}}}{1 - X_{\text{gas}}}, \quad \frac{1 - X_{\text{gas}}}{X_{\text{gas}}}, \quad (3.19)$$

in case of a flip of a H molecule, an exchange of a H with a G molecule, or an exchange of a G with a H molecule, respectively. For  $X_{\text{gas}} = 0$ , only flips of H molecules are considered, because no G molecules are available in the system.

For the measurement of observables (mainly  $X$  and  $X_{\text{net}}$ ) at the stationary state of the growth process, three characteristic time scales are introduced: (i) The adlayer equilibration time,  $\tau_L$ , measuring the time needed for an adlayer to come to equilibrium (measured in Monte Carlo steps, on average, per lattice site). (ii) The growth equilibration time,  $\tau_G$ , measuring the time needed for the growth process to reach a stationary state (measured in attached layers). (iii) The sampling time,  $\tau_S$ , specifying the number of measurements after the growth process has reached stationarity. One measurement is performed for each attached and equilibrated layer, i. e.  $\tau_S$  is also measured in attached layers.

Adequate intervals were set to  $\tau_L = 1\,000 - 5\,000$ ,  $\tau_G = 25 - 200$  and  $\tau_S = 100 - 800$ , in order to obtain sufficiently accurate expectation values for measured quantities. The last interval was justified by examining the time-displaced autocorrelation function between successively attached and equilibrated layers [66]. As adlayers were initialized randomly, very small correlation times  $< 2$ , measured in attached layers, resulted. Moreover, comparisons between results from identical and independent experiments supported the choice of intervals being sufficient in order to describe the main features of the growth model as well as to verify the validity of the Markov mean-field approach (see also Section 3.6.1).

Periodic boundary conditions were applied for the square lattice. For an investigation of finite size effects, simulations were performed for lattice sizes  $s_L$  in the range of  $32 \times 32$  to  $128 \times 128$ . For uniformly distributed random numbers of high quality, the random number generator ranlux was used in all calculations [62].

# Chapter 4

## Growth-Induced Polarity Formation in Solid Solutions: Supplementary Material

In the last two chapters a theoretical model for the investigation of growth-induced polarity formation in solid solutions  $H_{1-X}G_X$  of polar host (H) and non-polar guest (G) molecules was presented. This model was described analytically by means of a Markov mean-field (MMF) approximation and Monte Carlo simulations (MCS) were carried out. Based on these two approaches a thorough discussion on the phenomenology of polarity formation in solid solutions was given.

Chapters 2 and 3 are reprints of [91] and [92], respectively, i. e. a restriction to the most important material of the subject had to be made. In the present chapter the statistical analysis of Section 3.5.3 is deepened.

### 4.1 Influence of $X_{\text{gas}}$ , $T$ and Energy Range on $(X, X_{\text{net}})$ Density Distributions

The effect of a variation of  $X_{\text{gas}}$  and temperature  $T$  as well as an extended range of possible interaction energies on  $(X, X_{\text{net}})$  density distributions was shortly discussed in Section 3.5.3. Here this issue is taken up again.

From an experimental point of view,  $X_{\text{gas}}$  and temperature  $T$  are the only two parameters which can be varied, (although  $T$  only within a limited range given by the growth process of the solid solution). Therefore, it is of interest to study the *general*, i. e. in a statistical sense, influence of these two parameters on  $X$  and  $X_{\text{net}}$  for the present model. Fig. 4.1, 4.2 and 4.3 show density distributions of  $(X, X_{\text{net}})$  pairs for  $X_{\text{gas}} = 0.25, 0.5$  and  $0.75$  and

$T = 300$  and  $450$  K, respectively. The *same* 50 000 sets of interaction energies as in Fig. 3.6 were used (energies were randomly chosen within the range of  $-10 \dots 2$  kJ/mol). Additionally, for each 2D histogram the distribution of  $\Delta E_m$  and  $\Delta E_n$  values corresponding mainly to (A) H crystals with little inclusions of G, (B) and (D) solid solutions, (C) intermediate compounds HG, (E) G crystals with little inclusions of H, and total percentages of  $(X, X_{\text{net}})$  values in regions (A) - (E) are given.

Besides a slight shift of the  $(X, X_{\text{net}})$  densities towards larger  $X$  values (e. g. noted in the percentages), the histograms as well as the distributions in  $(\Delta E_m, \Delta E_n)$  space show no significant differences with a variation of  $X_{\text{gas}}$  at constant temperature. This insensitivity to  $X_{\text{gas}}$  is due to the fact that  $X_{\text{gas}}$  enters the molecular attachment probabilities only as a constant factor, while the various interaction energies appear in the exponent of the exponentials (see Eqs. 3.5). The smallest differences with a change of  $X_{\text{gas}}$  (for both temperatures) occur for region (C), i. e. intermediate compounds. Since an ordered structure may only form if  $\Delta E_m \ll 0$ , the Gibbs factors are mainly determined by this energy difference and the relative influence of  $X_{\text{gas}}$  becomes even smaller.

An increase of temperature from 300 to 450 K for constant  $X_{\text{gas}}$  has two effects: (i)  $|X_{\text{net}}|$  decreases, due to higher thermal disorder (see especially the upper left part and region (C) in the histograms). (ii) The energy ranges in  $(\Delta E_m, \Delta E_n)$  space for which solid solutions may form, i. e. regions (B) and (D), become wider. Therefore, percentages for finding  $(X, X_{\text{net}})$  values in these regions increase also. As already mentioned in Section 3.5.2, a necessary condition for the formation of solid solutions over a wide range of  $X$  are  $\Delta E_p$ ,  $\Delta E_m$  and  $\Delta E_n$  values being balanced to one another, i. e. deviating only little from each other and being generally small. Exactly this results, if the temperature is increased.

Limiting the range of interaction energies to  $-10 \dots 2$  kJ/mol is only realistic for certain groups of molecules. In order to investigate the influence of different energy ranges on the  $(X, X_{\text{net}})$  density distribution, two additional calculations with the ranges  $-20 \dots 5$  kJ/mol and  $-50 \dots 10$  kJ/mol were performed, each containing 50 000 energy sets (for constant  $T = 300$  K and  $X_{\text{gas}} = 0.25$ ). The results are shown in Fig. 4.4. It shows clearly, that the larger the energy range, the more tend  $(X, X_{\text{net}})$  values to the following limiting cases:

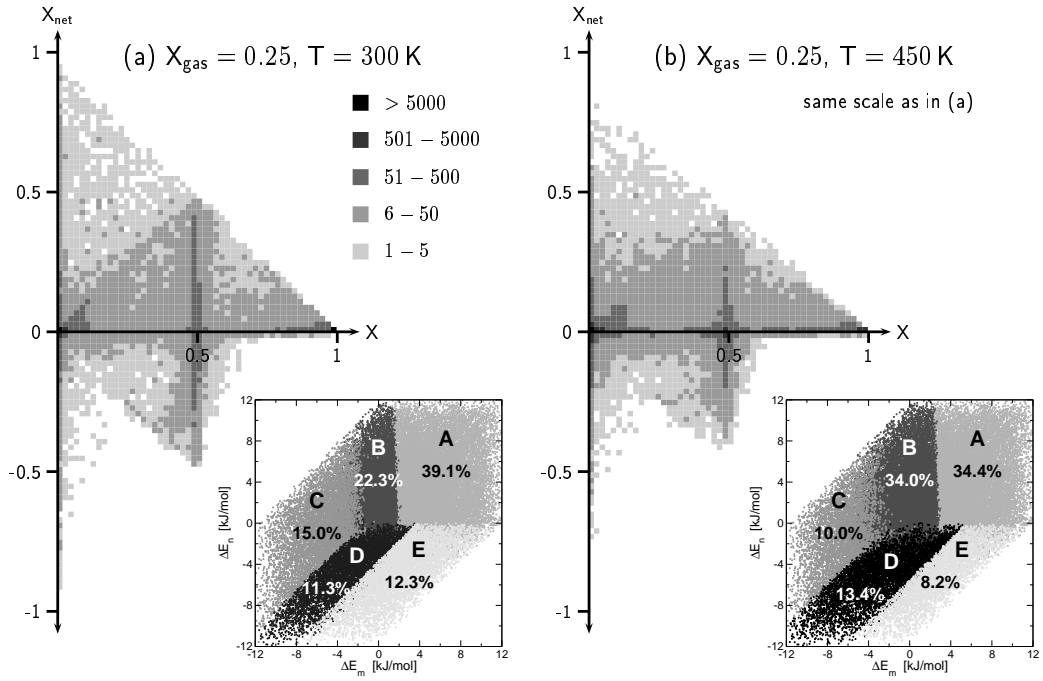
- (i)  $X \approx 0$  and  $0 \leq |X_{\text{net}}| \leq 1$  ( $\Delta E_n \gg 0$ ), i. e. region (A),
- (ii)  $X \approx |X_{\text{net}}|$  ( $\Delta E_p \gg 0$ ,  $\Delta E_m < 0$ ), i. e. region (B), but only the positive diagonal,

- (iii)  $X \approx 1 - |X_{\text{net}}|$  ( $\Delta E_p \approx 0$ ,  $\Delta E_m < 0$ ,  $\Delta E_n < 0$ ), i. e. regions (B) and (D), but only the negative diagonal,
- (iv)  $X \approx 0.5$  and  $0 \leq |X_{\text{net}}| \leq 0.5$  ( $\Delta E_m \ll 0$ ), i. e. region (C),
- (v)  $X \approx 1$  and  $X_{\text{net}} \approx 0$  ( $\Delta E_n \ll 0$ ), i. e. region (E).

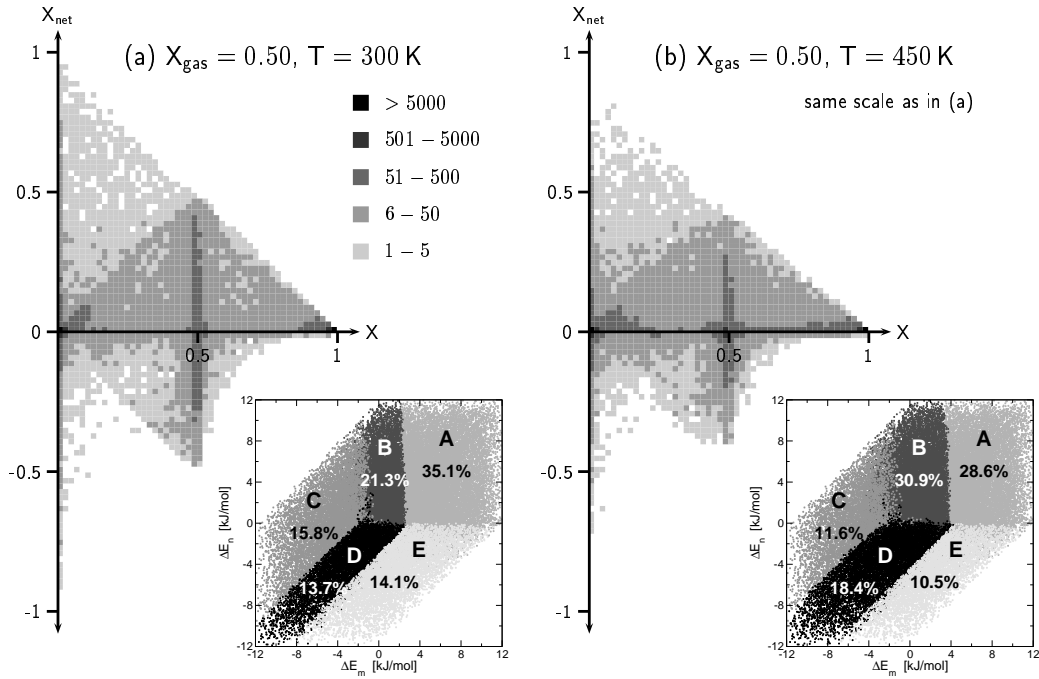
(Determining energy differences are specified in parenthesis.) Both, the high densities on the diagonals as well as near the point ( $X = 0.5$ ,  $X_{\text{net}} = 0.5$ ) are a result of an increased probability for  $\Delta E_f \gg 0$  and  $\Delta E_A \gg 0$  and therefore, leading to a very high orientational selectivity by H and G molecules, respectively.

Due to a lower probability of finding  $\Delta E_p$ ,  $\Delta E_m$  and  $\Delta E_n$  values being close to each other, the percentages of ( $X$ ,  $X_{\text{net}}$ ) values in regions (B) and (D) decrease with larger energy range. However, the widths as well as the placements of the two strips defining regions (B) and (D) in ( $\Delta E_m$ ,  $\Delta E_n$ ) space remain unchanged compared with those in Fig. 4.1 - 4.3 (for  $T = 300$  K). *This underlines again the fact that, in the present model, formation of solid solutions is mainly determined by  $\Delta E_m$  and  $\Delta E_n$  independent of other interaction energies*, (i. e. the energy differences of  $\downarrow \cdots |$  and  $|\cdots \uparrow$  with respect to  $\downarrow \cdots \uparrow$ ).

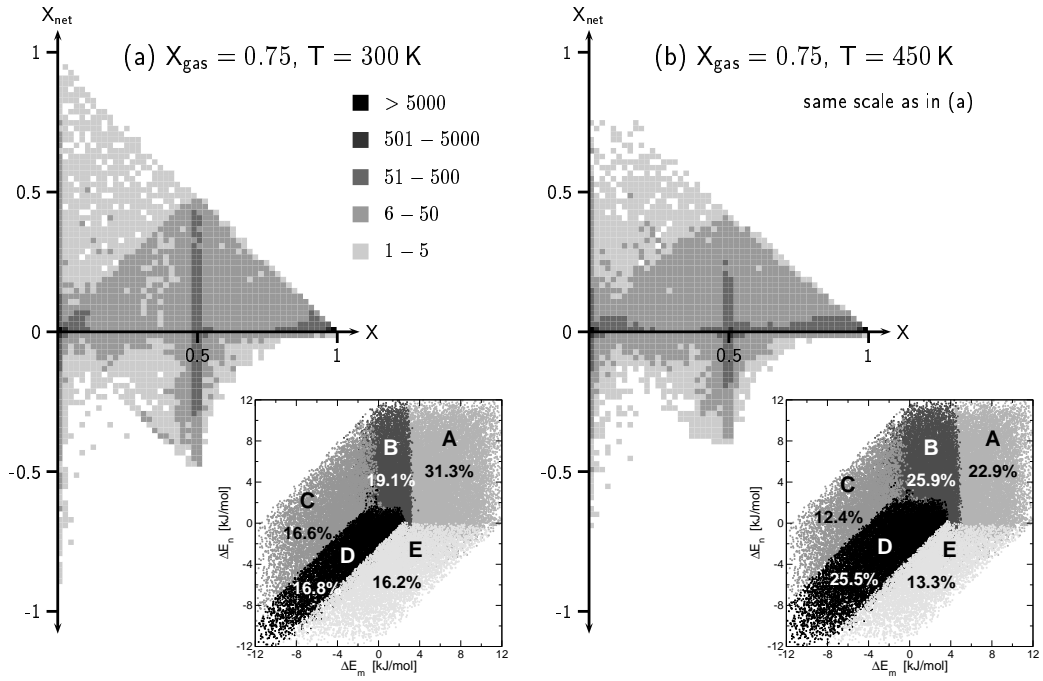
All calculations for Fig. 4.1 - 4.4 were carried out within the Markov mean-field approach. Even though the MMF approximation gives some erroneous results for  $X_{\text{net}}$  values around  $X \approx 0.5$  compared to Monte Carlo simulations (see Section 3.6.1), it is not expected that significant differences would occur for a similar MCS study. The conclusions made in this section refer mainly to the distribution of  $X$  and the *absolute* value of  $X_{\text{net}}$ . Nevertheless, a comparison with MCS results would have been of great interest. However, the MCS results shown in Fig. 3.6 took approximately two weeks of computer time using four conventional PCs. This would correspond to 16 weeks for calculating eight histograms as presented here and was not feasible, unfortunately.



**Figure 4.1:** *Upper figures:* 2D histograms of the density distributions of  $(X, X_{\text{net}})$  pairs for 50 000 randomly chosen sets of interaction energies in the range of  $-10 \dots 2$  kJ/mol calculated with the MMF model. Resolution for both axis: 0.02. *Lower figures:* Distribution of  $\Delta E_m$  and  $\Delta E_n$  values (from the same energy sets) corresponding to  $X$  values in the ranges: (A)  $0 \leq X < 0.02$ , (B)  $0.02 \leq X \leq 0.49$ , (C)  $0.49 < X < 0.51$ , (D)  $0.51 \leq X \leq 0.98$ , (E)  $0.98 < X \leq 1$ , and total percentages of  $(X, X_{\text{net}})$  values in regions (A) - (E).

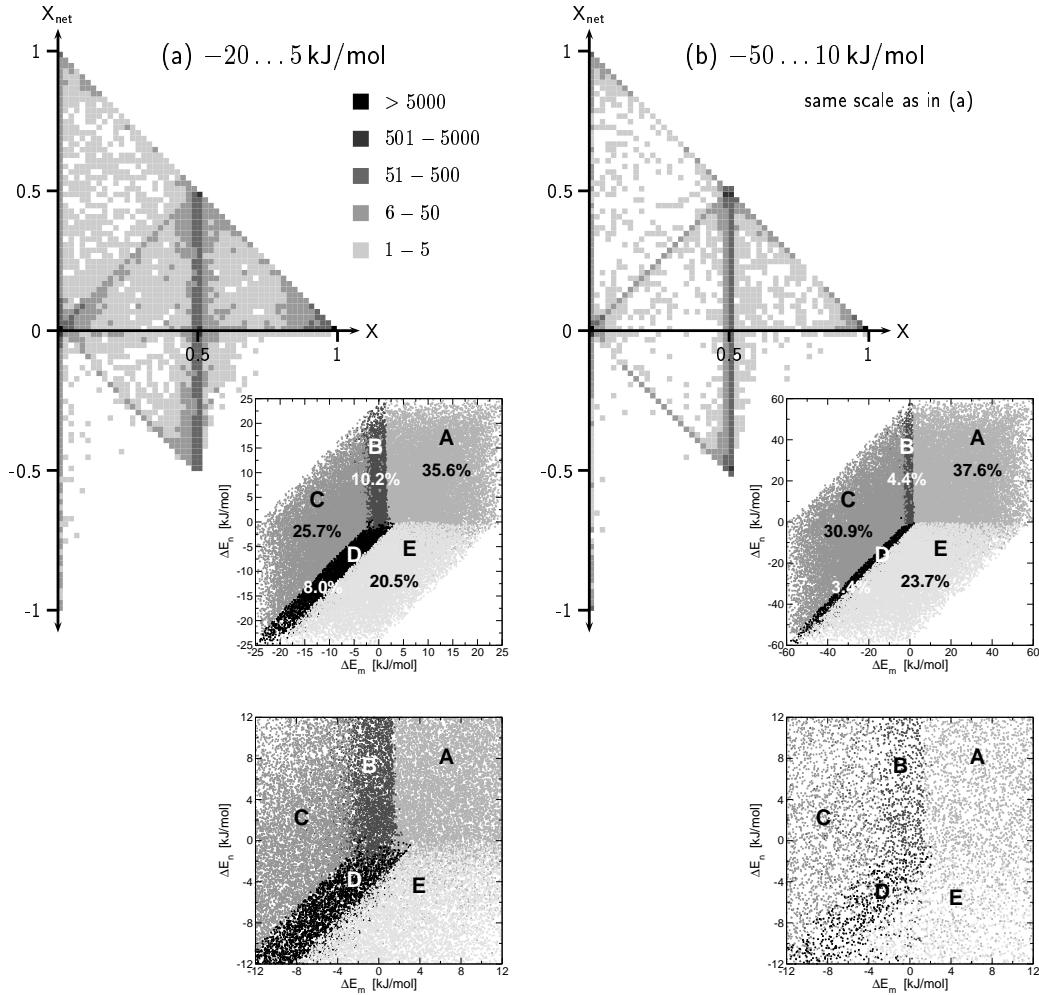


**Figure 4.2:** *Upper figures:* 2D histograms of the density distributions of  $(X, X_{\text{net}})$  pairs for 50 000 randomly chosen sets of interaction energies in the range of  $-10 \dots 2$  kJ/mol calculated with the MMF model. Resolution for both axis: 0.02. *Lower figures:* Distribution of  $\Delta E_m$  and  $\Delta E_n$  values (from the same energy sets) corresponding to  $X$  values in the ranges: (A)  $0 \leq X < 0.02$ , (B)  $0.02 \leq X \leq 0.49$ , (C)  $0.49 < X < 0.51$ , (D)  $0.51 \leq X \leq 0.98$ , (E)  $0.98 < X \leq 1$ , and total percentages of  $(X, X_{\text{net}})$  values in regions (A) - (E).



**Figure 4.3:** *Upper figures:* 2D histograms of the density distributions of  $(X, X_{\text{net}})$  pairs for 50 000 randomly chosen sets of interaction energies in the range of  $-10 \dots 2$  kJ/mol calculated with the MMF model. Resolution for both axis: 0.02. *Lower figures:* Distribution of  $\Delta E_m$  and  $\Delta E_n$  values (from the same energy sets) corresponding to  $X$  values in the ranges: (A)  $0 \leq X < 0.02$ , (B)  $0.02 \leq X \leq 0.49$ , (C)  $0.49 < X < 0.51$ , (D)  $0.51 \leq X \leq 0.98$ , (E)  $0.98 < X \leq 1$ , and total percentages of  $(X, X_{\text{net}})$  values in regions (A) - (E).





**Figure 4.4:** *Upper figures:* 2D histograms of the density distributions of  $(X, X_{\text{net}})$  pairs for 50 000 randomly chosen sets of interaction energies for two different energy ranges calculated with the MMF model ( $T = 300$  K,  $X_{\text{gas}} = 0.25$ ). Resolution for both axis: 0.02. *Lower figures:* Distribution of  $\Delta E_m$  and  $\Delta E_n$  values (from the same energy sets) corresponding to  $X$  values in the ranges: (A)  $0 \leq X < 0.02$ , (B)  $0.02 \leq X \leq 0.49$ , (C)  $0.49 < X < 0.51$ , (D)  $0.51 \leq X \leq 0.98$ , (E)  $0.98 < X \leq 1$ , and total percentages of  $(X, X_{\text{net}})$  values in regions (A) - (E). For comparison, sections of these distributions with the same intervals as in Fig. 4.1 - 4.3 are given.



## Chapter 5

# Growth-Induced Polarity Formation in Solid Solutions of Two Polar Components: A Statistical Analysis

### 5.1 Introduction

In a logical continuation of the previous studies, in this chapter, growth-induced polarity formation in solid solutions  $H_{1-X}G_X$  of *two polar* components is investigated. That is, building blocks are host (H) molecules of the type  $A - \pi - D$ , ( $A$ : electronic acceptor terminal;  $D$ : electronic donor terminal;  $\pi$ : delocalized  $\pi$ -electron system connecting  $A$  and  $D$ ), with a dipole moment  $\mu_{el}^H$ , and guest (G) molecules of the type  $A' - \pi - D'$ , ( $A'$ : electronic acceptor terminal;  $D'$ : electronic donor terminal;  $\pi$ : delocalized  $\pi$ -electron system connecting  $A'$  and  $D'$ ), with a dipole moment  $\mu_{el}^G$ . Unlike solid solutions investigated in Chapters 2 and 3, in the present case, polarity originates not only from H molecules, but also from G molecules.

Principally, the same growth model as in Section 3.3 is considered: Crystals are subjected to slow layer-by-layer growth from the gas phase. Molecules are arranged on a square lattice featuring two orientational states (up and down, relative to the projection of the molecular dipoles onto the growth direction). Adlayers relax to thermal equilibrium with respect to (i) the up and down orientation of the dipole moment of H *and* G molecules, and (ii) an exchange of H and G molecules. Using the notation of Section 3.3, the occupation of a lattice site is uniquely denoted by one of the states  $\{A, D, A', D'\}$ , referring to the molecular terminal being oriented toward the nutrient. Previously grown

layers are kept frozen. Ising-type nearest neighbor interactions are assumed. Growth takes place near thermal equilibrium, i. e. chemical potentials of H and G molecules are supposed to be the same in the solid and gas phase, and independent of the orientational state of the molecule in the crystal. For further details about the growth model, see Section 3.3.

Since, conceptually, an equivalent physical model is used, the present system with two polar components is expected to show the same characteristics as that with polar and non-polar molecules. In particular, the notions of orientational selectivity (see Section 3.5.1) and miscibility (see Section 3.5.2) apply also here. However, for the system with two polar molecules a minimal set of interaction energies comprises already 16 different values, see Table 5.1. This makes it impossible to derive simple (and useful) relations between interaction energies and specific behaviors of the system as it has been achieved for solid solutions of polar and non-polar components.

Therefore, we restrict ourselves to a statistical analysis only. A large number of energy sets is chosen randomly within a realistic range, allowing predictions on polarity formation in a probabilistic sense, (see also Section 3.5.3). Two points are addressed: (i) Comparison of  $(X, X_{\text{net}})$  density distributions between solid solutions with *non-polar* and *polar* G molecules, respectively. (ii) Comparison of  $X_{\text{net}}$  distributions for the three systems, (a) single-component crystals of polar (H) molecules only, (b) solid solutions of polar (H) and non-polar (G) molecules, and (c) solid solutions of polar (H) and polar (G) molecules. The overall yield of net polarity is calculated for each system. From a statistical point of view, this gives a measure of the potentiality of a system to provide polarity.

All results are obtained by means of Monte Carlo simulations, described in detail in Section 3.9 and Chapter 7. Additionally, an outline of a possible analytical description of growth-induced polarity formation in solid solutions with two polar components is given.

## 5.2 Definitions and Symmetry Relations

First, relevant definitions are given concerning macroscopic quantities and interaction energies. Some may have been stated already elsewhere, however, for clarity reasons they are repeated here.

The following three systems are considered: (a) Single-component crystals of polar (H) molecules only. (b) Solid solutions  $\text{H}_{1-X}\text{G}_X$  of polar (H) and non-polar (G) molecules. (c) Solid solutions  $\text{H}_{1-X}\text{G}_X$  of polar (H) and polar (G) molecules. Molar fractions of H and G molecules in the solid,  $0 \leq X_i \leq 1$ ,  $i \in \{A, D, N, A', D'\}$ , denoted by the corresponding molecular terminal

oriented toward the nutrient, are defined as follows:

$$\begin{aligned}
X_A & : \text{ polar H molecules, oriented downwards } (\downarrow) \\
X_D & : \text{ polar H molecules, oriented upwards } (\uparrow) \\
X_N & : \text{ non-polar G molecules, single orientation } (|) \\
X_{A'} & : \text{ polar G molecules oriented downwards } (\downarrow) \\
X_{D'} & : \text{ polar G molecules oriented upwards } (\uparrow)
\end{aligned}$$

(Orientations are with respect to the growth direction.)

The molar fraction of G molecules in the solid,  $0 \leq X \leq 1$ , the net polarity,  $-1 \leq X_{\text{net}} \leq 1$ , and the normalization condition for molar fractions  $X_i$ ,  $i \in \{A, D, N, A', D'\}$ , are given as:

(a) Single-component crystals of polar (H) molecules:

$$\begin{aligned}
X & = 0 \\
X_{\text{net}} & = X_A - X_D \\
X_A + X_D & = 1
\end{aligned} \tag{5.1}$$

(b) Solid solutions of polar (H) and non-polar (G) molecules:

$$\begin{aligned}
X & = 1 - X_A - X_D = X_N \\
X_{\text{net}} & = X_A - X_D \\
X_A + X_D + X_N & = 1
\end{aligned} \tag{5.2}$$

(c) Solid solutions of polar (H) and polar (G) molecules:

$$\begin{aligned}
X & = X_{A'} + X_{D'} \\
X_{\text{net}} & = (X_A - X_D) + (X_{A'} - X_{D'}) \\
X_A + X_D + X_{A'} + X_{D'} & = 1
\end{aligned} \tag{5.3}$$

Any physical property having its origin in polar properties of the molecules is assumed to be proportional to  $X_{\text{net}}$ . For system (c), this is only valid if  $\mu_{el}^G = \mu_{el}^H$ , (which is assumed for simplicity here). Otherwise,  $X_{\text{net}}^H$  and  $X_{\text{net}}^G$ , the separate net polarities for H and G components, respectively, have to be weighted with the absolute values of the dipole moments of H and G molecules.

Table 5.1 gives an overview of the different energy sets used in the three systems (a), (b) and (c). They are sufficient for a basic physical description with respect to the polar character of H (and G) molecules. However, they are considered *minimal*, because only nearest neighbor isotropic interactions for a simple square lattice are taken into account. Moreover, in case of

the two-component systems it is required that H and G molecules are of similar shape and crystallizing in isomorphous crystal structures (here square lattice). Note that in case of system (b), it is not assumed anymore that functional group terminals ( $N$ ) of non-polar G molecules require that  $N = A$  or  $D$ , as in Section 3.5. That is, in this chapter, longitudinal interactions between H and G molecules as well as between G molecules only are considered independently.

Based on these energy sets and the growth model, it is possible to identify symmetry relations between interaction energies and  $X$ ,  $X_{\text{net}}$ . Indeed, an exchange of acceptor/donor terminals ( $A$ ,  $D$ ,  $A'$ ,  $D'$ ) induces a change in  $X$  and/or  $X_{\text{net}}$ , without modifying the actual set of interaction energies. For systems (a), (b) and (c) the following symmetry relations arise:

- (a) Single-component crystals of polar (H) molecules only ( $X = 0$ ):

$$\left. \begin{array}{l} A \rightarrow D \\ D \rightarrow A \end{array} \right\} \Rightarrow X_{\text{net}} \rightarrow -X_{\text{net}}, \quad (5.4)$$

i. e. the point  $X_{\text{net}} = 0$  specifies a center of symmetry on the  $X_{\text{net}}$ -axis.

- (b) Solid solutions of polar (H) and non-polar (G) molecules:

$$\left. \begin{array}{l} A \rightarrow D \\ D \rightarrow A \end{array} \right\} \Rightarrow (X, X_{\text{net}}) \rightarrow (X, -X_{\text{net}}), \quad (5.5)$$

i. e. the  $X$ -axis specifies a 2-fold axis of symmetry in  $(X, X_{\text{net}})$  space.

- (c) Solid solutions of polar (H) and polar (G) molecules:

$$\left. \begin{array}{l} A \rightarrow A' \\ D \rightarrow D' \\ A' \rightarrow A \\ D' \rightarrow D \end{array} \right\} \Rightarrow (X, X_{\text{net}}) \rightarrow (1 - X, X_{\text{net}}), \quad (5.6a)$$

i. e. the vertical axis through  $X = 0.5$  specifies a 2-fold axis of symmetry in  $(X, X_{\text{net}})$  space.

$$\left. \begin{array}{l} A \rightarrow D \\ D \rightarrow A \\ A' \rightarrow D' \\ D' \rightarrow A' \end{array} \right\} \Rightarrow (X, X_{\text{net}}) \rightarrow (X, -X_{\text{net}}), \quad (5.6b)$$

i. e. the  $X$ -axis specifies a 2-fold axis of symmetry in  $(X, X_{\text{net}})$  space.

$$\left. \begin{array}{l} A \rightarrow D' \\ D \rightarrow A' \\ A' \rightarrow D \\ D' \rightarrow A \end{array} \right\} \Rightarrow (X, X_{\text{net}}) \rightarrow (1 - X, -X_{\text{net}}), \quad (5.6c)$$

i. e. the point  $(X = 0.5, X_{\text{net}} = 0)$  specifies a center of symmetry in  $(X, X_{\text{net}})$  space.

These symmetry relations are taken into consideration for the calculations of density distributions, see below.

## 5.3 Results and Discussion

### 5.3.1 $(X, X_{\text{net}})$ Density Distributions

In order to obtain representative  $(X, X_{\text{net}})$  density distributions for systems (b) and (c), independent Monte Carlo simulations were performed for a large number of energy sets, randomly chosen within a realistic range of  $-10 \dots 2$  kJ/mol for both systems ( $T = 300$  K).  $X_{\text{gas}}$  was set to 0.5, i. e. chemical potentials of H and G molecules were the same,  $\mu_H = \mu_G$ . Since we are interested only on the effect of polarity *formation* in centrosymmetric crystal structures, interaction energies were subjected to the condition that the antiparallel packing of molecules in lateral direction is in favor of the parallel packing for native polar H and G crystals, respectively, see the bottom row in Table 5.1.

For system (b) calculations were done for 50 000 energy sets. For each resulting  $(X, X_{\text{net}})$  pair the symmetry operation, according to Eq. (5.5), was applied in order to double the number of  $(X, X_{\text{net}})$  points. Correspondingly, for system (c) simulations for 25 000 energy sets were carried out, and symmetry operations applied, see Eqs. (5.6), yielding four times the number of  $(X, X_{\text{net}})$  points.

These additional  $(X, X_{\text{net}})$  pairs do not improve the statistical accuracy, however, a large amount of computer time could be saved by taking symmetry relations into account. This was especially important in case of system (c), where the adlayer equilibration time  $\tau_L$  was set to a high value in order to account for the larger number of possible adlayer configurations,  $4^{N_L}$  and  $\tau_L = 5\,000$ , compared to system (b),  $3^{N_L}$  and  $\tau_L = 1\,000$ . ( $N_L$  is the number of lattice sites in a layer, see Section 3.9 for definitions.)

Results are shown in Fig. 5.1. Symmetries in the 2D histograms are clearly

**Table 5.1:** Minimal sets of interaction energies for three different molecular systems with at least one polar component. Polar host (H) molecules:  $A-\pi-D$ , ( $A$ : acceptor terminal;  $D$ : donor terminal), two orientational states ( $\uparrow, \downarrow$ ). Non-polar guest (G) molecules:  $N-\pi-N$ , ( $N$ : functional group, often  $A$  or  $D$ ), single orientational state ( $|\cdot\rangle$ ). Polar guest (G) molecules:  $A'-\pi-D'$ , ( $A'$ : acceptor terminal;  $D'$ : donor terminal), two orientational states ( $\uparrow, \downarrow$ ). Energies are subdivided into *longitudinal* and *lateral* with respect to the growth direction of the crystals and furthermore, into interactions between H molecules only, G molecules only, and H and G molecules, respectively. Meaning of indices for lateral interactions:  $p$ , parallel;  $ap$ , antiparallel;  $m$ , mixed;  $n$ , neutral. The total number of energies and independent energy differences (in parenthesis) is given. The last row states the conditions on lateral interaction energies for centrosymmetric native crystal structures.

	Crystals of polar (H) molecules only	Solid solutions of polar (H) and non-polar (G) molecules	Solid solutions of polar (H) and polar (G) molecules
Longitudinal			
only H	$E_{AD} (-A \cdots D-)$ $E_{AA} (-A \cdots A-)$ $E_{DD} (-D \cdots D-)$		
only G		$E_{NN} (-N \cdots N-)$	$E_{A'D'} (-A' \cdots D'-)$ $E_{A'A'} (-A' \cdots A'-)$ $E_{D'D'} (-D' \cdots D'-)$
between H and G		$E_{NA} (-N \cdots A-)$ $E_{ND} (-N \cdots D-)$	$E_{AA'} (-A \cdots A'-)$ $E_{DA'} (-D \cdots A'-)$ $E_{AD'} (-A \cdots D'-)$ $E_{DD'} (-D \cdots D'-)$
Lateral			
only H	$E_p (\uparrow \cdots \uparrow)$ $E_{ap} (\uparrow \cdots \downarrow)$		
only G		$E_n ( \cdot\rangle \cdots  \cdot\rangle)$	$E_{p'} (\uparrow \cdots \uparrow)$ $E_{ap'} (\uparrow \cdots \downarrow)$
between H and G		$E_m ( \cdot\rangle \cdots \uparrow)$	$E_p^m (\uparrow \cdots \uparrow)$ $E_{ap}^m (\uparrow \cdots \downarrow)$
Total	5 (3)	10 (8)	16 (14)
Centric structures	$E_p > E_{ap}$	$E_p > E_{ap}$	$E_p > E_{ap}$ $E_{p'} > E_{ap'}$



apparent, i. e. a 2-fold axis of symmetry ( $X$ -axis) for system (b), and two 2-fold axis of symmetry ( $X$ -axis and perpendicular through  $X = 0.5$ ) and a center of symmetry ( $X = 0.5, X_{\text{net}} = 0$ ) for system (c), respectively. Note that these *perfect* symmetric density distributions in  $(X, X_{\text{net}})$  space are due to the procedure described above. Nevertheless, it has to be emphasized that symmetries are physical in the sense that, for an infinite large number of chosen energy sets, similar ideal 2D histograms would arise, also without applying any symmetry operations.

While for system (b) density distributions are constrained by the requirement  $|X_{\text{net}}| \leq 1 - X$ , any  $(X, X_{\text{net}})$  pair may be obtained in system (c), principally. In both systems, the strong influence of lateral interactions on miscibility between H and G molecules manifests in high  $(X, X_{\text{net}})$  densities for  $X$  values around 0, 0.5 and 1, respectively, (four nearest neighbors within a layer and only one between adjacent layers, see also Section 3.5.3).

For system (b) regions with relatively homogeneous  $(X, X_{\text{net}})$  densities may be located, e. g. the area with  $|X_{\text{net}}| < X$  or the vertical stripe through  $X = 0.5$ . In system (c) the density distribution in  $(X, X_{\text{net}})$  space is more inhomogeneous, because of two reasons: (i) Polar G molecules introduce additional orientational disorder. (ii) Longitudinal ( $E_{AA'}$ ,  $E_{DA'}$ ,  $E_{AD'}$ ,  $E_{DD'}$ ) and lateral ( $E_p^m$ ,  $E_{ap}^m$ ) interactions between H and G molecules are selective with respect to their dipole orientations. Oppositely, in system (b) *only* the longitudinal energies  $E_{NA}$  and  $E_{ND}$  between the two components show orientational selectivity, see Table 5.1. In system (c) large differences between  $(X, X_{\text{net}})$  densities arise particularly along the vertical line through  $X = 0.5$ , with high densities at  $|X_{\text{net}}| \approx 0$  and  $|X_{\text{net}}| \approx 1$ , respectively.

The influence of these energies (especially  $E_p^m$  and  $E_{ap}^m$ ) on  $X_{\text{net}}$  becomes best visible in a comparison between systems (b) and (c) for particular crystal structures. Fig. 5.2 shows the relative  $X_{\text{net}}$  distributions for H crystals with little inclusions of G (Fig. 5.2(a)), solid solutions  $H_{1-X}G_X$  (Fig. 5.2(b) and 5.2(d)), and intermediate compounds HG (Fig. 5.2(c)), respectively. For nearly pure H crystals,  $X_{\text{net}}$  distributions for systems (b) and (c) are almost the same, because polarity is governed mainly by interactions between H molecules only, see Fig. 5.2(a). This behavior changes completely as soon as a certain fraction of G molecules is present in crystals, the most pronounced effect being for intermediate compounds. In ordered structures HG of systems (b) and (c) the following situations occur, see Fig. 5.2(c):

System (b): H molecules are entirely surrounded by laterally non-selective G molecules. Therefore, a relatively large fraction of these structures shows high net polarity,  $0 < |X_{\text{net}}| < 0.5$ , determined by  $E_{AA}$  and  $E_{DD}$ . Besides, the  $X_{\text{net}}$  distribution does not vary a lot in this range, since energies are chosen uniformly.

System (c): Although H molecules are also surrounded by G molecules, lateral interactions between the two components may strongly influence the polar properties of crystals. This is often the case, because lateral orientational selectivity arises as soon as  $E_p^m (\uparrow \cdots \uparrow) \neq E_{ap}^m (\uparrow \cdots \downarrow)$ . Since this selectivity is enhanced by the presence of *four* lateral neighbors, ordered structures of the types H( $\downarrow$ )G( $\uparrow$ ) or H( $\uparrow$ )G( $\downarrow$ ) with  $X_{\text{net}} \approx 0$  and H( $\downarrow$ )G( $\downarrow$ ) or H( $\uparrow$ )G( $\uparrow$ ) with  $X_{\text{net}} \approx 1$ , are most probable. The  $X_{\text{net}}$  distribution decreases rapidly for  $|X_{\text{net}}| > 0$ , passes a minimum, and increases again considerably for  $|X_{\text{net}}| \rightarrow 1$ . Generally, large fluctuations are observed.

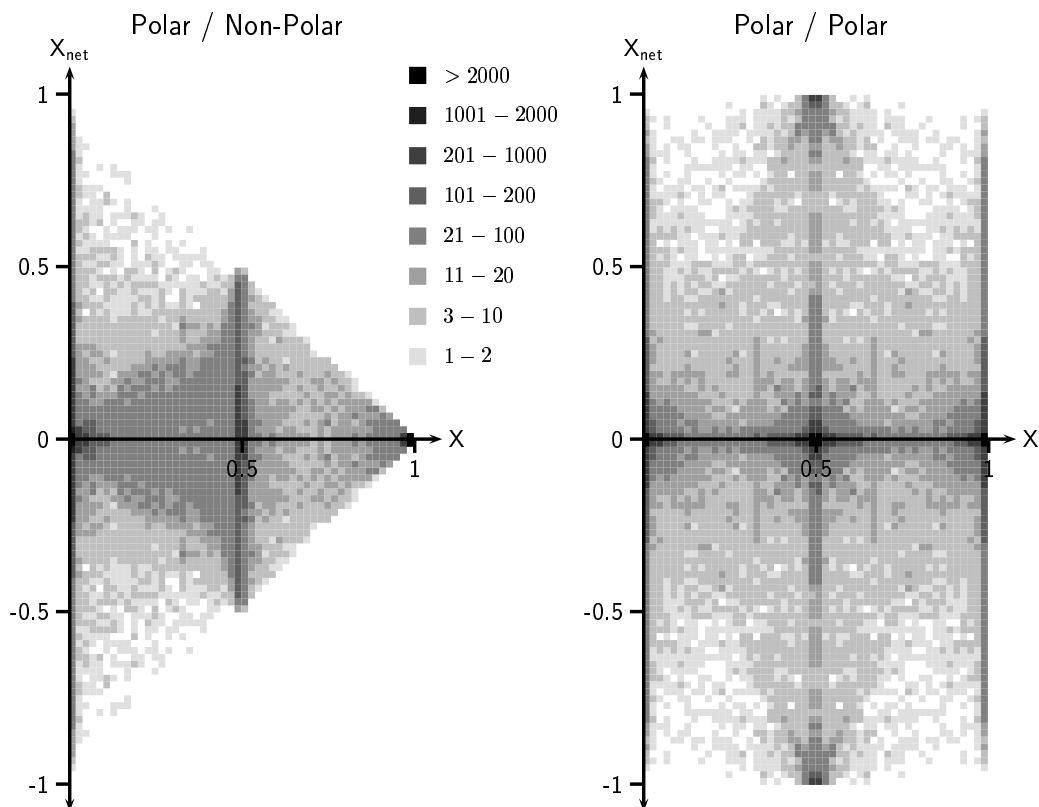
In case of solid solutions (Figs. 5.2(b) and 5.2(d)),  $X_{\text{net}}$  distributions for system (c) decrease slightly faster for  $|X_{\text{net}}| \rightarrow 0.5$  than those for system (b). For  $|X_{\text{net}}| > 0.5$  behaviors are similar as in case of intermediate compounds, Fig. 5.2(c). Because of the complex interplay between different lateral (and longitudinal) interactions, a simple interpretation of  $X_{\text{net}}$  distributions in case of solid solutions can not be given here.

The observations of Fig. 5.1 and Fig. 5.2 allow the following conclusion: For system (c) it is possible and also probable to obtain an almost complete parallel alignment of H and G molecules in the present model, i. e.  $|X_{\text{net}}| \approx 1$ , even though both native structures (H and G) favor centrosymmetric packings of molecules. This is only possible due to the large influence of lateral interactions between H and G components. However, the same interactions may diminish polarity, if the antiparallel packing of H and G molecules is preferred and  $X_{\text{net}} \approx 0$ . *Therefore, in order to obtain polarity in real systems, solid solution formation between two polar components is only reasonable, if antiparallel bindings between the two species are weak.* Otherwise, solid solutions with one polar and a non-polar component might be more advantageous.

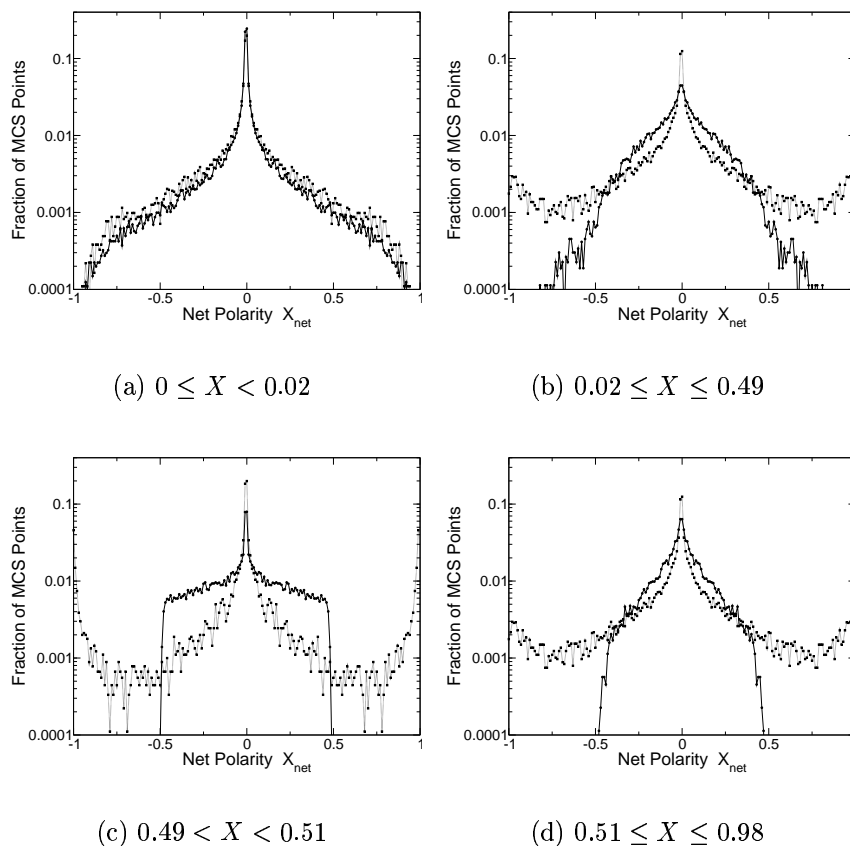
### 5.3.2 $X_{\text{net}}$ Distributions for Systems (a), (b) and (c)

For many application purposes a large vectorial alignment of polar H (or G) molecules is required. In this respect, formation of solid solutions  $\text{H}_{1-X}\text{G}_X$  is just a means to get net polarity ( $|X_{\text{net}}|$ ), especially in cases, where native crystal structures of the two components are centrosymmetric. However, the actual fraction of G molecules in the solid solutions ( $X$ ), is not of particular importance, provided that a large value of  $|X_{\text{net}}|$  is obtained.

Therefore, in this section we focus only on the statistical distribution of  $X_{\text{net}}$ , irrespective of  $X$ . Thereby, systems (b) and (c) are compared with system (a), i. e. single-component crystals of polar (H) molecules only ( $X = 0$ ). As such, it is possible to investigate the potential benefit of solid solution formation with respect to the evolvement of polarity. Furthermore, this analysis



**Figure 5.1:** 2D histograms showing density distributions of  $(X, X_{\text{net}})$  results for randomly chosen sets of interaction energies in the range of  $-10 \dots 2$  kJ/mol from Monte Carlo simulations (MCS),  $T = 300$  K,  $X_{\text{gas}} = 0.5$ . *Left:* Solid solutions  $\text{H}_{1-X}\text{G}_X$  of polar (H) and non-polar (G) molecules. MCS were performed for 50 000 energy sets and then symmetry relations were applied (2-fold axis of symmetry, see Eq. (5.5)). MCS parameters:  $s_L = 32 \times 32$ ,  $\tau_L = 1\,000$ ,  $\tau_G = 50$ ,  $\tau_S = 200$ . *Right:* Solid solutions of polar (H) and polar (G) molecules. MCS were performed for 25 000 energy sets and then symmetry relations were applied (two 2-fold axis of symmetry and a center of symmetry, see Eqs. (5.6)). MCS parameters:  $s_L = 32 \times 32$ ,  $\tau_L = 5\,000$ ,  $\tau_G = 50$ ,  $\tau_S = 200$ . Both figures contain the same number of points in  $(X, X_{\text{net}})$  space, namely 100 000. Resolution for both axis: 0.02. The same scale is applied in both figures. The number of energy sets is considered sufficient for representative density distributions, because similar results were obtained for smaller sets.



**Figure 5.2:**  $X_{\text{net}}$  distributions corresponding mainly to (A) H crystals with little inclusions of G, (B) and (D) solid solutions, (C) intermediate compounds HG. *Solid line with circles:* Solid solutions  $H_{1-X}G_X$  of polar (H) and non-polar (G) molecules, i. e. system (b). *Dotted line with squares:* Solid solutions of polar (H) and polar (G) molecules, i. e. system (c). Data is from the same Monte Carlo simulations as for Fig. 5.1. Distributions are normalized relative to the number of  $(X, X_{\text{net}})$  points in regions (a) - (d) for a given system. Resolution for  $-1 \leq X_{\text{net}} \leq 1$ : 0.01. Note that distributions are symmetric with respect to the vertical line through  $X_{\text{net}} = 0$ . Small deviations between the two points next to the left and right of this 2-fold axis of symmetry arise, because the point  $X_{\text{net}} = 0$  belongs to the right bin only. For system (b)  $X_{\text{net}}$  distributions drop to zero for  $|X_{\text{net}}| > 0.5$  in case of (C) and (D), due to the requirement  $|X_{\text{net}}| \leq 1 - X$ . For system (c)  $X_{\text{net}}$  distributions are the same in case of (B) and (D), due to symmetry relations.

allows to make statistical predictions on the possibility to form polarity for these common types of molecular systems.

For system (a), Monte Carlo simulations were performed for 50 000 randomly chosen energy sets in the same range as above ( $-10 \dots 2$  kJ/mol) using the equivalent two-layer system described in [5] and Section 6.5. As for systems (b) and (c), only centrosymmetric crystal structures were assumed, i. e.  $E_{ap} < E_p$ , see Table 5.1. Assuming that systems are far away from a critical region (phase transition) for most of the energy sets, the following simulation parameters were considered to be sufficient for the present analysis: 4 000 Monte Carlo trials per lattice site (on average) to equilibrate the two-layer system (lattice size  $s_L = 32 \times 32$ ), followed by 20 000 measurements (one after each sweep of the two layers). For each resulting  $X_{\text{net}}$  value, the negative counterpart ( $-X_{\text{net}}$ ) was also taken into account for the statistics, see Eq. (5.4). For systems (b) and (c) the same Monte Carlo data was used as for Fig. 5.1.

$X_{\text{net}}$  distributions are shown in Fig. 5.3. In all three systems a sharp peak arises at  $X_{\text{net}} = 0$ . This is a clear consequence of the strong influence of lateral interactions which are in favor of antiparallel packings of H (and G) molecules with respect to the orientations of their dipoles, see Table 5.1. However, the slope of the  $X_{\text{net}}$  distribution towards higher  $|X_{\text{net}}|$  values ( $|X_{\text{net}}| \rightarrow 0.5$ ) is considerably steeper for system (a), compared to those for systems (b) and (c), respectively. That is, from a statistical point of view, solid solution formation is certainly advantageous to yield net polarity  $|X_{\text{net}}| > 0$  in comparison to single-component systems (a) as found by the present model.

For system (b) at  $|X_{\text{net}}| \approx 0.5$  a fast drop in the  $X_{\text{net}}$  distribution is observed. This is a result of the fact that inclusion of non-polar (G) molecules in a centrosymmetric H structure may increase the vectorial alignment of polar (H) molecules, however, only at the expense of reducing the fraction of the H component (dilution effect). As depicted in Fig. 5.1, a relatively high density of  $(X, X_{\text{net}})$  points with  $|X_{\text{net}}| > 0$  (and especially  $|X_{\text{net}}| \approx 0.5$ ) is only observed at  $X \approx 0.5$ . Therefore, since  $|X_{\text{net}}| \leq 1 - X$ , for  $|X_{\text{net}}| > 0.5$  the probability must decrease rapidly.

The  $X_{\text{net}}$  distribution for system (c) passes a minimum at  $|X_{\text{net}}| \approx 0.75$ , and increases again towards  $|X_{\text{net}}| \rightarrow 1$  considerably.

Fig. 5.4 shows the total fraction of  $|X_{\text{net}}|$  results being equal or greater than a certain value ( $0 \leq |X_{\text{net}}| \leq 1$ ) for systems (a), (b) and (c), respectively. Again, for system (a) the probability to reach net polarity  $|X_{\text{net}}| > 0$  decreases much faster for low values of  $|X_{\text{net}}|$  in comparison to systems (b) and (c), respectively. The two-component systems show approximately the same behavior in the range  $0 < |X_{\text{net}}| \leq 0.1$ . For larger  $|X_{\text{net}}|$  values the curve for system (b) drops faster than that for system (c). Even more, the lowering

**Table 5.2:** Overall yield of net polarity,  $\langle |X_{\text{net}}| \rangle$ , (average of  $|X_{\text{net}}|$  over all  $X_{\text{net}}$  values), and percentages of cases with almost no net polarity ( $|X_{\text{net}}| < 0.01$ ), moderate net polarity ( $|X_{\text{net}}| > 0.2$ ), and high net polarity ( $|X_{\text{net}}| > 0.5$ ), respectively. (a) Single-component crystals of polar (H) molecules only. (b) Solid solutions of polar (H) and non-polar (G) molecules. (c) Solid solutions of polar (H) and polar (G) molecules.

	$\langle  X_{\text{net}}  \rangle$	$ X_{\text{net}}  < 0.01$ (%)	$ X_{\text{net}}  > 0.2$ (%)	$ X_{\text{net}}  > 0.5$ (%)
(a)	0.067	57.7	11.4	2.9
(b)	0.106	35.0	20.2	2.3
(c)	0.181	31.3	27.9	13.0

effect on polarity by dilution with non-polar (G) molecules becomes so large that at  $|X_{\text{net}}| \approx 0.45$  the curve of system (b) crosses the one of system (a). That is, the probability to get  $|X_{\text{net}}|$  above this value is even slightly higher for system (a) than for system (b).

Table 5.2 summarizes essential figures for the three systems, including the overall yields of net polarity,  $\langle |X_{\text{net}}| \rangle$ , i. e. the averages of  $|X_{\text{net}}|$  over all  $|X_{\text{net}}|$  values for each system. For system (c) this measure is almost three times larger than for system (a), illustrating clearly the high potential of solid solutions with two polar components to form structures with large  $|X_{\text{net}}|$ .

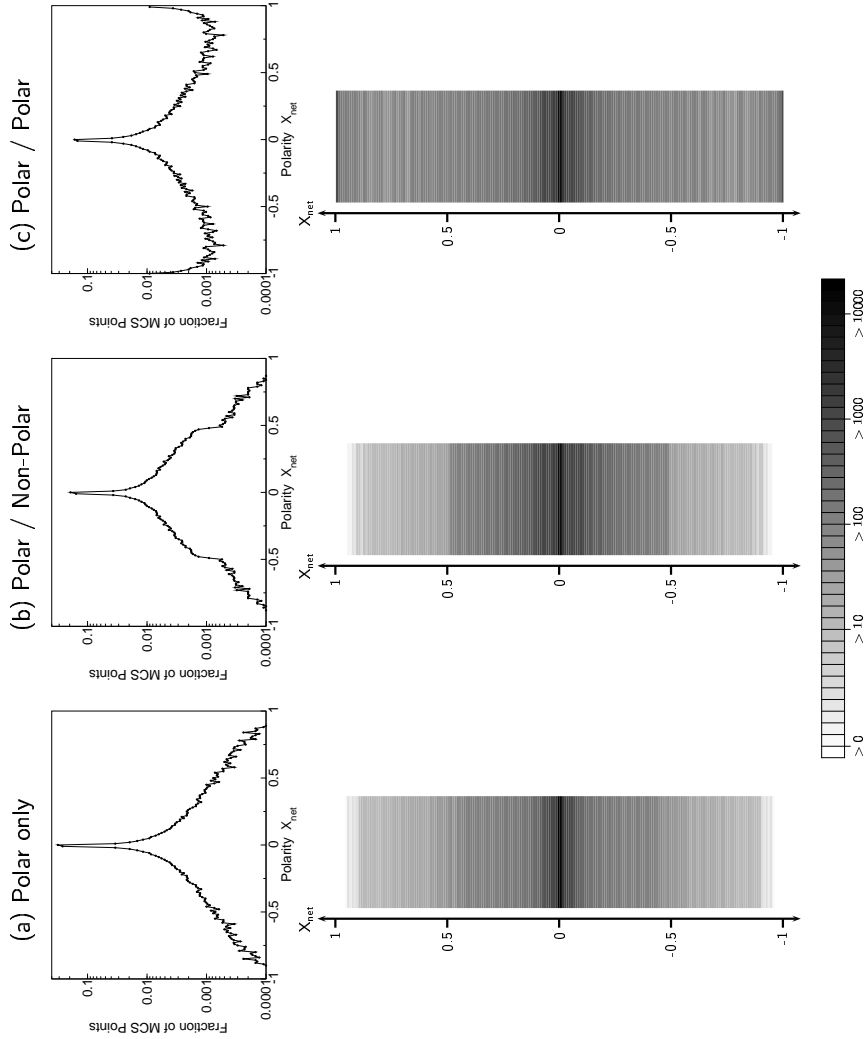
### 5.3.3 An Analytical Approach

Systems (a), (b) and (c) were investigated by means of Monte Carlo simulations only. This was considered sufficient (and reliable) for a statistical analysis. However, following the derivations of Section 3.4.1, an analytical description of system (c) in terms of a Markov mean-field approximation is straightforward. Here, a short outline of this approach is given.

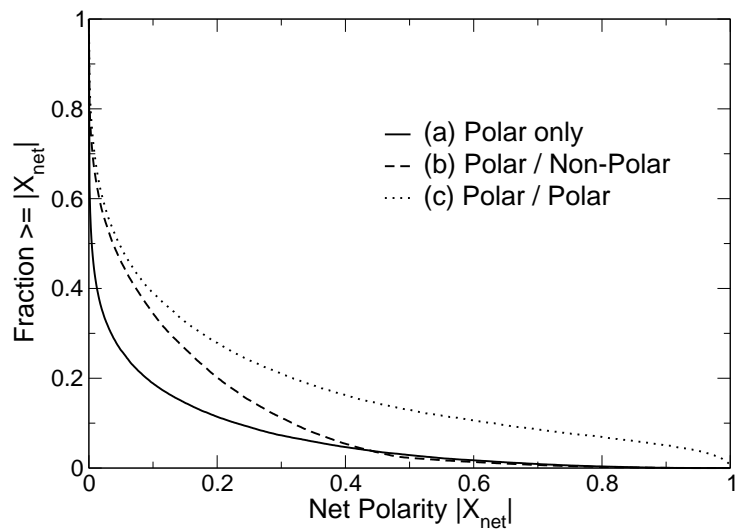
The layer-by-layer growth process has reached a stationary state, if molar fractions  $X_i$ ,  $i \in \{A, D, A', D'\}$ , of H and G molecules are the same in the substrate layer and the adlayer. This can be expressed by the matrix equation (see also Eq. (3.6))

$$\begin{pmatrix} X_A^g \\ X_D^g \\ X_{A'}^g \\ X_{D'}^g \end{pmatrix} = \begin{pmatrix} P_{AD}^g & P_{DD}^g & P_{A'D}^g & P_{D'D}^g \\ P_{AA}^g & P_{DA}^g & P_{A'A}^g & P_{D'A}^g \\ P_{AD'}^g & P_{DD'}^g & P_{A'D'}^g & P_{D'D'}^g \\ P_{AA'}^g & P_{DA'}^g & P_{A'A'}^g & P_{D'A'}^g \end{pmatrix} \begin{pmatrix} X_A^g \\ X_D^g \\ X_{A'}^g \\ X_{D'}^g \end{pmatrix}, \quad (5.7)$$

where the superscript  $g$  indicates that independent molar fractions must be considered for two sublattices  $g = I, II$ . (The decomposition into two



**Figure 5.3:** Two different representations ( $x,y$ -graphs and density bars) of  $X_{\text{net}}$  distributions for randomly chosen sets of interaction energies in the range of  $-10 \dots 2$  kJ/mol from Monte Carlo simulations (MCS),  $T = 300$  K. (a) Single-component crystals of polar (H) molecules only. MCS were performed for 50 000 energy sets and then symmetry relations were applied (center of symmetry, see Eq. (5.4)). Results were obtained by use of the equivalent two-layer system, see Section 6.5 and [5],  $s_L = 32 \times 32$ . (b) Solid solutions  $H_{1-X}G_X$  of polar (H) and non-polar (G) molecules. (c) Solid solutions of polar (H) and polar (G) molecules. For (b) and (c), data is from the same Monte Carlo simulations as for Fig. 5.1, taking only  $X_{\text{net}}$  values into consideration (arbitrary  $X$ ). The number of points in the range  $-1 \leq X_{\text{net}} \leq 1$  is the same (100 000) for systems (a), (b) and (c). The resolution for the range  $-1 \leq X_{\text{net}} \leq 1$  is 0.01 in both representations and a logarithmic scaling is applied. Note that distributions are symmetric with respect to  $X_{\text{net}} = 0$ . Small deviations between the two points (or stripes) next to the left and right of this center of symmetry arise, because the point  $X_{\text{net}} = 0$  belongs to the right (upper) bin only.



**Figure 5.4:** Fraction of net polarity  $|X_{\text{net}}|$  ( $0 \leq |X_{\text{net}}| \leq 1$ ) being equal or greater than a certain value for randomly chosen sets of interaction energies in the range of  $-10 \dots 2$  kJ/mol and  $T = 300$  K. (a) Single-component crystals of polar (H) molecules only. (b) Solid solutions  $\text{H}_{1-X}\text{G}_X$  of polar (H) and non-polar (G) molecules. (c) Solid solutions of polar (H) and polar (G) molecules. Data is from the same Monte Carlo simulations as for Fig. 5.1 in case of systems (b) and (c), and Fig. 5.3 in case of system (a), respectively. The resolution for probabilities is 0.001. Note that at  $|X_{\text{net}}| = 0$  the probability is unity for all systems. For systems (a) and (b) a cross-over takes place at  $|X_{\text{net}}| \approx 0.45$ .



sublattices is necessary to describe antiparallel packings.)  $P_{s's}^g$  is the transition probability that an admolecule, (specified by its molecular terminal  $s \in \{D, A, D', A'\}$  oriented toward the substrate), will be attached onto a molecule of the substrate layer, (specified by its molecular terminal  $s' \in \{A, D, A', D'\}$  oriented toward the nutrient), belonging to a site of sublattice  $g$ . Transition probabilities  $P_{s's}^g$  are given by normalized Gibbs factors ( $\beta = 1/k_B T$ )

$$P_{s's}^g = \frac{1}{Z_{s'}} x_s e^{-\beta f_{s's}^g}, \quad (5.8a)$$

with

$$Z_{s'} = \sum_{s \in \{A, D, A', D'\}} x_s e^{-\beta f_{s's}^g}, \quad s' \in \{A, D, A', D'\}. \quad (5.8b)$$

$x_s$  is the factor arising from chemical potentials  $\mu_H, \mu_G$  of H and G molecules, respectively, (see Eqs. (3.1)), and is

$$x_s = \begin{cases} 1 - X_{\text{gas}} & : s \in \{A, D\} \\ X_{\text{gas}} & : s \in \{A', D'\} \end{cases}. \quad (5.9)$$

( $X_{\text{gas}}$  is the molar fraction of G molecules in the gas phase,  $0 \leq X_{\text{gas}} \leq 1$ .) The energy terms  $f_{s's}^g$  take into account longitudinal energies explicitly and lateral energies within a mean-field correction. Since they can be derived easily for system (c) from Table 3.1, they are not stated here. With the normalization condition

$$X_A^g + X_D^g + X_{A'}^g + X_{D'}^g = 1, \quad g = I, II, \quad (5.10)$$

Eq. (5.7) can be solved numerically for molar fractions  $X_i, i \in \{A, D, A', D'\}$ , using a similar procedure as described in Section 3.8.

For an increasing number of different interaction energies, local correlations within an adlayer become more and more important, which can not be described sufficiently by a mean-field approximation. Therefore, it is expected that the agreement between Monte Carlo simulations and an analytical description (as presented above) decreases from system (a) to system (c). Nevertheless, it could be an interesting subject, to investigate the influence of these local effects on polarity formation for the three systems considered here. A comparison between the two approaches with respect to predictions on the overall yield of net polarity,  $\langle |X_{\text{net}}| \rangle$ , for a large number of energy sets (see above), would be of particular interest.

## 5.4 Conclusion

Applying the growth model introduced in Section 3.3, three different molecular systems were investigated: (a) Single-component crystals of polar (H) molecules, (b) solid solutions  $H_{1-X}G_X$  of polar (H) and non-polar (G) molecules, and (c) solid solutions  $H_{1-X}G_X$  of polar (H) and polar (G) molecules. These systems were compared with one another in terms of a statistical analysis based on Monte Carlo simulations. This study was focused mainly on differences in distributions of  $X_{\text{net}}$  and  $(X, X_{\text{net}})$  pairs, respectively, between systems (a), (b) and (c).

The fundamental difference between systems (b) and (c) is that in case of non-polar G molecules, polarity formation is mainly determined by *longitudinal* interaction energies only, while in case of polar G molecules, it is strongly influenced by *lateral* interaction energies too. In both systems, significant net polarity ( $|X_{\text{net}}| > 0$ ) may result for ordered structures HG ( $X = 0.5$ ).

The probability to show *no polarity* at all is of the same order of magnitude for all three systems and by far the most probable case (centrosymmetric native crystal structures assumed). However, in systems (b) and (c) the decrease of  $X_{\text{net}}$  distributions is considerable smaller in comparison with system (a) in the range  $0 < |X_{\text{net}}| \leq 0.5$ . *This shows, that solid solution formation is a powerful way to obtain growth-induced polar properties.* A high degree of polarity (i. e.  $|X_{\text{net}}| > 0.5$ ) is only realistic for system (c), where H and G components are polar.

The statistical analysis applied in this study has shown to give sufficient information to derive essential differences between the systems investigated. This approach is potentially useful, if even more complex systems are considered, e. g. crystal structures with a larger number of molecular interactions, three (or multi-) component systems or anisotropic interactions.

From a methodical point of view, a comparison between Monte Carlo simulations and the Markov mean-field approximation for the description of systems (a), (b) and (c) could clarify the validity and limitations of such an analytical theory.

# Chapter 6

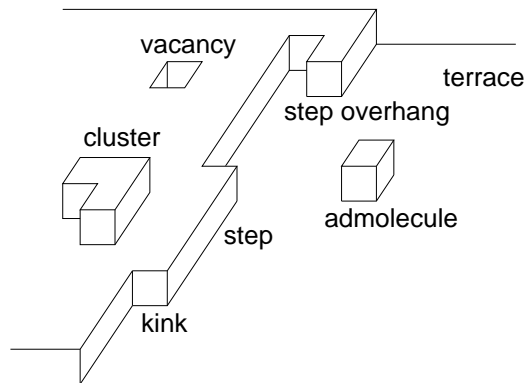
## Influence of the Growth Mechanism on Macroscopic Polarity Formation

### 6.1 Introduction

It has been shown that the appearance of polarity in molecular crystals with centrosymmetric structure (as well as the reduction of polar properties for crystals with polar symmetry) is caused by an *orientational disorder* up vs down of the dipoles of molecules during their attachment on growing crystal faces, see [43, 39, 40] (and the previous chapters about polarity formation in two-component systems).

Theoretically, growth-induced polarity formation has been described by a *layer-by-layer* growth model [40, 5]. Adlayers of polar molecules are attached successively to the crystal surface (substrate), the uppermost layer being allowed to relax to thermal equilibrium with respect to an up and down orientation of molecular dipoles, taking Ising-type nearest neighbor interactions into account, while formerly grown layers are kept frozen. After many attached layers, net polarity may result, due to a certain fraction of grown-in faulted orientations of molecular dipoles (orientational disorder). In this model, growth-induced polarity formation is a phenomenon mainly *thermodynamic* in its nature, since crystal growth takes place near thermal equilibrium.

However, the assumption of a flat crystal surface during growth is only valid for conditions of low temperature. At higher temperatures the surface becomes rough, see Fig. 6.1 [79]. Surface roughening gives rise to altered bindings in the molecular neighborhood and consequently to different attachment



**Figure 6.1:** Surface configuration of a crystal during growth. Above a certain temperature defects arise and the surface becomes rough. Molecules perform surface diffusion due to weak bond connections. They may form clusters or slide along a step until they reach a kink site and finally crystallize because molecular bindings with neighboring molecules at this position are strong enough against thermal vibrations. The degree of surface roughening influences the up and down orientation of dipoles during attachment of polar molecules.

probabilities for the up and down orientations of molecular dipoles, in comparison to the layer-by-layer growth.

Moreover, thermal relaxation of a *complete* adlayer requires sufficient time to equilibrate before newly attached molecules prevent reorientation of the underlying molecules due to a high energy of activation for such events in the bulk. That is, the growth rate must be much slower than characteristic equilibration times of the surface layer. However, this implies a high mobility of molecules on the surface, e. g. by surface diffusion or desorption-resorption mechanisms. Therefore, the assumption of a layer-by-layer growth model is valuable only for specific situations and the growth process as well as the surface morphology may have a considerable influence on the evolution of polarity.

The relationship between interface kinetics, i. e. deposition, evaporation and surface diffusion processes, and the surface morphology as well as their influence on the growth rate have been extensively studied for a long time, both analytically and with computer simulations, see e. g. [45, 28, 79, 60, 46, 47]. However, only a few studies have investigated the influence of the growth mechanism on the evolvment of a macroscopic growth-induced crystal property. (One example shows the interplay between phase ordering and roughening for growing films of binary alloys, see [54, 56, 55] and [17, 18].)

In this chapter, we investigate the influence of the *growth mechanism* on macroscopic polarity formation in single-component systems of polar molecules. The attachment of molecules, and with that the *final* orientational

state of their dipoles, occurs at characteristic positions on the crystal surface, depending on the strengths of molecular bindings, the rates of kinetic processes and geometrical constraints determined by the molecular packing. Here, five growth schemes are considered. The layer-by-layer growth process (0) is compared with four different growth models: (i) growth along steps, (ii) growth along kink sites, (iii) cluster growth, and (iv) random deposition, (for details, see below). These *idealized* growth processes reflect particularly a *reduced cooperativity* between molecules during their attachment on surface sites in real crystals. However, they still keep basic features of the original growth model (0). That is, kinetic or structural causes leading to a specific growth process are not investigated here, but solely its influence on the *thermodynamic* contribution to orientational order.

By means of Monte Carlo simulations, the evolution of polarity is investigated for each growth model, especially in the asymptotic limit after many steps of growth. Furthermore, growth models (i) - (iv) are analyzed with respect to the appearance of a continuous phase transition, as it has been observed for the layer-by-layer growth model (0) [40, 5]. By introducing an *effective* lateral coordination number  $z_{\perp}^{\text{eff}}$  for each growth model, results from an analytical description in terms of a Markov mean-field approximation (originally describing the layer-by-layer growth model [40]) are compared with simulations.

In Ref. [5] it was proven that the asymptotic statistics of the layer-by-layer growth model, i. e. the distribution of up and down oriented molecular dipoles after an arbitrary large number of attached layers, is equivalent to the canonical distribution of a two-layer system with appropriate interactions. In a second part of this chapter we investigate whether a similar approximative relation holds also for the other growth models presented here. Therein, this two-layer system is modified in such a way, that it accounts for a reduced lateral neighborhood during equilibration of molecular dipoles according to the corresponding growth models (i) - (iv). Even though an exact equivalence between growth processes and corresponding two-layer systems has not been found, a good agreement gives an indication of the thermodynamic nature of growth-induced polarity in growth models (i) - (iv).

## 6.2 The Growth Models and their Description by Monte Carlo Simulations

### 6.2.1 The Five Growth Models

All growth models considered here have the following rules and properties in common: Building blocks are polar molecules of the type  $A - \pi - D$  ( $A$ : electronic acceptor terminal;  $D$ : electronic donor terminal;  $\pi$ : delocalized  $\pi$ -electron system connecting  $A$  and  $D$ ), carrying a dipole moment  $\mu_{el}$  pointing from  $A$  to  $D$ . (In this chapter only single-component systems of polar molecules are considered.)

Crystals grow in the positive  $z$  direction. In  $x$  and  $y$  direction growth is limited by the dimensions of a rectangular seeding state. Molecules are arranged on the sites of a square lattice. The number of molecules in a completely filled layer is denoted by  $N = n_x n_y$ , where usually  $n_x = n_y$ . For the particular type of molecules involved (elongated principal axis), only one degree of freedom for their attachment on a surface site is taken into account: Either upwards ( $\uparrow$ ) or downwards ( $\downarrow$ ) with respect to the projection of their dipole moment onto the  $z$  direction, pointing their donor ( $D$ ) or acceptor ( $A$ ) terminal toward the nutrient, respectively. That is, molecules feature simply two directional states ( $s = \pm 1$ ).

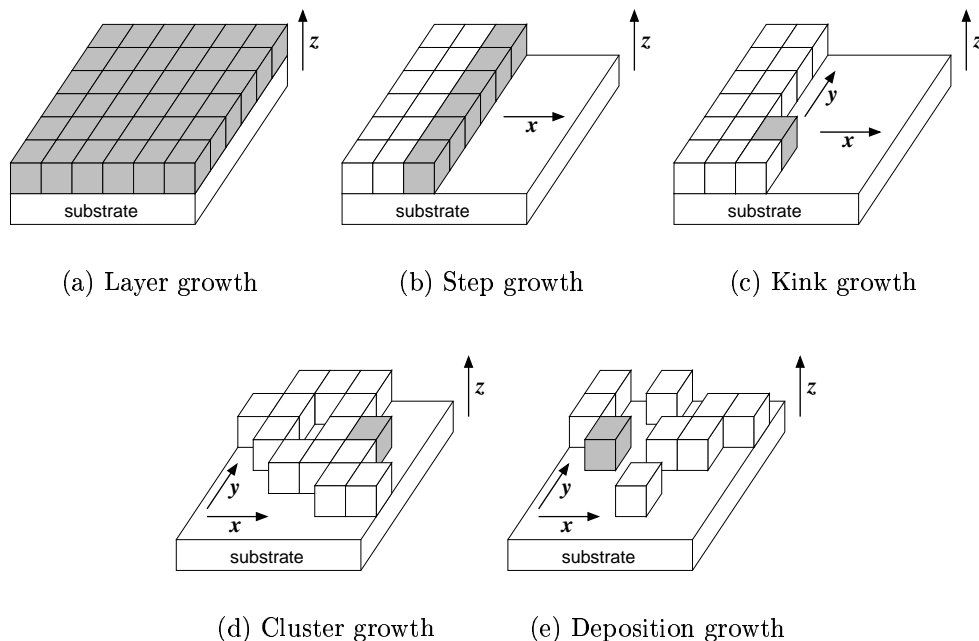
Upon growth molecules are subjected to thermal relaxation with respect to the orientational state of their dipoles, taking nearest neighbor interactions among molecules within the same layer (lateral) and between adjacent layers (longitudinal) into account. Pair interaction energies depend on the directional state of the two molecules involved (see definitions of interaction energies between polar (H) molecules only in Table 5.1). Laterally, isotropic interactions are assumed. Basic parameters are the energy differences  $\Delta E_{\perp} = E_p - E_{ap}$  (lateral) as well as  $\Delta E_A = E_{AA} - E_{AD}$  and  $\Delta E_D = E_{DD} - E_{AD}$  (longitudinal).

The five growth models are ranged according to a reduced cooperativity between neighboring molecules:

- (0) *Layer growth*: The crystal grows layer-by-layer, i. e. complete adlayers of molecules are attached to the surface, see Fig 6.2(a). Thermal relaxation of an adlayer takes place after all molecules are attached. Previously grown layers are kept frozen, i. e.  $180^\circ$  orientational flips of molecular dipoles are not allowed in the bulk. Within a layer molecules are surrounded by four nearest neighbor molecules (lateral coordination number  $z_{\perp} = 4$ ). This growth process assumes a slow growth rate, where the time for the growth of a layer is much larger than the sur-

face layer relaxation time (high mobility of molecules on the surface). Growth mechanism (0) was thoroughly discussed in [40, 5]. Here, it represents the *reference case*.

- (i) *Step growth*: Crystal growth takes place along surface steps by the attachment of complete columns of molecules, see Fig. 6.2(b). Molecules at the edge of a step are subjected to thermal relaxation with respect to their dipole orientations. Formerly attached molecules, i.e. in the interior of the surface as well as in the bulk, are considered to be frozen. Once the step has reached the border of the crystal, i.e. a complete layer of molecules has been filled, a new step is formed and the process starts over for a new adlayer. Here,  $z_{\perp} = 3$ , but only two of the neighboring molecules thermalize simultaneously (those being in the same column). Growth model (i) is characterized by a fast equilibration for molecules along the edge of a step, but a high energy of activation for the whole surface layer, due to the reduced mobility of molecules being completely surrounded by neighboring molecules.
- (ii) *Kink growth*: Attachment takes place at kink sites, see Fig. 6.2(c). By adding molecules, an initial kink position slides along a step until it reaches the border of the crystal. A new kink site is formed and molecules are attached, one after the other, along the edge of the step in the same manner until the entire surface layer is filled. Afterwards, the process is continued above the completed layer. Only molecules at the kink position are allowed to thermalize, while any previously attached molecules (surface layer and bulk) are kept frozen ( $z_{\perp} = 2$ ).
- (iii) *Cluster growth*: Starting from a seed molecule on the flat crystal surface, one of its neighboring sites is occupied randomly by another molecule. Likewise, subsequently impinging molecules are attached randomly at neighboring sites (the perimeter) of this growing cluster, see Fig. 6.2(d). Once a molecule is thermalized within the cluster, it is kept frozen thereafter. The process is continued until the cluster has filled the whole surface, see also [19]. Upon completion of a layer, a new seed molecule is attached randomly (and thermalized) on the surface and a next cluster starts to grow ( $1 \leq z_{\perp} \leq 4$ , for the seed molecule,  $z_{\perp} = 0$ ). In this growth model molecules are highly mobile as long as they do not encounter lateral interactions with molecules belonging to the adlayer.
- (iv) *Deposition Growth*: Molecules are randomly deposited on the crystal surface, see Fig. 6.2(e). They thermalize and are frozen immediately



**Figure 6.2:** The five growth models. Molecules are represented as cubic building blocks. *Shaded units:* Molecules, being allowed to thermalize simultaneously with respect to an up and down orientation of their dipoles. White parts (adlayer and substrate) are kept frozen. For details, see text.

after being attached to the surface ( $0 \leq z_{\perp} \leq 4$ ), see also [77]. Sites of a new layer start to be occupied by molecules only, when the previous layer has been completed. Except relaxation during the impingement on the surface, molecules feature no mobility at all in this growth process. Such a situation may occur for fast growth rates and surface morphologies which do not show surface diffusion nor rapid desorption from unfavorable positions.

Details of growth mechanisms (0) - (iv) in terms of Monte Carlo simulations are discussed in Section 6.2.2, including the treatment of boundary conditions.

All growth models describe a state of minimal free energy *only* for certain units of the surface layer: (0) a complete adlayer, (i) a column of molecules, (ii) - (iv) a single molecule. Therefore, growth processes lead to a metastable bulk state, being justified only if re-orientational flips of molecules are not taking place after crystallization is completed.

It is clear that neither does a real crystal grow exactly according to one of the processes described above, nor do they cover the entire range of possi-



ble growth schemes. (For instance, spiral growth is another typical process which is not considered here [85]).

Nevertheless, these growth models represent a logical decomposition of complexity given by real growing crystal surfaces, which is focusing on those processes which may influence polarity formation. In real crystals, combinations of these growth mechanisms can occur. Here, they are treated separately, in order to analyze their individual influence on growth-induced polarity formation. As already mentioned above, kinetic or structural conditions leading to a certain growth scheme are not studied here.

## 6.2.2 Monte Carlo Simulations

So far, general characteristics of the five growth mechanisms were described as well as possible instances for their occurrence. Here, technical details of implementation using Monte Carlo simulations are briefly discussed.

Each growth process starts off by the definition of the type of seeding state, e. g. uniform  $\uparrow$  or  $\downarrow$ , random, or antiparallel. Ideally, in the asymptotic limit of many grown layers ( $z \rightarrow \infty$ ) macroscopic polarity does not depend on this initial state. However, this issue needs a careful analysis for each growth process in simulations.

For the thermalization of a unit (i. e. adlayer, column, or single molecule, respectively), nearest neighbor couplings among molecules within the surface layer (lateral) and longitudinal interactions with molecules on corresponding sites of the previously grown frozen substrate layer (or, initially, the seeding state) are taken into account. Laterally, periodic boundary conditions are applied for all growth models. In order to fulfill periodicity in case of step (i) and kink (ii) growth, respectively, the following rule is applied: For *border* molecules on the surface, if necessary nearest neighbor molecules do not exist on the growing adlayer, lateral couplings to molecules of the *substrate* layer (on corresponding sites of the opposite border) are taken into account instead. Defined as such, constant  $z_{\perp} = 3$  (i) and  $z_{\perp} = 2$  (ii) is provided for *all* molecules in these growth models. In case of cluster (iii) and deposition (iv) growth, the appearance of variable lateral molecular neighborhoods ( $0 \leq z_{\perp} \leq 4$ ) is intended.

In the case of layer and step growth, adlayers (0) or columns (i) of molecules are initialized randomly, and then, thermalized using the Metropolis algorithm [66, 58]. The equilibration time  $\tau_E$  (measured in Monte Carlo steps, on average, per molecule) is expected to be much smaller for step growth (i) than for layer growth (0), since no critical slowing down is observed for 1D columns of molecules. Here, the following orders of magnitude are considered to be sufficient:  $\tau_E \approx N^2$  for layer growth and  $\tau_E \approx n_x$  or  $n_y$  for step growth.

In cases (ii) - (iv), where only one molecule is thermalized at the time, the probabilities for the up and down dipole orientations,  $p(\uparrow)$  and  $p(\downarrow)$ , respectively, are given by normalized Boltzmann factors. That is,

$$p(\downarrow) = \frac{1}{1 + e^{-\beta(E_{\uparrow} - E_{\downarrow})}}, \quad (6.1)$$

where  $E_{\downarrow}$  and  $E_{\uparrow}$  are the sums of interactions between a thermalizing molecule (in down or up state, respectively) and its nearest neighbors and  $p(\uparrow) = 1 - p(\downarrow)$ , ( $\beta = 1/k_B T$ ).

In case of step growth (i), the first column of molecules is always attached at the border of the crystal. Correspondingly, in case of kink growth (ii), the first molecule is attached at a corner of the crystal. (Note that this does not introduce any bias against the evolution of polarity.) Due to the fourfold symmetry of the square lattice as well as the assumption of isotropic lateral interactions, it is sufficient to consider step growth from one border and kink growth from one corner of a crystal only. Besides, for growth model (i) and (ii), the same directionality is kept during attachments of molecules on the surface.

The growth equilibration time  $\tau_G$  measures the number of attached layers until the growth process has lost its memory from the initial seeding state. Generally, this takes place already after a few grown layers for all growth models investigated here. Therefore,  $50 \leq \tau_G < 1000$  is considered as sufficient.

Measurements of physical quantities are performed after an adlayer has been completed. The sampling time  $\tau_S$  (measured in completed adlayers) denotes the number of measurements (here,  $10^3 < \tau_S < 10^6$ ). Measurements are carried out after  $\tau_G$  growth steps.

## 6.3 Results

Throughout this study, growth models (0) - (iv) are analyzed for four different longitudinal coupling parameters,  $\Delta E_f = \Delta E_A - \Delta E_D$ , [kJ/mol]:

- (1)  $\Delta E_A = 15, \quad \Delta E_D = 10 \quad (\Delta E_f = 5)$
- (2)  $\Delta E_A = 5, \quad \Delta E_D = 2 \quad (\Delta E_f = 3)$
- (3)  $\Delta E_A = 3, \quad \Delta E_D = 1 \quad (\Delta E_f = 2)$
- (4)  $\Delta E_A = 2, \quad \Delta E_D = 1 \quad (\Delta E_f = 1)$

They are chosen as such in order to investigate the influence of decreasing longitudinal couplings on the evolution of orientational order for the different growth schemes. Growth models are analyzed for varying lateral energy

differences  $\Delta E_{\perp}$ . Temperature  $T = 300$  K is kept constant in all Monte Carlo simulations. For given parameters, tests have shown that simulation results do not depend on the initial seeding state. However, in order to avoid erroneous frozen configurations (anti-phase boundaries) in case of antiferromagnetic ordering within adlayers ( $\Delta E_{\perp} > 0$ ), a centrosymmetric seeding state has been selected.

### 6.3.1 Polarity Formation

Macroscopic net polarity,  $X_{\text{net}}$ , is defined as the difference between downwards ( $\downarrow$ ) and upwards ( $\uparrow$ ) oriented molecular dipoles in the asymptotic limit of many attached layers ( $z \rightarrow \infty$ ). In Monte Carlo simulations,  $X_{\text{net}}$  corresponds to the mean value from  $\tau_S$  layer polarizations, (which are denoted by  $x_{\text{net}}$ ).

Figs. 6.3 - 6.6 show  $X_{\text{net}}$  obtained from Monte Carlo simulations for growth models (0) - (iv) as a function of the lateral energy difference ( $\Delta E_{\perp}$ ). At  $\Delta E_{\perp} = 0$  kJ/mol, i. e. no lateral coupling, attachment of molecules is described by isolated 1D chains and all growth models become equivalent. Therefore,  $X_{\text{net}}$  curves from growth models (0) - (iv) must cross each other at this value. (This is a good test for the verification of algorithms for the simulation of the different growth mechanisms.)

Step (i) and kink (ii) growth show principally the same behavior for  $X_{\text{net}}$  in comparison to the layer-by-layer growth model (0). Growing crystals tend towards a completely antiferromagnetic ( $X_{\text{net}} = 0$ ) or ferromagnetic ( $X_{\text{net}} = 1$ ) ordering for  $\Delta E_{\perp} \rightarrow \pm\infty$ , respectively, see also Table 6.3. Further on, a bump is observed in the slopes of  $X_{\text{net}}$  curves for  $\Delta E_{\perp} > 0$  in growth models (0) - (ii), indicating a singularity (see below). However, for all longitudinal energy parameters (Figs. 6.3 - 6.6), the transition from ferromagnetic to antiferromagnetic ordering is smoother for step (i) and kink (ii) growth, compared to the layer growth (0). That is, it holds  $X_{\text{net}}(\text{layer}) > X_{\text{net}}(\text{step}) > X_{\text{net}}(\text{kink})$  for  $\Delta E_{\perp} < 0$ , and  $X_{\text{net}}(\text{layer}) < X_{\text{net}}(\text{step}) < X_{\text{net}}(\text{kink})$  for  $\Delta E_{\perp} > 0$ .

For large longitudinal coupling parameters (relative to  $\Delta E_{\perp}$ ), cluster (iii) and deposition (iv) growth show a very similar behavior in  $X_{\text{net}}$  as kink (i) growth, see Fig. 6.3. However, the smaller these longitudinal interactions, the more deviate growth models (iii) and (iv) from growth schemes (0) - (ii). For  $\Delta E_{\perp} < 0$ ,  $X_{\text{net}}$  may even pass a maximum in case of cluster and deposition growth. Generally, in these two growth processes  $X_{\text{net}}$  decreases slower towards zero for  $\Delta E_{\perp} \rightarrow \infty$ .

For a discussion of these observations, see Section 6.6.

### 6.3.2 Phase Transition

For the layer-by-layer growth model (0) a continuous phase transition from a disordered to an antiferromagnetic ordered (AFO) state was found [5, 40]. Here, we investigate whether such a phase transition is preserved in growth models (i) - (iv), despite a reduced cooperativity between neighboring molecules in these growth processes.

A suitable order parameter,  $\phi$ , to examine the existence of an AFO phase transition by means of Monte Carlo simulations is given as

$$\phi = \frac{1}{2} \langle |x_{\text{net}}(g) - x_{\text{net}}| \rangle_{\text{max}}, \quad (6.2)$$

where  $x_{\text{net}}(g)$  ( $g = I, II$ ) denote the two sublattice polarizations (sublattice  $I$ ,  $x+y = \text{even}$ ; sublattice  $II$ ,  $x+y = \text{odd}$ ).  $\langle \rangle_{\text{max}}$  means the value corresponding to the maximum of the distribution.

Besides, the specific heat  $C_V = \partial U / \partial T$  at constant volume is measured ( $U$  is the internal energy). A sharp peak in  $C_V$  indicates the appearance of a phase transition, see e. g. [2] or [32, 66] for the Ising model. In Monte Carlo simulations, the specific heat per molecule,  $c_V$ , can be obtained from energy fluctuations as (see [66])

$$c_V = \frac{k_B \beta^2}{N} (\langle E^2 \rangle - \langle E \rangle^2). \quad (6.3)$$

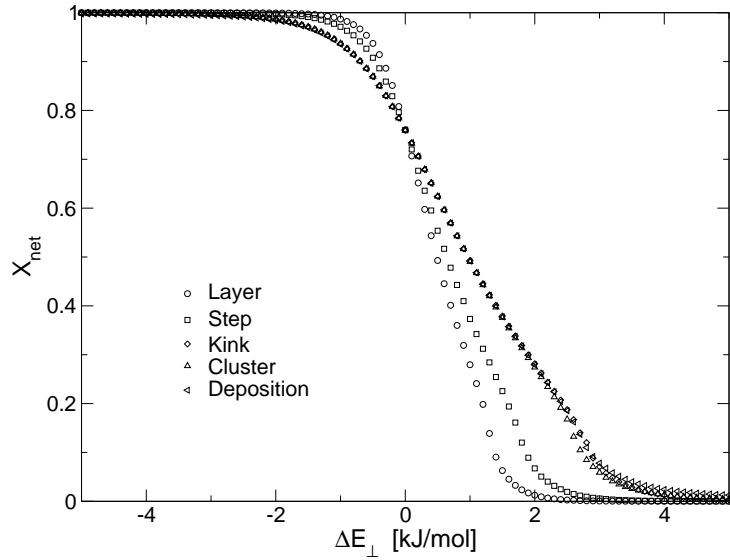
$E$  is the energy sum of all lateral and longitudinal intermolecular couplings of a *completed* adlayer.

In Figs. 6.7 - 6.10 and Figs. 6.11 - 6.14 results are given for  $\phi$  and  $c_V$ , respectively, in dependence on  $\Delta E_{\perp}$  for growth models (0) - (iv). Note that in curves with  $\phi$ , the positive range of  $\Delta E_{\perp}$  is shown only, since this order parameter is always zero for  $\Delta E_{\perp} < 0$ .

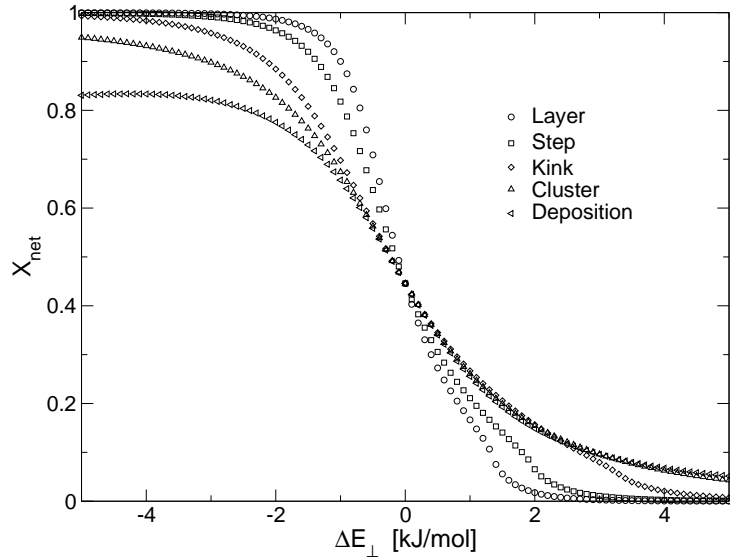
For growth models (0) - (ii), the rapid increase of  $\phi$  as well as the sharp peak of  $c_V$  (at corresponding critical  $\Delta E_{\perp} > 0$ ) for any given longitudinal couplings clearly indicate an AFO phase transition. Additionally, a *diffuse* transition from a ferromagnetic ordered ( $\Delta E_{\perp} < 0$ ) to a disordered ( $\Delta E_{\perp} = 0$ ) state is observed from curves of the specific heat  $c_V$ .

Contrarily, in case of cluster (iii) and deposition (iv) growth, for medium and small longitudinal coupling parameters (Figs. 6.8 - 6.10 and 6.12 - 6.14, respectively),  $\phi$  remains zero for any  $\Delta E_{\perp} > 0$  and  $c_V$  shows only a minimum at  $\Delta E_{\perp} = 0$  (all growth models must have the same  $c_V$  at this point). That is, neither an AFO phase transition, nor a diffuse transition is existent for these growth schemes here. However, this changes for  $\Delta E_A = 15$  and  $\Delta E_D = 10$  [kJ/mol] (Figs. 6.7 and 6.11), where also cluster and deposition growth

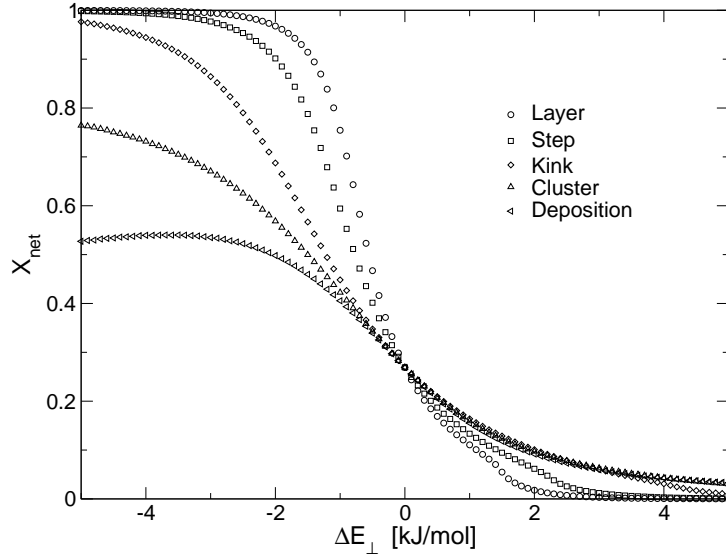
show the characteristic behavior in  $\phi$  and  $c_V$  for the existence of an AFO phase transition (corresponding curves resemble strongly those of kink (ii) growth, compare also with Fig. 6.3).



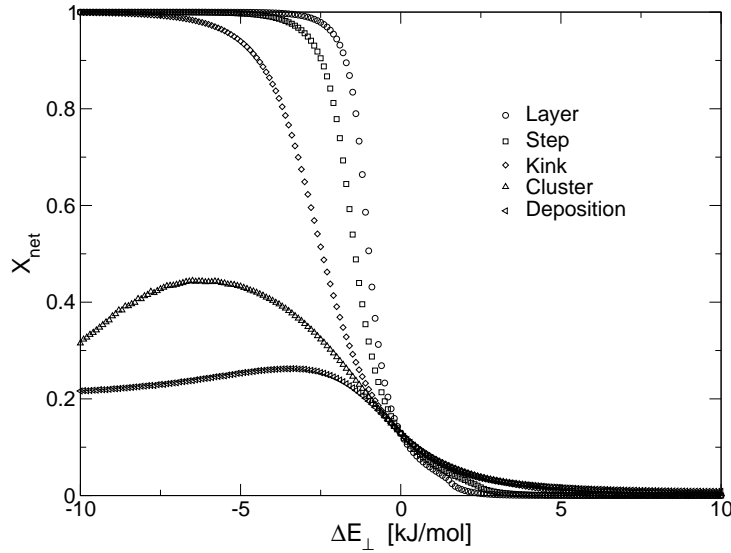
**Figure 6.3:** Net polarity ( $X_{\text{net}}$ ) vs lateral coupling difference ( $\Delta E_{\perp}$ ) for growth models (0) - (iv) from Monte Carlo simulations.  $\Delta E_A = 15$  and  $\Delta E_D = 10$  [kJ/mol],  $T = 300$  K.  $s_L = 50 \times 50$ ;  $\tau_G = 200$ ;  $\tau_S = 10\,000$  (i),  $200\,000$  (ii),  $100\,000$  (iii) and (iv); centrosymmetric seeding state. For layer-by-layer growth (0), results are obtained from the equivalent two-layer system ( $\tau_G = 20\,000$ ,  $\tau_S = 100\,000$ ).



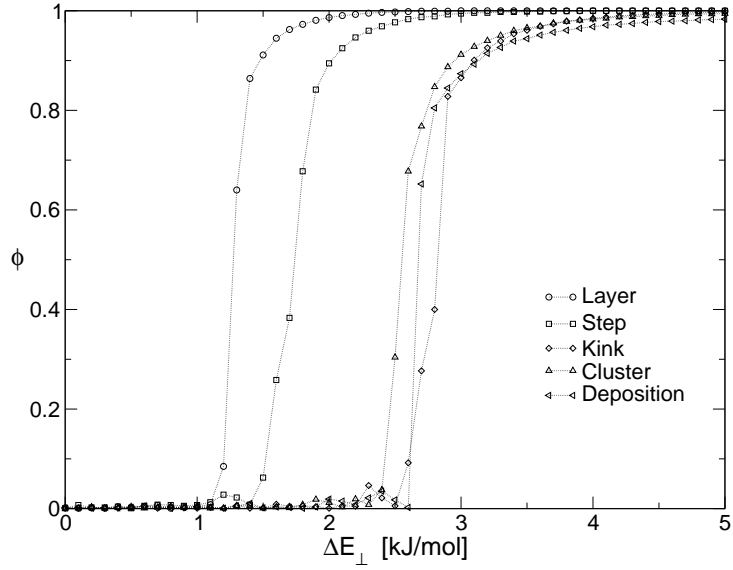
**Figure 6.4:** Net polarity ( $X_{\text{net}}$ ) vs lateral coupling difference ( $\Delta E_{\perp}$ ) for growth models (0) - (iv) from Monte Carlo simulations.  $\Delta E_A = 5$  and  $\Delta E_D = 2$  [kJ/mol],  $T = 300$  K.  $s_L = 50 \times 50$ ;  $\tau_G = 200$ ;  $\tau_S = 10\,000$  (i),  $200\,000$  (ii),  $100\,000$  (iii) and (iv); centrosymmetric seeding state. For layer-by-layer growth (0), results are obtained from the equivalent two-layer system ( $\tau_G = 20\,000$ ,  $\tau_S = 100\,000$ ).



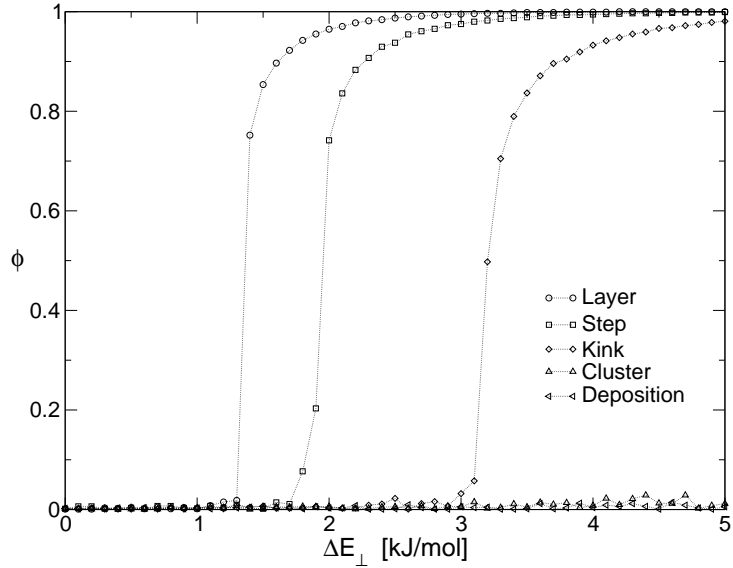
**Figure 6.5:** Net polarity ( $X_{\text{net}}$ ) vs lateral coupling difference ( $\Delta E_{\perp}$ ) for growth models (0) - (iv) from Monte Carlo simulations.  $\Delta E_A = 3$  and  $\Delta E_D = 1$  [kJ/mol],  $T = 300$  K.  $s_L = 50 \times 50$ ;  $\tau_G = 200$ ;  $\tau_S = 10\,000$  (i),  $200\,000$  (ii),  $100\,000$  (iii) and (iv); centrosymmetric seeding state. For layer-by-layer growth (0), results are obtained from the equivalent two-layer system ( $\tau_G = 20\,000$ ,  $\tau_S = 100\,000$ ).



**Figure 6.6:** Net polarity ( $X_{\text{net}}$ ) vs lateral coupling difference ( $\Delta E_{\perp}$ ) for growth models (0) - (iv) from Monte Carlo simulations.  $\Delta E_A = 2$  and  $\Delta E_D = 1$  [kJ/mol],  $T = 300$  K.  $s_L = 50 \times 50$ ;  $\tau_G = 200$ ;  $\tau_S = 10\,000$  (i),  $200\,000$  (ii),  $100\,000$  (iii) and (iv); centrosymmetric seeding state. For layer-by-layer growth (0), results are obtained from the equivalent two-layer system ( $\tau_G = 20\,000$ ,  $\tau_S = 100\,000$ ).

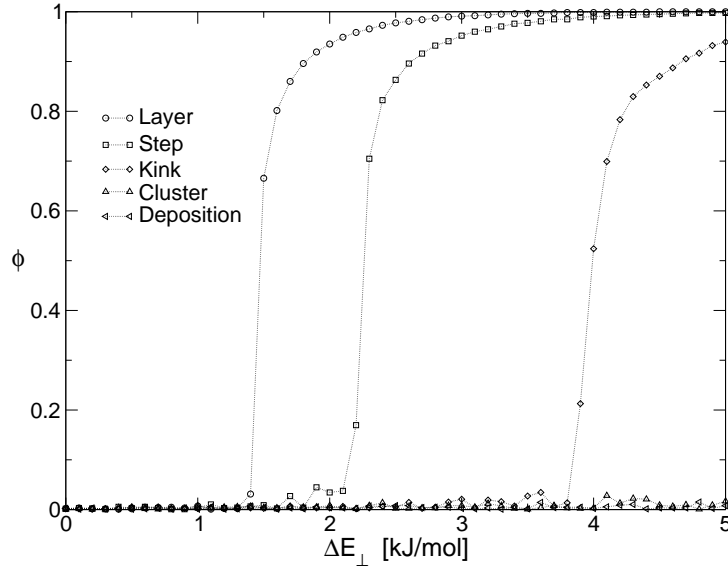


**Figure 6.7:** Order parameter ( $\phi$ ) vs lateral coupling difference ( $\Delta E_{\perp}$ ) for growth models (0) - (iv) from Monte Carlo simulations.  $\Delta E_A = 15$  and  $\Delta E_D = 10$  [kJ/mol],  $T = 300$  K.  $s_L = 50 \times 50$ ;  $\tau_G = 200$ ;  $\tau_S = 10\,000$  (i),  $200\,000$  (ii),  $100\,000$  (iii) and (iv); centrosymmetric seeding state. For layer-by-layer growth (0), results are obtained from the equivalent two-layer system ( $\tau_G = 20\,000$ ,  $\tau_S = 100\,000$ ). Dotted lines are guidelines for the eyes only.

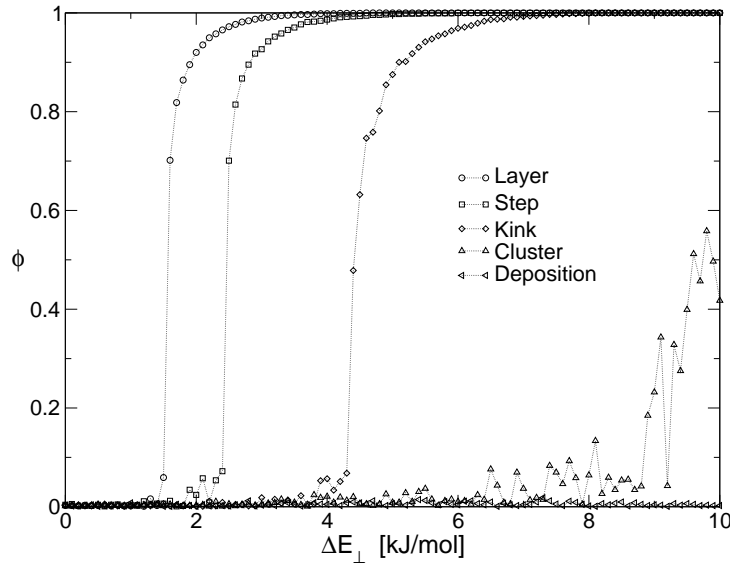


**Figure 6.8:** Order parameter ( $\phi$ ) vs lateral coupling difference ( $\Delta E_{\perp}$ ) for growth models (0) - (iv) from Monte Carlo simulations.  $\Delta E_A = 5$  and  $\Delta E_D = 2$  [kJ/mol],  $T = 300$  K.  $s_L = 50 \times 50$ ;  $\tau_G = 200$ ;  $\tau_S = 10\,000$  (i),  $200\,000$  (ii),  $100\,000$  (iii) and (iv); centrosymmetric seeding state. For layer-by-layer growth (0), results are obtained from the equivalent two-layer system ( $\tau_G = 20\,000$ ,  $\tau_S = 100\,000$ ). Dotted lines are guidelines for the eyes only.

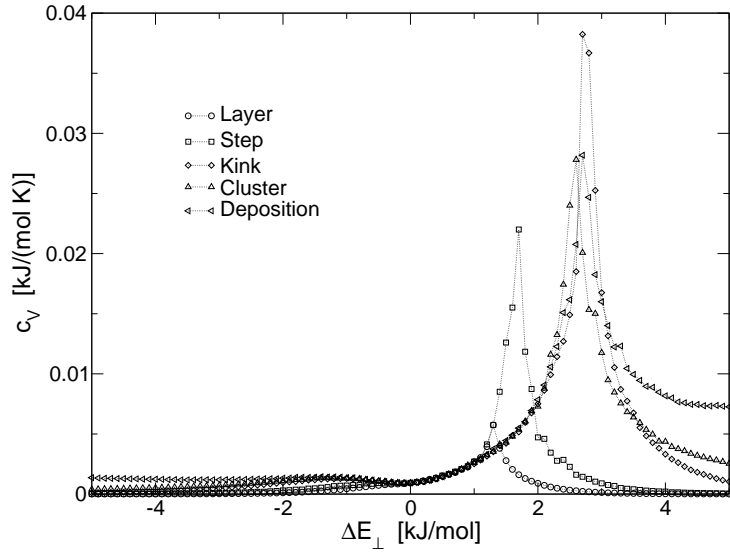




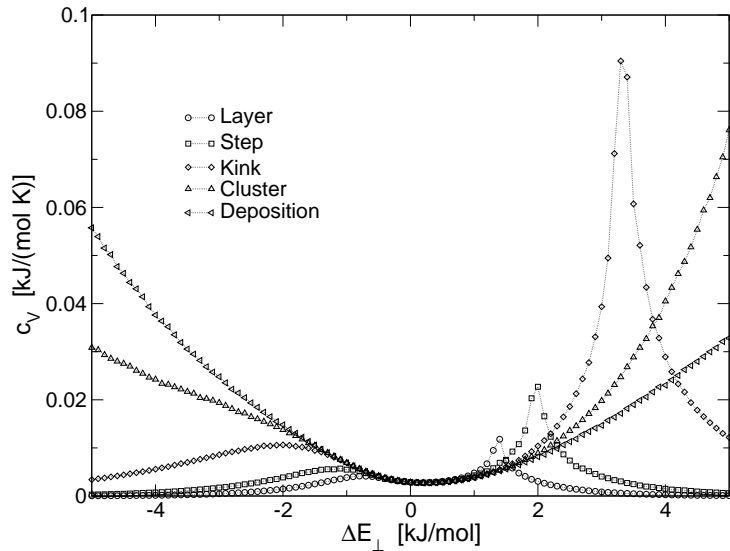
**Figure 6.9:** Order parameter ( $\phi$ ) vs lateral coupling difference ( $\Delta E_{\perp}$ ) for growth models (0) - (iv) from Monte Carlo simulations.  $\Delta E_A = 3$  and  $\Delta E_D = 1$  [kJ/mol],  $T = 300$  K.  $s_L = 50 \times 50$ ;  $\tau_G = 200$ ;  $\tau_S = 10\,000$  (i),  $200\,000$  (ii),  $100\,000$  (iii) and (iv); centrosymmetric seeding state. For layer-by-layer growth (0), results are obtained from the equivalent two-layer system ( $\tau_G = 20\,000$ ,  $\tau_S = 100\,000$ ). Dotted lines are guidelines for the eyes only.



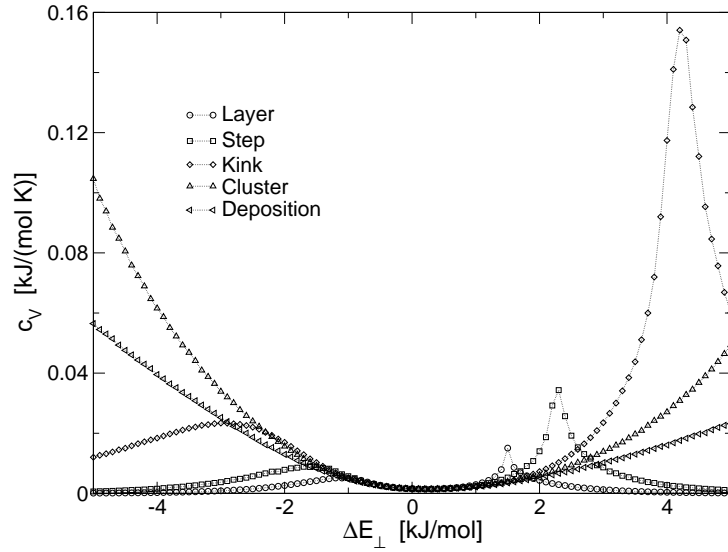
**Figure 6.10:** Order parameter ( $\phi$ ) vs lateral coupling difference ( $\Delta E_{\perp}$ ) for growth models (0) - (iv) from Monte Carlo simulations.  $\Delta E_A = 2$  and  $\Delta E_D = 1$  [kJ/mol],  $T = 300$  K.  $s_L = 50 \times 50$ ;  $\tau_G = 200$ ;  $\tau_S = 10\,000$  (i),  $200\,000$  (ii),  $100\,000$  (iii) and (iv); centrosymmetric seeding state. For layer-by-layer growth (0), results are obtained from the equivalent two-layer system ( $\tau_G = 20\,000$ ,  $\tau_S = 100\,000$ ). Dotted lines are guidelines for the eyes only.



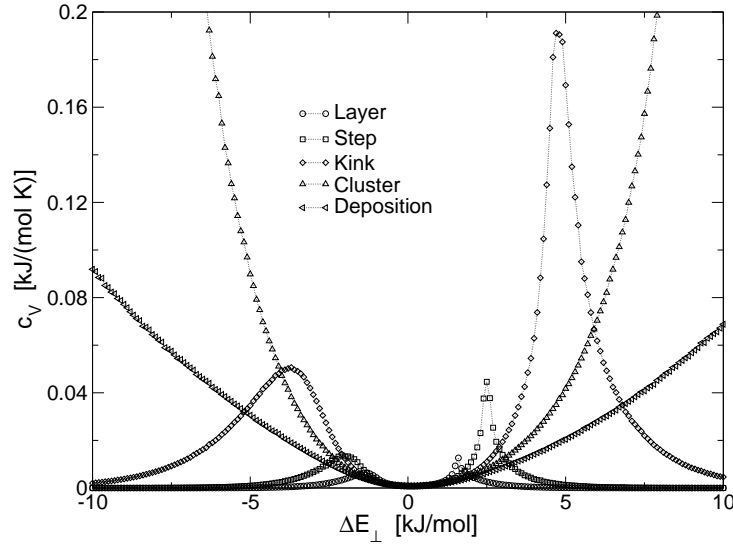
**Figure 6.11:** Specific heat ( $c_V$ ) vs lateral coupling difference ( $\Delta E_\perp$ ) for growth models (0) - (iv) from Monte Carlo simulations.  $\Delta E_A = 15$  and  $\Delta E_D = 10$  [kJ/mol],  $T = 300$  K.  $s_L = 50 \times 50$ ;  $\tau_G = 200$ ;  $\tau_S = 10\,000$  (i),  $200\,000$  (ii),  $100\,000$  (iii) and (iv); centrosymmetric seeding state. For layer-by-layer growth (0), results are obtained from the equivalent two-layer system ( $\tau_G = 20\,000$ ,  $\tau_S = 100\,000$ ). Dotted lines are guidelines for the eyes only.



**Figure 6.12:** Specific heat ( $c_V$ ) vs lateral coupling difference ( $\Delta E_\perp$ ) for growth models (0) - (iv) from Monte Carlo simulations.  $\Delta E_A = 5$  and  $\Delta E_D = 2$  [kJ/mol],  $T = 300$  K.  $s_L = 50 \times 50$ ;  $\tau_G = 200$ ;  $\tau_S = 10\,000$  (i),  $200\,000$  (ii),  $100\,000$  (iii) and (iv); centrosymmetric seeding state. For layer-by-layer growth (0), results are obtained from the equivalent two-layer system ( $\tau_G = 20\,000$ ,  $\tau_S = 100\,000$ ). Dotted lines are guidelines for the eyes only.



**Figure 6.13:** Specific heat ( $c_V$ ) vs lateral coupling difference ( $\Delta E_\perp$ ) for growth models (0) - (iv) from Monte Carlo simulations.  $\Delta E_A = 3$  and  $\Delta E_D = 1$  [kJ/mol],  $T = 300$  K.  $s_L = 50 \times 50$ ;  $\tau_G = 200$ ;  $\tau_S = 10\,000$  (i),  $200\,000$  (ii),  $100\,000$  (iii) and (iv); centrosymmetric seeding state. For layer-by-layer growth (0), results are obtained from the equivalent two-layer system ( $\tau_G = 20\,000$ ,  $\tau_S = 100\,000$ ). Dotted lines are guidelines for the eyes only.



**Figure 6.14:** Specific heat ( $c_V$ ) vs lateral coupling difference ( $\Delta E_\perp$ ) for growth models (0) - (iv) from Monte Carlo simulations.  $\Delta E_A = 2$  and  $\Delta E_D = 1$  [kJ/mol],  $T = 300$  K.  $s_L = 50 \times 50$ ;  $\tau_G = 200$ ;  $\tau_S = 10\,000$  (i),  $200\,000$  (ii),  $100\,000$  (iii) and (iv); centrosymmetric seeding state. For layer-by-layer growth (0), results are obtained from the equivalent two-layer system ( $\tau_G = 20\,000$ ,  $\tau_S = 100\,000$ ). Dotted lines are guidelines for the eyes only.

## 6.4 Markov Mean-Field Approximation

A straightforward approach for the analytical description of growth models (i) - (iv) is to apply the Markov mean-field approximation of the layer-by-layer growth model (0), however introducing an effective lateral coordination number  $z_{\perp}^{\text{eff}}$ , which accounts for a reduced cooperativity during thermalization of molecules on surface sites, ( $z_{\perp}^{\text{eff}} = 4$  for the layer-by-layer growth model).

The analytical treatment of the layer-by-layer growth model (0) in terms of a Markov mean-field approximation has been described in detail in Chapter 3 (for two-component systems), [40] and [5]. Here, the equations (in a compact form) for the calculation of  $X_{\text{net}}$  are summarized, which result from those in Chapter 3 for a single-component crystal of polar molecules only, i. e.  $X_{\text{gas}} = 0$ .

$X_A^g$  is the fraction of polar molecules with  $A$ -terminal oriented toward the nutrient ( $s = -1$ ) for sublattice  $g = I, II$ . The fraction of molecules with  $D$ -terminal oriented toward the nutrient ( $s = +1$ ),  $X_D^g$ , is given by normalization conditions  $X_A^g + X_D^g = 1$ ,  $g = I, II$ . It follows

$$X_A^I = \frac{1 + e^{\beta f_{AA}^I}}{2 + e^{\beta f_{AA}^I} + e^{\beta f_{DD}^I}}, \quad (6.4)$$

$$X_A^{II} = \frac{1 + e^{\beta f_{AA}^{II}}}{2 + e^{\beta f_{AA}^{II}} + e^{\beta f_{DD}^{II}}}, \quad (6.5)$$

with

$$f_{AA}^I = \Delta E_A + z_{\perp}^{\text{eff}} \Delta E_{\perp} (1 - 2X_A^{II}), \quad (6.6a)$$

$$f_{DD}^I = \Delta E_D - z_{\perp}^{\text{eff}} \Delta E_{\perp} (1 - 2X_A^{II}), \quad (6.6b)$$

$$f_{AA}^{II} = \Delta E_A + z_{\perp}^{\text{eff}} \Delta E_{\perp} (1 - 2X_A^I), \quad (6.6c)$$

$$f_{DD}^{II} = \Delta E_D - z_{\perp}^{\text{eff}} \Delta E_{\perp} (1 - 2X_A^I). \quad (6.6d)$$

$z_{\perp}^{\text{eff}}$  denotes the *average* number of occupied neighbor sites during thermalization of molecules on the crystal surface for growth models (0) - (iv), see Table 6.2. Eqs. (6.4) and (6.5) are solved numerically, see Appendix 3.8. Finally,  $X_{\text{net}}$  is given as

$$X_{\text{net}} = X_A^I + X_A^{II} - 1. \quad (6.7)$$

Note that  $z_{\perp}^{\text{eff}}$  is the only characteristic parameter distinguishing growth models (0) - (iv) in this approximation. That is, kink (ii), cluster (iii) and deposition (iv) growth are equivalent within the present description, because

they all have  $z_{\perp}^{\text{eff}} = 2$  (see Table 6.2). Furthermore, it has to be emphasized that the mean-field estimate of the lateral couplings assumes thermalization of molecules after an adlayer has been completely occupied by molecules. However, this is not the case for growth models (i) - (iv). Therefore, it is already clear that the present mean-field approach may only provide reasonable results for homogeneous distributions of up and down oriented molecules on the crystal surface.

Comparisons of  $X_{\text{net}}$  between growth models and corresponding two-layer systems (see below) from Monte Carlo simulations as well as the present Markov mean-field approximation are given in Section 6.5.3.

## 6.5 The Two-Layer Systems

For the *layer growth* model (0) it was proven that the asymptotic statistics of the system consisting of the thermalized adlayer and the previously attached substrate layer is equivalent to the canonical distribution of a *two-layer system* with appropriate interactions, see Ref. [5]. In this section, we address the question whether similar relations may hold for the other growth models discussed here, at least within certain ranges of intermolecular couplings.

In order to provide a basis for the argumentation below, the case of the layer-by-layer growth model is shortly reviewed (using the same notations as in [5]).

### 6.5.1 The Equivalent Two-Layer System for the Layer Growth Model (0)

In the layer growth model (0) the asymptotic distribution  $\pi_{\sigma}$  denotes the probability distribution that the thermalized uppermost layer (surface) is in state  $\sigma$  ( $\sigma = 1, \dots, 2^N$ ) after infinitely many growth steps ( $z \rightarrow \infty$ ). A state  $\sigma$  is specified by the values of all dipole orientations,  $\{s_{xy}\}$ ,  $x = 1, \dots, n_x$ ,  $y = 1, \dots, n_y$ . The proof in [5] states that  $\pi_{\sigma}$  is equal to the *thermal equilibrium* distribution of *one* layer of a two-layer system with the following structure and interactions:

- The system consists of two layers ( $L, L'$ ) of the same geometry (square lattice) and size as the layers in the growth model. Each lattice site is occupied by a polar molecule in state up or down ( $s = \pm 1$ ).
- Within a layer ( $L$  or  $L'$ ) the same lateral interactions hold as in the layer growth model (periodic boundary conditions). That is, each molecule interacts with its four nearest neighbors according to  $\Delta E_{\perp}$ .

**Table 6.1:** Longitudinal energy differences for the layer growth model (GM) and the two-layer system (LL).  $s'$  and  $s$  denote corresponding sites on the substrate and adlayer (for GM) as well as layers  $L'$  and  $L$  (for LL), respectively.  $\leftarrow$  and  $\rightarrow$  represent the down and up dipole orientations of molecules, respectively.

$s'$	$s$	Growth model (GM)	Two-layer system (LL)
$\leftarrow$	$\leftarrow$	0	$-\Delta E_A$
$\leftarrow$	$\rightarrow$	$\Delta E_A$	0
$\rightarrow$	$\leftarrow$	$\Delta E_D$	0
$\rightarrow$	$\rightarrow$	0	$-\Delta E_D$

- Longitudinal interactions between the two layers are given in Table 6.1. Note that an exchange of the two layers does not affect the total energy, due to the symmetries in longitudinal interactions.

Furthermore, it was shown that even the distribution of layer *pairs* is the same:  $\Pi_{\sigma'\sigma}^{GM} = \Pi_{\sigma'\sigma}^{LL}$ . The first symbol refers to the growth process (GM;  $z \rightarrow \infty$ ) and denotes the probability of finding two consecutive layers in given states  $\sigma'$ ,  $\sigma$ . The second symbol denotes the two-layer system (LL) to have its first and second layer in states  $\sigma'$  and  $\sigma$ , respectively.

Besides being an interesting relation from a theoretical point of view, these equivalences stated for the one- and two-layer statistics have the following benefits:

- A *non-equilibrium* system (layer-by-layer growth model) is described by an *equilibrium* system (two-layer system) and therefore, being analyzed in the frame of equilibrium statistical physics. In particular, the investigation of phase transitions gets a well defined background.
- Any physical quantity (e. g.  $X_{\text{net}}$ ,  $\phi$ ,  $U$  or  $c_V$ ) of the layer growth process in the asymptotic limit ( $z \rightarrow \infty$ ) may be obtained *from measurements of the two-layer system in thermodynamic equilibrium*. Note that for the calculation of the internal energy  $U$  (and derived quantities) the *original* longitudinal energies have to be taken into account.
- The reduction to a two-layer system allows a more detailed sampling of the configuration space in Monte Carlo simulations (for the same amount of computer time), and therefore, leading to more precise measurements.

## 6.5.2 The Two-Layer Systems for Growth Models (i) - (iv)

Motivated by this result, it is interesting to investigate whether the asymptotic behavior of the other growth models presented here may also be represented approximatively by corresponding two-layer systems. The derivation of these two-layer systems is based on the following considerations.

As described above, for the layer growth model (0), only longitudinal couplings undergo a transformation in the two-layer system, while lateral couplings *within* a layer remain unchanged. Moreover, the entire deduction in [5] is independent of the detailed structure of the lateral molecular neighborhoods (and couplings). That is, the equivalence presented above remains valid even for different layer geometries, next nearest neighbor interactions (lateral) or inhomogeneous molecular environments (such as open boundary conditions) within a layer as long as corresponding modifications are taken into account in the two-layer system as well. However, requirements for an equivalence between growth model and two-layer system are that (1) each attached layer has the *same* lateral structure, (2) only a single longitudinal coupling to molecules of corresponding sites of the (previously grown) substrate layer are taken into account, and (3) thermalization takes place *after* all molecules of an adlayer are attached on the surface.

The corresponding two-layer systems for growth models (i) - (iv) are defined as follows: The systems consist of two layers ( $L$ ,  $L'$ ) of the same size than the layers of the growth models. Lattice sites are occupied by polar molecules in state up or down ( $s = \pm 1$ ). Between layers  $L$  and  $L'$  the same longitudinal couplings as shown in Table 6.1 are taken into account. This is a logical consequence of the fact that, for *vanishing* lateral interactions, growth models (0) - (iv) become equivalent, and therefore, these transformed longitudinal interactions must be valid for any two-layer system.

In order to represent the specific lateral molecular neighborhoods and couplings during the attachment of molecules on the crystal surface for growth models (i) - (iv), appropriate modifications are applied in the corresponding two-layer systems:

- (i) Only *three* of the four lateral intermolecular couplings within layers  $L$  and  $L'$  are taken into account during thermalization of a molecule. Always the same coupling is discarded (e. g. the interaction with the right neighbor). Note that this two-layer system corresponds *exactly* to a layer-by-layer growth model where only three lateral neighbors are taken into account.
- (ii) Only *two* of the four lateral intermolecular couplings within layers  $L$

and  $L'$  are taken into account during thermalization of a molecule. These two couplings must be perpendicular to each other. Always the same two couplings are discarded (e. g. the interactions with the right and upper neighbor). Note that this two-layer system corresponds *exactly* to a layer-by-layer growth model where only two lateral neighbors are taken into account.

- (iii) The lateral neighborhood within layers  $L$  and  $L'$  which is taken into account during thermalization of a molecule is chosen with a certain probability. Specifically, for each single molecule flip, a subset of the four lateral intermolecular couplings is randomly selected in Monte Carlo simulations according to the probability distribution for cluster growth, see Table 6.2.
- (iv) The same procedure is applied as in (iii), using the probability distribution for deposition growth, see Table 6.2.

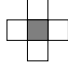
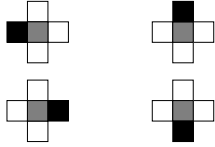
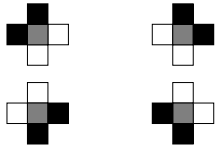

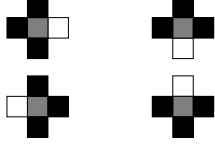

Probability distributions for cluster (iii) and deposition (iv) growth in Table 6.2 are dependent on the size of the lattice. However, for the actual lattice size,  $s_L = 50 \times 50$ , probabilities are already in the asymptotic limit of infinite large lattices. Note that for Monte Carlo simulations of the two-layer systems,  $\tau_G$  denotes the equilibration time of layers  $L$  and  $L'$  measured in Monte Carlo trials, on average, per molecule.  $\tau_S$  describes the number of measurements (one measurement is performed after  $2 \times n_x \times n_y$  trials, i. e. one sweep of the two-layer system). Within layers  $L$  and  $L'$  periodic boundary conditions are applied in all two-layer systems. It has to be emphasized that equilibration of two-layer systems takes place for entirely filled layers only, unlike thermalization of molecules in growth models (i) - (iv).

An exact equivalence between the asymptotic distributions of growth models (i) - (iv) and the equilibrium distributions of corresponding two-layer systems (as for the layer-by-layer growth process) can not be expected. While for the layer growth model (0) and its two-layer system the *thermalizing unit* is the same (namely an entire layer), this is not the case anymore for growth models (i) - (iv). For step (i) and kink (ii) growth, requirement (3) from above is not fulfilled, and, for cluster (iii) and deposition (iv) growth, requirements (1) and (3) are not satisfied anymore.

Nevertheless, the study of the agreement between the thermal equilibrium two-layer systems described here and corresponding non-equilibrium growth models (i) - (iv) is a good way to estimate the thermodynamic nature of macroscopic polarity formation in these growth models.



**Table 6.2:** Probabilities describing the occurrence of different *types* of lateral neighborhood configurations during thermalization of molecules on the crystal surface for growth models (0) - (iv). A type of configuration is characterized by the number of occupied neighbor sites. *Grey:* Thermalizing molecule. *Black:* Occupied neighbor site. *White:* Empty neighbor site. In case of two occupied neighboring sites, two different types of configurations exist. A dash denotes that corresponding configurations are not possible for a certain growth model. In case of step and kink growth, only one of the four possible configurations can occur (with probability one). In case of cluster and deposition growth, probabilities represent averages over 100 000 completed adlayers ( $s_L = 50 \times 50$ ). Individual configurations of a certain type occur with equal probability for growth models (iii) and (iv), respectively. Random selection of the lateral neighborhood (intermolecular couplings) in the two-layer systems for cluster and deposition growth is based on the corresponding probability distributions presented here. The effective lateral coordination number ( $z_{\perp}^{\text{eff}}$ ) specifies the *average* number of occupied neighbor sites during thermalization of molecules on surface sites. Note that  $z_{\perp}^{\text{eff}}$  is the same for kink, cluster and deposition growth.

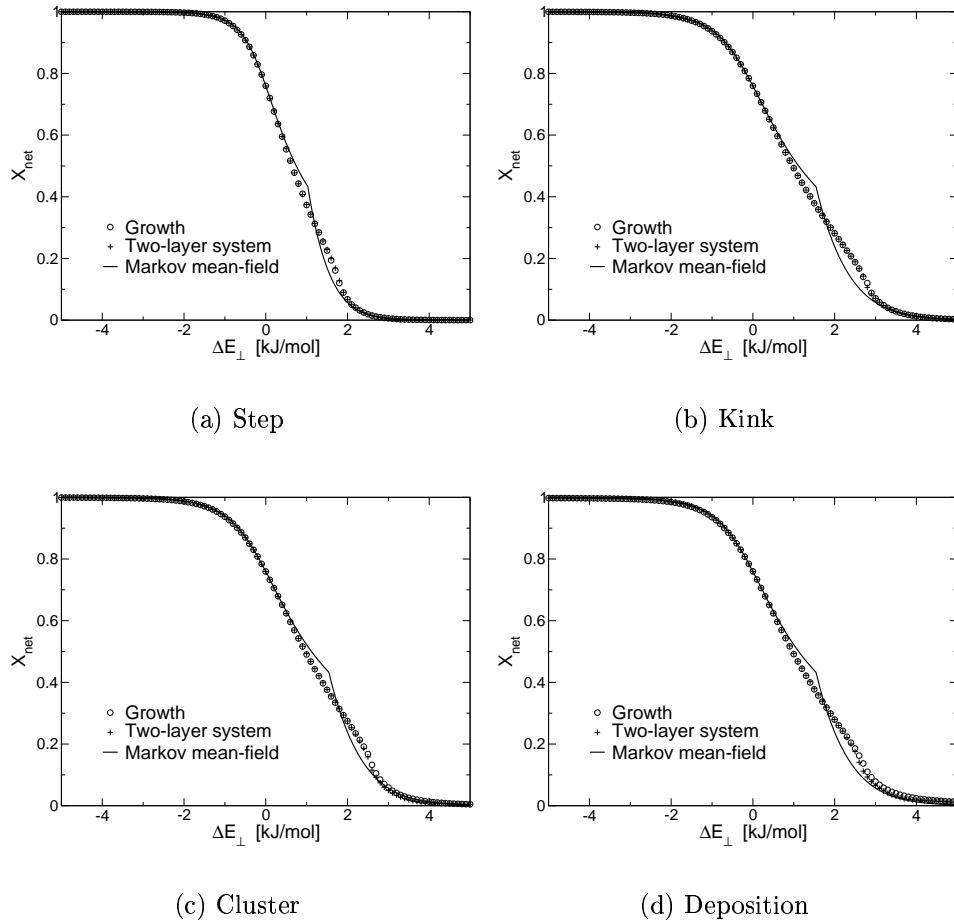
Configuration	Growth model				
	Layer	Step	Kink	Cluster	Deposition
	—	—	—	0.0004	0.2000
	—	—	—	0.4329	0.2000
	—	—	1.0	0.2337	0.1333
	—	—	—	0.0320	0.0667
	—	1.0	—	0.1681	0.2000
	1.0	—	—	0.1329	0.2000
$z_{\perp}^{\text{eff}}$	4.0	3.0	2.0	2.0	2.0

### 6.5.3 Comparisons of $X_{\text{net}}$ between Growth Models, Two-Layer Systems and Analytical Description

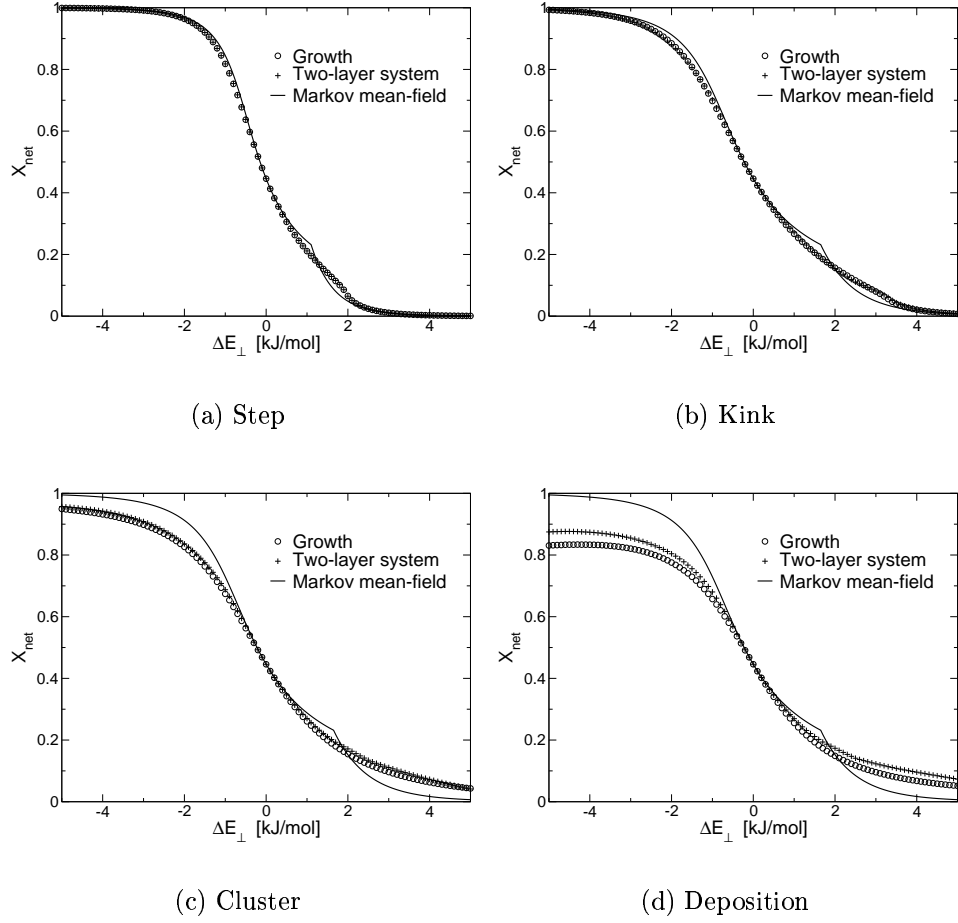
Figs. 6.15 - 6.18 show  $X_{\text{net}}$  in dependence on the lateral coupling difference ( $\Delta E_{\perp}$ ) obtained from Monte Carlo simulations for growth models (i) - (iv) and corresponding two-layer systems as well as for the Markov mean-field approximation (choosing the same four longitudinal coupling parameters as in Section 6.3). A detailed comparison between Markov mean-field approximation and Monte Carlo simulations for the layer-by-layer growth model (0) is given in [40, 5], therefore, it is not considered anymore here. Remind that kink (ii), cluster (iii) and deposition (iv) growth are indistinguishable in terms of the mean-field approach, since all have  $z_{\perp}^{\text{eff}} = 2$ . That is, corresponding curves are the same in Figs. 6.15 - 6.18.

Generally, the agreement of  $X_{\text{net}}$  between growth models (i) - (iv) on one hand, and corresponding two-layer systems on the other hand, decreases towards smaller longitudinal energy differences. This effect is most pronounced for cluster (iii) and deposition (iv) growth. Nevertheless, in case of step (i) and kink (ii) growth, the similarities with the corresponding two-layer systems are remarkable (for step growth even nearly identical). In case of cluster (iii) and deposition (iv) growth, except for the maxima of  $X_{\text{net}}$  for  $\Delta E_{\perp} < 0$ , the correspondence with the two-layer systems is reasonable, in consideration of the strong non-equilibrium character of these growth schemes.

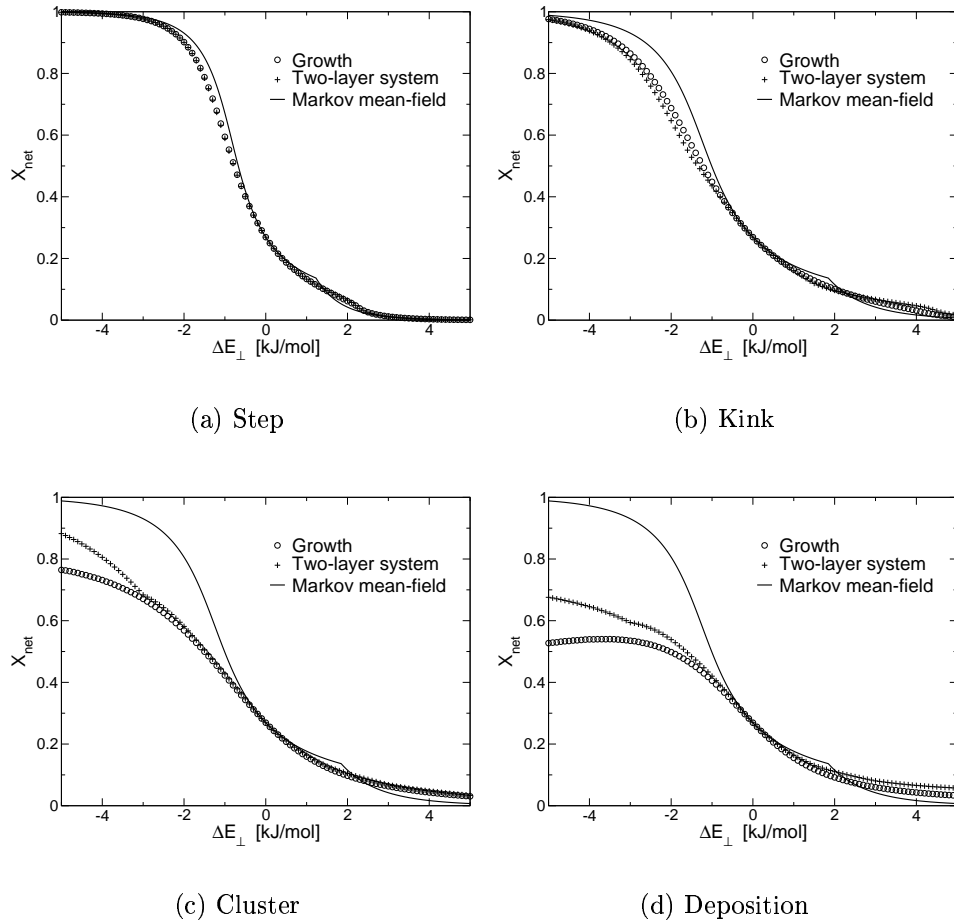
In contrast, in addition to the expected large divergences for cluster (iii) and deposition (iv) growth, results from the analytical approach show relatively large deviations even for kink (ii) growth for small longitudinal coupling parameters. For step growth (i), the Markov mean-field approximation gives a sufficient agreement compared with Monte Carlo simulations. Note that the discontinuity in the slope of  $X_{\text{net}}$  from the analytical description corresponds to the AFO phase transition (see [40, 5]), which remains for any  $z_{\perp}^{\text{eff}} \neq 0$ . For a detailed discussion, see Section 6.6.



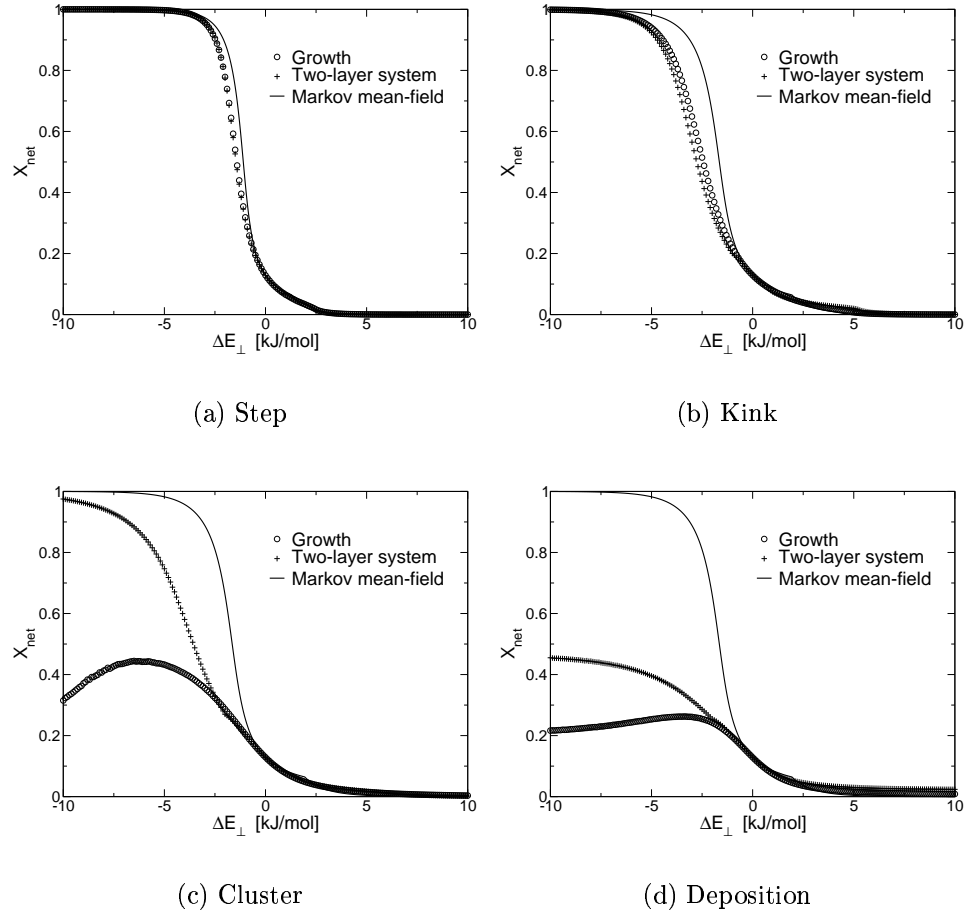
**Figure 6.15:** Comparison of net polarity ( $X_{\text{net}}$ ) between growth models (i) - (iv) and corresponding two-layer systems (from Monte Carlo simulations), and Markov mean-field approximation.  $\Delta E_A = 15$  and  $\Delta E_D = 10$  ( $\Delta E_f = 5$ ) [kJ/mol],  $T = 300$  K. Two-layer systems:  $s_L = 50 \times 50$ ,  $\tau_G = 20\,000$ ,  $\tau_S = 100\,000$ , centrosymmetric seeding state. Growth models: Same data as for Fig. 6.3.



**Figure 6.16:** Comparison of net polarity ( $X_{\text{net}}$ ) between growth models (i) - (iv) and corresponding two-layer systems (from Monte Carlo simulations), and Markov mean-field approximation.  $\Delta E_A = 5$  and  $\Delta E_D = 2$  ( $\Delta E_f = 3$ ) [kJ/mol],  $T = 300$  K. Two-layer systems:  $s_L = 50 \times 50$ ,  $\tau_G = 20\,000$ ,  $\tau_S = 100\,000$ , centrosymmetric seeding state. Growth models: Same data as for Fig. 6.4.



**Figure 6.17:** Comparison of net polarity ( $X_{\text{net}}$ ) between growth models (i) - (iv) and corresponding two-layer systems (from Monte Carlo simulations), and Markov mean-field approximation.  $\Delta E_A = 3$  and  $\Delta E_D = 1$  ( $\Delta E_f = 2$ ) [kJ/mol],  $T = 300$  K. Two-layer systems:  $s_L = 50 \times 50$ ,  $\tau_G = 20\,000$ ,  $\tau_S = 100\,000$ , centrosymmetric seeding state. Growth models: Same data as for Fig. 6.5.



**Figure 6.18:** Comparison of net polarity ( $X_{\text{net}}$ ) between growth models (i) - (iv) and corresponding two-layer systems (from Monte Carlo simulations), and Markov mean-field approximation.  $\Delta E_A = 2$  and  $\Delta E_D = 1$  ( $\Delta E_f = 1$ ) [kJ/mol],  $T = 300$  K. Two-layer systems:  $s_L = 50 \times 50$ ,  $\tau_G = 20\,000$ ,  $\tau_S = 100\,000$ , centrosymmetric seeding state. Growth models: Same data as for Fig. 6.6.

**Table 6.3:** Snapshots of completed adlayers from Monte Carlo simulations for growth models (0) - (iv) and varying  $\Delta E_{\perp}$ .  $\Delta E_A = 2$ ,  $\Delta E_D = 1$  [kJ/mol],  $T = 300$  K. Lattice size  $s_L = 16 \times 16$ . In all cases, more than 1 000 growth steps (completed adlayers) preceded before snapshots have been taken.

$\Delta E_{\perp}$	-20	-8	-4	-2	0	2	4	8	20
Layer									
Step									
Kink									
Cluster									
Deposition									

## 6.6 Discussion

The equivalent principal behavior of step (i) and kink (ii) growth processes compared to the layer-by-layer growth model (0), i. e. same limiting values of  $X_{\text{net}}$  for  $\Delta E_{\perp} \rightarrow \pm\infty$  (see Figs. 6.3 - 6.6) and existence of an AFO phase transition (see Figs. 6.7 - 6.10 and Figs. 6.11 - 6.14, respectively), is the result of an ordered fashion and *constant directionality* of molecules attachments during growth. This is of particular importance in case of kink growth, where molecules are frozen immediately after being attached and thermalized on the surface. Due to a reduced cooperativity between neighboring molecules during thermalization for step ( $z_{\perp} = 3$ ) and kink ( $z_{\perp} = 2$ ) growth, the orientational disorder is correspondingly higher in these processes compared to the layer-by-layer growth, see Table 6.3. Therefore, the transition from the ferromagnetic to the antiferromagnetic ordered state with increasing  $\Delta E_{\perp}$  is less pronounced for growth schemes (i) and (ii).

Because the attachment of molecules proceeds in an ordered way, step (i) and kink (ii) growth models show a good agreement with their corresponding two-layer systems with respect to  $X_{\text{net}}$  (see Figs. 6.15 - 6.18). That is, despite a limited mobility of molecules within an adlayer (frozen states), evolution of polarity in models (i) and (ii) is sufficiently described by thermal equilibrium systems (taking into account a reduced number of lateral neigh-

bors) and therefore, remains mainly a thermodynamically driven process. As a consequence, even the Markov mean-field approximation yields generally comparable results for  $X_{\text{net}}$  in case of step and kink growth. However, for kink (i) growth, the weak cooperativity of molecules within an adlayer can not be compensated always by longitudinal couplings upon growth and therefore, the analytical approach may considerably deviate from simulation results, see Fig. 6.18(b). A decreasing validity of mean-field estimates with a reduction of the number of interacting particles is well known also for other models [10].

Cluster (iii) and deposition (iv) growth processes as presented here are generally different from growth models (0) - (ii), because of two reasons: First, molecules are allowed to attach randomly on the surface (for growth model (iii) only along the perimeter of the cluster). Second, in case of cluster growth, thermalization of the seed molecule (i.e. the first molecule being attached on the flat crystal surface) is determined *only* by longitudinal couplings and, in case of deposition growth, even a large number of molecules thermalize without any influence of lateral interactions ( $z_{\perp} = 0$ ). That is, for large  $|\Delta E_{\perp}|$ , the orientational states of these isolated molecules strongly determine the dipole orientations of subsequently attached molecules, see Table 6.3.

Indeed, in case of cluster growth and  $\Delta E_{\perp} \rightarrow -\infty$ ,  $X_{\text{net}}$  tends towards the *same* value as for  $\Delta E_{\perp} = 0$ , since all molecules within an adlayer feature the same orientational state as the seed molecule, which is thermalized without the influence of any lateral coupling, see Table 6.4. Therefore, cluster growth shows *always* a maximum in  $X_{\text{net}}$  curves for  $-\infty < \Delta E_{\perp} < 0$ . (Note that  $|x_{\text{net}}|$  still reaches unity for  $\Delta E_{\perp} \rightarrow -\infty$ ).

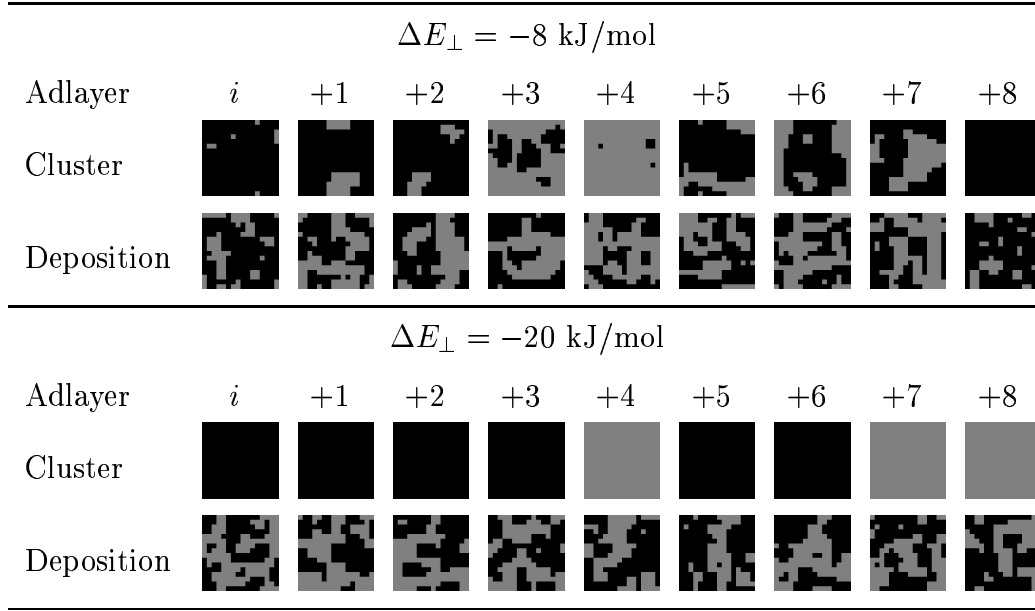
In case of deposition growth, the effect of a single isolated molecule on the orientational order of an *entire* adlayer is less pronounced, since several molecules thermalize without any lateral coupling on the crystal surface simultaneously, see Tables 6.3 and 6.4. Nevertheless, also here a maximum in  $X_{\text{net}}$  may be observed and, for  $\Delta E_{\perp} \rightarrow -\infty$ ,  $|X_{\text{net}}|$  and  $|x_{\text{net}}|$  can tend to a constant value smaller than one.

For  $\Delta E_{\perp} > 0$ , cluster (iii) and deposition (iv) growth show for  $X_{\text{net}}$  similar behaviors as growth models (0) - (ii), because  $X_{\text{net}} \approx 0$  can be obtained also for a slightly randomly disordered antiferromagnetic state, see Table 6.3.

Except for one case (see Figs. 6.7 and 6.11), cluster and deposition growth feature no AFO phase transition anymore, because of the two reasons mentioned above. The differences of orientational states of molecules between subsequently grown layers, give rise to large energy fluctuations and therefore, increasing specific heat  $c_V$  away from  $\Delta E_{\perp} = 0$  in growth models (iii)



**Table 6.4:** Snapshots of subsequently completed adlayers from Monte Carlo simulations for cluster (iii) and deposition (iv) growth models.  $\Delta E_A = 2$ ,  $\Delta E_D = 1$  [kJ/mol],  $T = 300$  K. Lattice size  $s_L = 16 \times 16$ .  $i$  denotes an arbitrary start of the sequence (after more than 1000 grown layers).



and (iv).

Taking into account the specific probability for the occurrence of a certain lateral neighborhood with  $0 \leq z_{\perp} \leq 4$ , corresponding two-layer systems may account to a certain extent for the strong local correlations and high orientational disorder arising in cluster (iii) and deposition (iv) growth models, see Figs. 6.15 - 6.18. However, a maximum in  $X_{\text{net}}$  for  $-\infty < \Delta E_{\perp} < 0$ , as being observed for growth models (iii) and (iv), can not be reproduced in corresponding two-layer systems, because all molecules are thermalized simultaneously in the two layers  $L$  and  $L'$ . This diminishes the strong influence of single molecules being thermalized without any lateral coupling ( $z_{\perp} = 0$ ) on the global orientational state of a layer.

Of particular interest are the cluster (iii) and deposition (iv) growth cases with  $\Delta E_A = 15$  and  $\Delta E_D = 10$  [kJ/mol]. Both show similar values for  $X_{\text{net}}$ ,  $\phi$  and  $c_V$  (i. e. also an AFO phase transition) as obtained for kink (i) growth, see Fig. 6.3, 6.7 and 6.11.

In the different growth models, the influence of lateral couplings on the evolution of polarity is determined by two factors: first, the number of lateral neighbors to compete with the longitudinal one, and second, the detailed

attachment process, being either of ordered or random character for models (0) - (ii) and (iii), (iv), respectively. In case longitudinal interactions are predominantly high, the second factor is less and less significant because the orientational state of a thermalizing molecule is not determined anymore by the history of previously attached molecules, but only by its local neighborhood which is on average given by the effective lateral coordination number  $z_{\perp}^{\text{eff}}$ . As a consequence, for sufficiently large longitudinal couplings, cluster (iii) and deposition (iv) growth give similar results for  $X_{\text{net}}$  than kink (ii) growth, because all have  $z_{\perp}^{\text{eff}} = 2$  (see Table 6.2). (Logically, also a satisfactory agreement with corresponding two-layer systems and the analytical approach is obtained, see Fig. 6.15(c) and 6.15(d).) For a confirmation of these considerations it would be interesting to investigate a growth model with non-integer value for  $z_{\perp}^{\text{eff}}$ .

## 6.7 Conclusion

The present study has shown that the growth mechanism can have a significant influence on macroscopic polarity formation. However, as long as the attachment of molecules proceeds in a *ordered fashion* and with *constant directionality* (step (i) and kink (ii) growth), the evolution of polarity remains mainly a thermodynamically driven process, featuring principally the same characteristics as the layer-by-layer growth model (0). Indeed, even though thermalization within an adlayer is reduced to a column of molecules (step) or even a single molecule (kink) only, in growth models (i) and (ii) the same limiting values of  $X_{\text{net}}$  for  $\Delta E_{\perp} \rightarrow \pm\infty$  as well as an AFO phase transition are manifest like for the layer-by-layer growth process. Furthermore, the asymptotic statistics of growth models (i) and (ii) are in good agreement with the equilibrium statistics of corresponding two-layer systems, confirming the thermodynamic nature of growth-induced polarity formation for step and kink growth.

If the attachment of molecules proceeds *randomly* (cluster (iii) and deposition (iv) growth), principally different behaviors can appear (e. g. maximum of  $X_{\text{net}}$ ) and non-thermodynamic effects may strongly influence macroscopic polarity.

However, for all growth models (i) - (iv) and sufficiently strong longitudinal intermolecular couplings, the influence of the lateral neighborhood on growth-induced polarity formation is satisfactorily summarized by an effective lateral coordination number  $z_{\perp}^{\text{eff}}$ . This is especially remarkable in case of cluster (iii) and deposition (iv) growth, where the random character of molecules attachments results in highly inhomogeneous local environments.

In real crystals, since polarity evolves differently for layer/step/kink growth, formation of regions with different polarity may arise depending on the predominant growth mode in a crystal sector. This may result in even higher orientational disorder, due to this combined effect.



# Chapter 7

## The Program POLARITY

POLARITY is the program which has been developed in order to investigate all the systems and models presented in this thesis by means of Monte Carlo simulations. In particular, these are (i) a layer-by-layer growth model for two-component systems of polar (H) and non-polar or polar (G) molecules, (ii) five different growth models (layer-by-layer, step, kink, cluster, deposition) for single-component systems of polar (H) molecules only, and (iii) corresponding two-layer systems for these five growth models.

The program is written in C/C++. Control and definition of parameters is achieved via an input file. It is not the intention to give a thorough description of the algorithms and technical details of this program here. Nevertheless, in order to provide an overview of the possibilities of POLARITY, the different parameters appearing in the input file are briefly explained and a list of all physical quantities obtained from simulations is presented.

### 7.1 The Input File

In the input file of POLARITY, *program* and *system* parameters are distinguished, respectively. Program parameters specify the chemical system and model to be investigated as well as lattice size, number of measurements and others. These parameters are kept unchanged upon start of the program. System parameters are the molar fraction of G molecules in the gas phase,  $X_{\text{gas}}$  ( $0 \leq X_{\text{gas}} \leq 1$ , only relevant for two-component systems), the temperature  $T$  [K], and the different longitudinal and lateral interaction energies with nearest neighbor molecules [kJ/mol]. These parameters may vary during execution of the program.

To assign a value (or values) to a parameter, its name must be given, followed by the value(s). Only one parameter assignment per line is allowed.

If a parameter is missing in the input file, a default value is assigned. Lines beginning with # are treated as comments. In case of any invalid specifications, an error message is returned.

Here, a standard input file is presented and all parameters are shortly explained. Even though this input file is subdivided into program parameters and system parameters, principally, no specific ordering of parameters has to be kept.

```
#####
#                                                                 #
#           Polarity 1.0 - Input File                             #
#                                                                 #
#####

### Program Parameters #####
```

Header of the input file and beginning of the *program* parameters section.

```
### Chemical System #####
# 0 = polar (H) molecules only
# 1 = polar (H) and non-polar (G) molecules
# 2 = polar (H) and polar (G) molecules
ChemicalSystem 0
```

The chemical system: (0) Single-component system of polar (H) molecules only. (1) Two-component system of polar (H) and non-polar (G) molecules. (2) Two-component system of two polar (H, G) molecules.

```
### Model #####
# 0 = single adlayer on substrate (exact)
# 1 = single adlayer on substrate (MCS)
# 2 = growth (MCS)
# 3 = "two-layer system" for growth (MCS)
Model 2
```

The type of model: (0) Exact summation of the partition function for a system consisting of a (frozen) substrate and a single adlayer; mainly used for tests of the Monte Carlo algorithms for small lattice sizes only. Note that for a two-component system of polar (H, G) molecules and a lattice size  $s_L = 5 \times 5$ , the partition function already contains  $4^{25}$  terms. (1) Monte Carlo simulation (MCS) of the same model than for (0). (2) Monte Carlo simulation of a growth model described in this thesis, and (3) corresponding two-layer systems (see Chapter 6). Note that (3) is only valid for single-component systems of polar (H) molecules only. In this thesis models (2) and (3) were considered.

```

### Attachment Type #####
# 0 = layer-by-layer
# 1 = step
# 2 = kink
# 3 = cluster
# 4 = deposition
Attachment 0

```

Attachment types referring to the growth processes described in Chapter 6, or corresponding two-layer systems. Note that in case of two-component systems only the layer-by-layer growth model (0) is allowed so far.

```

### Layer Size X,Y (max 1024) #####
SizeX 50
SizeY 50

```

```

### Initial States #####

```

```

# H : polar molecules
# G : non-polar / polar molecules
# x : fraction of G molecules in the gas

```

```

# 0 = empty
# 1 = DOWN, H(1)
# 2 = UP, H(1)
# 3 = random, H(1)
# 4 = ideal antiferro, H(1)
# 5 = random, H(1-x)G(x)
# 6 = random, G(1)

```

```

### Initial State of Substrate #####
subInit 3

```

```

### Initial State of Adlayer/Step #####
newInit 3

```

Lattice sizes in  $x$  and  $y$  direction,  $n_x$  and  $n_y$ , respectively. In case of step growth, the length of a column of molecules is given by  $n_y$ . Initial seeding state (substrate) as well as initial state for a growth unit, i.e. an adlayer (layer-by-layer growth), or a column of molecules (step growth), before thermalization. For kink, cluster and deposition growth, only the value for the initial seeding state is relevant.

```

### Equilibration Time for One Unit (sweeps/unit) #####
UnitSweeps 2500

```

The number of Monte Carlo trials per molecule, on average, for a thermalizing unit, i.e. an adlayer (layer-by-layer growth), a column of molecules (step

growth), or both, layers  $L$  and  $L'$  (two-layer systems). For kink, cluster and deposition growth, this parameter is irrelevant.

```
### Equilibration Time for Growth (adlayers) #####
GrowthEquilibrationTime 200
```

The number of grown and completed adlayers before any measurements are performed. This parameter is irrelevant for two-layer systems.

```
### Correlation Time (sweeps/unit or adlayers) #####
CorrelationTime 0
```

The correlation time  $\tau$  of a specific physical quantity (default  $X_{\text{net}}$ ) for subsequent measurements. For test runs,  $\tau$  is set to zero and an estimate is obtained from the output (see below), which can be used for production runs thereafter. A unit refers to layers  $L$  and  $L'$  (two-layer systems, model 3) or a single adlayer (single adlayer on substrate, model 1).  $\tau$  is of relevance for the calculation of statistical errors.

```
### Measurement Interval (sweeps/unit or adlayers) #####
MeasureInterval 1
```

The number of grown and completed adlayers (growth model 2), or the number of sweeps of a unit (models 3, 1) between subsequent measurements. A unit refers to layers  $L$  and  $L'$  (two-layer systems, model 3) or a single adlayer (single adlayer on substrate, model 1).

```
### Number of Measurements per Experiment #####
nMeasurements 20000
```

```
### Number of Experiments #####
nExperiments 1
```

The number of measurements in each experiment and the number of independent experiments (an experiment is specified by a given set of system parameters). Note that in case of growth models (2), measurements are performed after an adlayer has been completed, irrespective of the specific attachment type.

```
### Output Level #####
# 0 = each measurement
# 1 = each experiment
# 2 = each system parameter set
# 3 = each system parameter set (with energies)
OutputLevel 2
```



The output level denoting the frequency at which printing of physical quantities takes place: (0) After each measurement (only those observables are displayed, which can be directly measured, but no derived quantities and no error estimates are given). (1) After each experiment (quantities and error estimates are averaged for one experiment). (2) and (3) Once after a completed run for a given system parameter set (quantities and error estimates are averaged for all experiments).

```
### Images Saving #####
```

```
# SaveImages [level, 0 = no image saving
#             1 = one image per parameter set
#             2 = one image per measurement ]
#           [cross-section x value]
#           [cross-section y value]
#           [cross-section x increment]
#           [cross-section y increment]
#           [zoom-factor, 1 - 50]
```

```
SaveImages 0 1 0 0 1 1
```

```
#####
```

Specifications for the sampling of snapshots of completed adlayers. Images are stores in the PPM format.

```
### System Parameters #####
```

```
### Definitions #####
```

```
# Format:
# [name] [start] [step] [number of steps] [level]

# total number of steps per parameter = step + 1
# 0 <= level < 10
# parameters with the same level loop simultaneously
```

End of the program parameters section and beginning of the *system* parameters section. Each system parameter is characterized by a start value, an increment value, the number of increments to be performed and an index (level). Parameters with the same index increment simultaneously. Parameters with a higher index increment only if parameters with the next lower index reached their specified number of increment steps (these parameters are reset to their start values again). As such, it is possible to perform production runs for any combinations of varying system parameters. Besides, system parameters (especially interactions energies) may be chosen randomly within

certain ranges as being applied in  $(X, X_{\text{net}})$  density plots, see e. g. Chapter 5. For interaction energies, the orientational states of the reference molecule and the neighbor molecule have to be specified, additionally. They are denoted as empty (an empty site, for completeness included), DOWN (H, ↓), UP (H, ↑), down (G, ↓), up (G, ↑), neutral (G, |), see Table 5.1. Note that it is possible to specify non-isotropic interactions in this program. Therefore, in case of isotropic interactions, the two corresponding coupling energies must be incremented *always* simultaneously and with the same increment (see the specification below for  $E_p$ ).

```
### Fraction of G molecules in the Gas #####
Gx 0.0 0.0 0 0
```

```
### Temperature #####
Temperature 300.0 0.0 0 0
```

```
### Longitudinal Interaction Energies #####
```

```
# 1. index: reference molecule
# 2. index: neighbour molecule (on substrate)
```

```
# e : empty
# D : Donor (H)
# A : Acceptor (H)
# d : donor (G)
# a : acceptor (G)
# N : N-terminal (G)
```

```
Elong empty empty 0.0 0.0 0 0 # ee
Elong DOWN empty 0.0 0.0 0 0 # eD
Elong UP empty 0.0 0.0 0 0 # eA
Elong down empty 0.0 0.0 0 0 # ed
Elong up empty 0.0 0.0 0 0 # ea
Elong neutral empty 0.0 0.0 0 0 # eN
```

```
Elong empty DOWN 0.0 0.0 0 0 # Ae
Elong DOWN DOWN 0.0 0.0 0 0 # AD
Elong UP DOWN 5.0 0.0 0 0 # AA
Elong down DOWN 0.0 0.0 0 0 # Ad
Elong up DOWN 0.0 0.0 0 0 # Aa
Elong neutral DOWN 0.0 0.0 0 0 # AN
```

```
Elong empty UP 0.0 0.0 0 0 # De
Elong DOWN UP 2.0 0.0 0 0 # DD
Elong UP UP 0.0 0.0 0 0 # DA
Elong down UP 0.0 0.0 0 0 # Dd
Elong up UP 0.0 0.0 0 0 # Da
Elong neutral UP 0.0 0.0 0 0 # DN
```

Elong	empty	down	0.0	0.0	0	0	#	ae
Elong	DOWN	down	0.0	0.0	0	0	#	aD
Elong	UP	down	0.0	0.0	0	0	#	aA
Elong	down	down	0.0	0.0	0	0	#	ad
Elong	up	down	0.0	0.0	0	0	#	aa
Elong	neutral	down	0.0	0.0	0	0	#	aN
Elong	empty	up	0.0	0.0	0	0	#	de
Elong	DOWN	up	0.0	0.0	0	0	#	dD
Elong	UP	up	0.0	0.0	0	0	#	dA
Elong	down	up	0.0	0.0	0	0	#	dd
Elong	up	up	0.0	0.0	0	0	#	da
Elong	neutral	up	0.0	0.0	0	0	#	dN
Elong	empty	neutral	0.0	0.0	0	0	#	Ne
Elong	DOWN	neutral	0.0	0.0	0	0	#	ND
Elong	UP	neutral	0.0	0.0	0	0	#	NA
Elong	down	neutral	0.0	0.0	0	0	#	Nd
Elong	up	neutral	0.0	0.0	0	0	#	Na
Elong	neutral	neutral	0.0	0.0	0	0	#	NN

### Lateral Interaction Energies #####

# 1. index: reference molecule  
# 2. index: neighbour molecule (within adlayer)

# e : empty  
# D : DOWN (H)  
# U : UP (H)  
# d : down (G)  
# u : up (G)  
# n : neutral (G)

Elat	empty	empty	0.0	0.0	0	0	#	ee
Elat	DOWN	empty	0.0	0.0	0	0	#	De
Elat	UP	empty	0.0	0.0	0	0	#	Ue
Elat	down	empty	0.0	0.0	0	0	#	de
Elat	up	empty	0.0	0.0	0	0	#	ue
Elat	neutral	empty	0.0	0.0	0	0	#	ne
Elat	empty	DOWN	0.0	0.0	0	0	#	eD
Elat	DOWN	DOWN	-5.0	0.1	100	1	#	DD
Elat	UP	DOWN	0.0	0.0	0	0	#	UD
Elat	down	DOWN	0.0	0.0	0	0	#	dD
Elat	up	DOWN	0.0	0.0	0	0	#	uD
Elat	neutral	DOWN	0.0	0.0	0	0	#	nD
Elat	empty	UP	0.0	0.0	0	0	#	eU
Elat	DOWN	UP	0.0	0.0	0	0	#	DU
Elat	UP	UP	-5.0	0.1	100	1	#	UU

Elat	down	UP	0.0	0.0	0	0	#	dU
Elat	up	UP	0.0	0.0	0	0	#	uU
Elat	neutral	UP	0.0	0.0	0	0	#	nU
Elat	empty	down	0.0	0.0	0	0	#	ed
Elat	DOWN	down	0.0	0.0	0	0	#	Dd
Elat	UP	down	0.0	0.0	0	0	#	Ud
Elat	down	down	0.0	0.0	0	0	#	dd
Elat	up	down	0.0	0.0	0	0	#	ud
Elat	neutral	down	0.0	0.0	0	0	#	nd
Elat	empty	up	0.0	0.0	0	0	#	eu
Elat	DOWN	up	0.0	0.0	0	0	#	Du
Elat	UP	up	0.0	0.0	0	0	#	Uu
Elat	down	up	0.0	0.0	0	0	#	du
Elat	up	up	0.0	0.0	0	0	#	uu
Elat	neutral	up	0.0	0.0	0	0	#	nu
Elat	empty	neutral	0.0	0.0	0	0	#	en
Elat	DOWN	neutral	0.0	0.0	0	0	#	Dn
Elat	UP	neutral	0.0	0.0	0	0	#	Un
Elat	down	neutral	0.0	0.0	0	0	#	dn
Elat	up	neutral	0.0	0.0	0	0	#	un
Elat	neutral	neutral	0.0	0.0	0	0	#	nn

#####

End of the system parameters section and end of the input file.

## 7.2 The Output

The following physical quantities are obtained from POLARITY (along with corresponding error estimates):

- $X_{\text{net}}$  : Difference between downwards and upwards oriented molecular dipoles (H and G molecules).
- $|X_{\text{net}}|$  : Absolute value of  $X_{\text{net}}$ .
- $X_{\text{net}}(I)$  : Difference between downwards and upwards oriented molecular dipoles (H molecules only), on sublattice  $I$  ( $x + y = \text{even}$ ).
- $X_{\text{net}}(II)$  : Difference between downwards and upwards oriented molecular dipoles (H molecules only), on sublattice  $II$  ( $x + y = \text{odd}$ ).
- $X$  : Molar fraction of G molecules in the solid.
- $G_c^{(2)}(1, 1)$  : Two-point connected correlation function [66] given as

$$G_c^{(2)}(1, 1) = \langle s_{x,y} s_{x+1,y+1} \rangle - \langle s_{x,y} \rangle \langle s_{x+1,y+1} \rangle,$$

where  $s_{x,y}$  ( $\pm 1$ ) denotes the orientational state of a H molecule at the position  $(x, y)$  and  $\langle \rangle$  is the average over an entire adlayer.

- $G_c^{(2)}(1, 0)$  : Two-point connected correlation function given as

$$G_c^{(2)}(1, 0) = \langle s_{x,y} s_{x+1,y} \rangle - \langle s_{x,y} \rangle \langle s_{x+1,y} \rangle.$$

- $U$  : Internal energy per molecule.
- $c_V$  : Specific heat per molecule, see Eq. 6.3. (An error estimate will be implemented later, using e. g. the bootstrap or jack-knife method, respectively, see [66]).
- $\tau$  : Correlation time of a physical quantity (default  $X_{\text{net}}$ ) for subsequent measurements. It is obtained by numerical integration of the time-displaced autocorrelation  $\chi(t)$  of the corresponding quantity, see [66].  $\tau$  gives a measure of the statistical correlations between subsequent measurements.
- $\phi$  : Order parameter, see Eq. 6.2.

## 7.3 Outlook

For the moment, POLARITY is considered to be still in a scientific development phase, because of the following two reasons: (i) Some features of the program are not yet accessible and controllable with the present input file (i. e. specifications must be directly carried out in the program and therefore a good knowledge of the code is required). (ii) Further extensions are planned, see Chapter 8. However, later, it is intended to make POLARITY available to the interested scientific community. Because of that, a real time graphical output along with a simple graphical user interface, based on OpenGL, GLUT and GLUI<sup>1</sup>, (as being already implemented for the predecessor of the present code, SIMULA), will be provided as well. This is particular useful for rapid investigation of the development of a system in certain situations.

---

<sup>1</sup>OpenGL: [www.opengl.org](http://www.opengl.org); GLUT: OpenGL Utility Toolkit; GLUI: GLUT-based C++ user interface library

# Chapter 8

## Conclusion and Outlook

It has been shown that the concept of layer-by-layer growth (solid-on-solid model) with thermal equilibrium formation of the surface layer (Ising model) represents a valuable and sufficient theoretical description to account for fundamental phenomena of growth-induced polarity formation in two-component systems. The main adaptation compared to the growth model used for analyzing single-component systems consisted in assuming thermal equilibrium with respect to the up and down orientation of the dipoles of H (and G) molecules *and* to an exchange of H and G molecules. The investigation mainly focused on the interplay between orientational ordering (ratio between up and down) and miscibility of the two components in the solid, according to different sets of interaction energies, assuming native structures (H, G) as centrosymmetric.

Based on this model, the following main conclusions can be drawn: Macroscopic polarity may increase considerably in mixed crystals of polar (H) and non-polar (G) molecules, due to orientational selectivity by G molecules as well as a reduced influence of lateral interactions between H molecules during the growth process. It was shown that longitudinal interactions are mainly responsible for polarity formation while lateral interactions were driving the miscibility between the two compounds. The polar behavior of two-component systems of polar (H) and non-polar (G) molecules could be classified in three types (dilution, coupled effect, creation of polarity), according to the value of  $X_{\text{net}}$  found for the corresponding single-component systems of polar (H) molecules only and to the selectivity of non-polar (G) molecules for the up and down orientation of H molecules. Probabilities to obtain certain configurations with  $(X, X_{\text{net}})$  within assumed but realistic ranges of interaction energies and by considering only centric pure H structures, were summarized in density plots. It could be shown that even small ratios of non-polar (G) molecules in the crystal may strongly effect polarity, which

is of particular interest when considering that many real systems represent cases of limited miscibility. Besides, high polarity was observed for ordered structures HG, where G molecules effect a shielding against the tendency of H molecules to pack in a centrosymmetric fashion they would do alone. In systems with two polar components, principally, notions of orientational selectivity and miscibility still apply. However, the strong influence of longitudinal *and* lateral interactions on the evolution of polarity results in more pronounced effects and to inhomogeneous  $(X, X_{\text{net}})$  density distributions. A statistical analysis of the three systems (single-component systems of polar (H) molecules only, two-component systems of polar (H) and non-polar (G) molecules and two-component systems of two polar (H, G) molecules) has shown that two-component systems are clearly favorable with respect to polarity formation in comparison with single-component systems.

Assuming a square lattice and isotropic interactions, the present model is dedicated only to the investigation of general behaviors and qualitative predictions on growth-induced polarity formation in single- and two-component systems. For more quantitative statements, the geometrical details of molecules and crystal structure as well as precise strengths of molecular couplings of a real system have to be taken into account. Implementation of other lattice symmetries with inhomogeneous energetic environments or next-nearest neighbor interactions is considered straightforward by means of Monte Carlo simulations. However, such modifications are only reasonable in recognition of a specific case. The combination of the present layer-by-layer growth model with molecular modeling methods is a promising route for the understanding and quantitative prediction of polarity formation in a specific system [26, 25].

Besides the above issues towards a closer description of reality with respect to growth-induced polarity formation, kinetic effects as well as the specific growth mechanism of different crystal faces must be considered. Here, for the first time, the influence of different growth processes on the evolution of polarity was investigated. Four distinct growth models were introduced and compared with the layer-by-layer growth model, namely, growth along steps, along kinks, cluster growth and random deposition. These growth processes reflect particularly a reduced cooperativity between molecules during their attachment on a crystal surface.

With respect to macroscopic polarity formation, growth along steps or kinks shows principally the same behavior compared to the original layer-by-layer growth model. That is, a continuous phase transition from a disordered to an antiferromagnetic ordered state could be observed, as well as same limiting values for infinite lateral couplings. Further on, the asymptotic statistics af-



ter many steps of growth is in good agreement with the thermal equilibrium distribution of the corresponding two-layer systems, showing that as long as growth proceeds in an ordered fashion and with a constant directionality (like for kink and step growth), polarity formation remains mainly a thermodynamically driven process.

To the contrary, in case attachment of molecules proceeds in a random fashion (cluster and deposition growth), a complete different behavior can be observed, particularly in the asymptotic limit of very strong lateral polar couplings (both systems may show a maximum of polarity in this region). Due to strong local effects of ordering, these two growth models can be only partially represented by the corresponding equilibrium two-layer systems. Nevertheless, for any growth process (i. e. also for cluster and deposition growth), the reduced lateral cooperativity between molecules during their attachment on the crystal surface can be compensated by sufficiently strong longitudinal interactions upon growth. In such cases, the local lateral environment can be represented by an effective lateral coordination number, whatever the growth process.

Principally, an extension of the present analysis to two-component systems is possible. However, here a careful treatment of chemical potentials is necessary when considering the attachment of two types of molecules in different growth models.

Besides, the introduction of different kinetic processes, such as deposition, evaporation and surface diffusion along with the up and down orientation of molecular dipoles is contemplated. The interplay of surface roughening and orientational order as well as the existence of order/disorder phase transitions in dependence of such processes would be of particular interest.

Finally, in consideration of the literature about two-layer Ising systems [3, 1, 7, 68, 81, 20, 61], the character of the AFO phase transition observed in two-layer systems presented here (especially in case of reduced lateral couplings and anisotropic longitudinal interactions) remains still an open issue. The Monte Carlo renormalization group (MCRG) method [84, 10, 66, 58] could be a promising route for the calculation of critical exponents and a thorough understanding.



# Bibliography

- [1] G. A. T. Allan. Critical temperatures of Ising lattice films. *Phys. Rev. B*, 1:352, 1970.
- [2] P. W. Atkins. *Physical Chemistry*. Oxford University Press, fifth edition, 1994.
- [3] L. E. Ballentine. Critical behaviour of a two-dimensional non-planar Ising lattice. *Physica*, 30:1231, 1964.
- [4] H. Bebie and J. Hulliger. Thermal equilibrium polarization: a near-surface effect in dipolar-based molecular crystals. *Physica A*, 278:327, 2000.
- [5] H. Bebie, J. Hulliger, S. Eugster, and M. Alaga-Bogdanović. Ising model of polarity formation in molecular crystals: From the growth model to the asymptotic equilibrium state. *Phys. Rev. E*, 66:021605, 2002.
- [6] H. A. Bethe. Statistical theory of superlattices. *Proc. Roy. Soc. London A*, 150:552, 1935.
- [7] K. Binder. Monte Carlo study of thin magnetic Ising films. *Thin Solid Films*, 20:367, 1974.
- [8] K. Binder. Applications of Monte Carlo methods to statistical physics. *Rep. Prog. Phys.*, 60:487, 1997.
- [9] K. Binder and D. W. Heermann. *Monte Carlo Simulation in Statistical Physics: An Introduction*. Springer Series in Solid-State Sciences. Springer, third edition, 1997.
- [10] J. J. Binney, N. J. Dowrick, A. J. Fisher, and M. E. J. Newman. *The Theory of Critical Phenomena: An Introduction to the Renormalization Group*. Oxford Science Publications. Clarendon Press, Oxford, 1992.

- [11] W. L. Bragg and E. J. Williams. The effect of thermal agitation on atomic arrangement in alloys. *Proc. Roy. Soc. London A*, 145:699, 1934.
- [12] W. L. Bragg and E. J. Williams. The effect of thermal agitation on atomic arrangement in alloys. II. *Proc. Roy. Soc. London A*, 151:540, 1935.
- [13] P. Brémaud. *Markov Chains, Gibbs Fields, Monte Carlo Simulation, and Queues*. Springer, 1999.
- [14] W. F. Brinkman, D. E. Haggan, and W. W. Troutman. A history of the invention of the transistor and where it will lead us. *IEEE J. Solid-State Circ.*, 32:1858, 1997.
- [15] W. K. Burton, N. Cabrera, and F. C. Frank. The growth of crystals and the equilibrium structure of their surfaces. *Phil. Trans. Royal Soc. London*, 243:299, 1951.
- [16] B. Drossel and M. Kardar. Model for growth of binary alloys with fast surface equilibration. *Phys. Rev. E*, 55:5026, 1997.
- [17] B. Drossel and M. Kardar. Phase ordering and roughening on growing films. *Phys. Rev. Lett.*, 85:614, 2000.
- [18] B. Drossel and M. Kardar. Interplay between phase ordering and roughening on growing films. *Eur. Phys. J. B*, 36:401, 2003.
- [19] M. Eden. A two-dimensional growth process. In J. Neyman, editor, *Proc. 4th Berkeley Symposium on Mathematical Statistics and Probability, Vol. IV*, page 223. University of California, Berkeley, 1961.
- [20] A. M. Ferrenberg and D. P. Landau. Monte Carlo study of phase transitions in ferromagnetic bilayers. *J. Appl. Phys.*, 70:6215, 1991.
- [21] U. Firkau. Zur Theorie des Ferromagnetismus und Antiferromagnetismus. *Ann. Phys. (Leipzig)*, 40:295, 1941.
- [22] A. Gavezzotti. Structure and intermolecular potentials in molecular crystals. *Modelling Simul. Mater. Sci. Eng.*, 10:1, 2002.
- [23] A. Gavezzotti. Towards a realistic model for the quantitative evaluation of intermolecular potentials and for the rationalization of organic crystal structures. part i. philosophy. *CrystEngComm*, 5:429, 2003.

- [24] A. Gavezzotti. Towards a realistic model for the quantitative evaluation of intermolecular potentials and for the rationalization of organic crystal structures. part ii. crystal energy landscapes. *CrystEngComm*, 5:439, 2003.
- [25] C. Gervais, T. Wüst, N. R. Behrnd, G. Couderc, and J. Hulliger. Impact of solid solution formation on polarity: Molecular modeling and experimental investigation of the system  $(4\text{-chloro-4'-nitrostilbene})_{1-x} - (4,4'\text{-dinitrostilbene})_x$ . In preparation.
- [26] C. Gervais, T. Wüst, N. R. Behrnd, M. Wübbenhorst, and J. Hulliger. Prediction of growth-induced polarity in centrosymmetric molecular crystals using force field methods. *Chem. Mater.*, in press.
- [27] G. H. Gilmer and P. Bennema. Simulation of crystal growth with surface diffusion. *J. Appl. Phys.*, 43:1347, 1972.
- [28] G. H. Gilmer and K. A. Jackson. Computer simulation of crystal growth. In E. Kaldis and H. J. Scheel, editors, *Crystal growth and materials*, page 80. North-Holland, Amsterdam, 1977.
- [29] J. M. Haile. *Molecular Dynamics Simulation, Elementary Methods*. John Wiley & Sons, Inc., 1997.
- [30] K. D. M. Harris and P. E. Jupp. Mathematical analysis of the alignment of guest molecules in solid one-dimensional inclusion compounds: the design of materials for applications in non-linear optics. *Chem. Phys. Lett.*, 274:525, 1997.
- [31] K. D. M. Harris and P. E. Jupp. Stochastic models for guest-guest interactions in one-dimensional inclusion compounds. *Proc. Roy. Soc. London A*, 453:333, 1997.
- [32] K. Huang. *Statistical Mechanics*. John Wiley & Sons, Inc., second edition, 1987.
- [33] J. Hulliger. On an intrinsic mechanism of surface defect formation producing polar, multidomain real-structures in molecular crystals. *Z. Kristallogr.*, 213:441, 1998.
- [34] J. Hulliger. Orientational disorder at growing surfaces of molecular crystals: general comments on polarity formation and on secondary defects. *Z. Kristallogr.*, 214:9, 1999.

- [35] J. Hulliger. New physical methods for a space resolved mapping of the macroscopic polarisation in molecular crystals and a stochastic theory for understanding. *Chimia*, 55:554, 2001.
- [36] J. Hulliger. Markov-type evolution of materials into a polar state. *Chem. Eur. J.*, 8:4579, 2002.
- [37] J. Hulliger. Connective tissue polarity unraveled by a Markov-chain mechanism of collagen fibril segment self-assembly. *Biophys. J.*, 84:3501, 2003.
- [38] J. Hulliger. *Encyclopedia of Supramolecular Chemistry*, page 1120. Marcel Dekker Inc., New York, 2004.
- [39] J. Hulliger, M. Alaga-Bogdanović, and H. Bebie. Growth-induced effects of polarity in molecular crystals: Comparison of Schottky- and Markov-type models with Monte Carlo simulations. *J. Phys. Chem. B*, 105:8504, 2001.
- [40] J. Hulliger, H. Bebie, S. Kluge, and A. Quintel. Growth-induced evolution of polarity in organic crystals. *Chem. Mater.*, 14:1523, 2002.
- [41] J. Hulliger, O. König, and R. Hoss. Polar inclusion-compounds of perhydrotriphenylene (PHTP) and efficient nonlinear-optical molecules. *Adv. Mater.*, 7:719, 1995.
- [42] J. Hulliger, S. W. Roth, and A. Quintel. The prediction and production of polarity in crystalline supramolecular materials. In D. Braga et al., editor, *Crystal Engineering: From Molecules and Crystals to Materials*, page 349. Kluwer Academic Publishers, the Netherlands, 1999.
- [43] J. Hulliger, S. W. Roth, A. Quintel, and H. Bebie. Polarity of organic supramolecular materials: A tunable crystal property. *J. Solid State Chem.*, 152:49, 2000.
- [44] E. Ising. Beitrag zur Theorie des Ferromagnetismus. *Ztschr. f. Phys.*, 31:253, 1925.
- [45] K. A. Jackson. Mechanism of growth. In *Liquid metals and solidification*, page 174. Am. Soc. Metals, 1958.
- [46] K. A. Jackson. Computer modeling of atomic scale crystal growth processes. *J. Cryst. Growth*, 198/199:1, 1999.

- [47] K. A. Jackson. The interface kinetics of crystal growth processes. *Interface Sci.*, 10:159, 2002.
- [48] M. Kato, M. Kiguchi, N. Sugita, and Y. Taniguchi. Second-order nonlinearity of mixtures including p-nitroaniline derivatives. *J. Phys. Chem. B*, 101:8856, 1997.
- [49] A. I. Kitaigorodsky. *Mixed Crystals*. Springer, 1984.
- [50] Ch. Kittel. *Thermal Physics*. John Wiley & Sons, Inc., 1969.
- [51] S. Kluge, F. Budde, I. Dohnke, P. Rechsteiner, and J. Hulliger. Phase-sensitive second-harmonic microscopy reveals polarity of topologically centrosymmetric molecular crystals. *Appl. Phys. Lett.*, 81:247, 2002.
- [52] S. Kluge, I. Dohnke, F. Budde, and J. Hulliger. Polarity formation in solid solutions:  $(4,4'$ -dinitrostilbene) $_{1-x}$  –  $(4$ -chloro- $4'$ -nitrostilbene) $_x$ ,  $1 > x > 0$ . *CrystEngComm*, 5:67, 2003.
- [53] W. Kossel. Zur Theorie des Kristallwachstums. *Nachr. Ges. Wiss. Göttingen*, page 135, 1927.
- [54] M. Kotrla and M. Předota. Interplay between kinetic roughening and phase ordering. *Europhys. Lett.*, 39:251, 1997.
- [55] M. Kotrla, M. Předota, and F. Slanina. Kinetic roughening and phase ordering in the two-component growth model. *Surf. Sci.*, 402-404:249, 1998.
- [56] M. Kotrla, F. Slanina, and M. Předota. Scaling in a two-component surface-growth model. *Phys. Rev. B*, 58:10003, 1998.
- [57] D. P. Landau. Finite-size behavior of the Ising square lattice. *Phys. Rev. B*, 13:2997, 1976.
- [58] D. P. Landau and K. Binder. *A Guide to Monte Carlo Simulations in Statistical Physics*. Cambridge University Press, 2000.
- [59] A. R. Leach. *Molecular Modelling, Principles and Applications*. Prentice Hall, second edition, 2001.
- [60] A. C. Levi and M. Kotrla. Theory and simulation of crystal growth. *J. Phys.: Condens. Matter*, 9:299, 1997.

- [61] Z. B. Li, Z. Shuai, Q. Wang, H. J. Luo, and L. Schülke. Critical exponents of the two-layer Ising model. *J. Phys. A: Math. Gen.*, 34:6069, 2001.
- [62] M. Lüscher. A portable high-quality random number generator for lattice field theory simulations. *Comp. Phys. Comm.*, 79:100, 1994.
- [63] A. Marbeuf, Ll. Casas, E. Estop, and D. Mikailitchenko. From all-atom vision to molecular pairwise-interactions: the mean-field approach in molecular alloys. *J. Phys. Chem. Solids*, 64:827, 2003.
- [64] A. Marbeuf, D. Mikailitchenko, A. Würger, H. A. J. Oonk, and M. A. Cuevas-Diarte. Unified stability concept of mixed molecular lattices: random alloys or complexes. *Phys. Chem. Chem. Phys.*, 2:261, 2000.
- [65] R. B. McLellan. Thermodynamics of solid solutions. *Mater. Sci. Eng.*, 9:121, 1972.
- [66] M. E. J. Newman and G. T. Barkema. *Monte Carlo Methods in Statistical Physics*. Clarendon Press, Oxford, 1999.
- [67] J. F. Nye. *Physical Properties of Crystals*. Clarendon Press, Oxford, 1992.
- [68] J. Oitmaa and I. G. Enting. Critical behaviour of a two-layer Ising system. *J. Phys. A: Math. Gen.*, 8:1097, 1975.
- [69] L. Onsager. Crystal statistics. i. a two-dimensional model with an order-disorder transition. *Phys. Rev.*, 65:117, 1944.
- [70] R. Peierls. On Ising's model of ferromagnetism. *Proc. Cambridge phil. Soc.*, 32:477, 1936.
- [71] R. Peierls. Statistical theory of adsorption with interaction between the adsorbed atoms. *Proc. Cambridge phil. Soc.*, 32:471, 1936.
- [72] R. Peierls. Statistical theory of superlattices with unequal concentrations of the components. *Proc. Roy. Soc. London A*, 154:207, 1936.
- [73] V. Pereyra, P. Nielaba, and K. Binder. Spin-one-Ising model for  $(\text{CO})_{1-x}(\text{N}_2)_x$  mixtures: a finite size scaling study of random-field-type critical phenomena. *Z. Phys. B*, 97:179, 1995.
- [74] M. Polak and L. Rubinovich. The interplay of surface segregation and atomic order in alloys. *Surf. Sci. Reports*, 38:127, 2000.



- [75] W. H. Press, S. A. Teukolsky, W. T. Vetterling, and B. P. Flannery. *Numerical Recipes in C*. Cambridge University Press, second edition, 1992.
- [76] A. Quintel and J. Hulliger. A theoretical base for optimising intermolecular interactions driving polarity formation in channel-type host-guest materials. *Chem. Phys. Lett.*, 312:567, 1999.
- [77] D. Richardson. Random growth in a tessellation. *Proc. Cambridge phil. Soc.*, 74:515, 1973.
- [78] S. W. Roth, P. J. Langley, A. Quintel, M. Wübbenhorst, P. Rechsteiner, P. Rogin, O. König, and J. Hulliger. Statistically controlled self-assembly of polar molecular crystals. *Adv. Mater.*, 10:1543, 1998.
- [79] Y. Saito. *Statistical Physics of Crystal Growth*. World Scientific, 1996.
- [80] H. R. Schwarz. *Numerische Mathematik*. B. G. Teubner Stuttgart, 1993.
- [81] L. Sneddon. Ising antiferromagnets in a magnetic field. *J. Phys. C*, 12:3051, 1979.
- [82] A. J. Stone. *The Theory of Intermolecular Forces*. Clarendon Press, Oxford, 1996.
- [83] H. I. Süss, T. Wüst, A. Sieber, R. Althaus, F. Budde, H. P. Lüthi, G. D. McManus, J. Rawson, and J. Hulliger. Alignment of radicals into chains by a Markov mechanism for polarity formation. *CrystEngComm*, 4:432, 2002.
- [84] R. H. Swendsen. Monte Carlo renormalization group. *Phys. Rev. Lett.*, 42:859, 1979.
- [85] R. H. Swendsen, P. J. Kortman, D. P. Landau, and H. Muller-Krumbhaar. Spiral growth of crystals: Simulations on a stochastic model. *J. Cryst. Growth*, 35:73, 1976.
- [86] M. Vaida, L. J. W. Shimon, Y. Weisinger-Lewin, F. Frolow, M. Lahav, L. Leiserowitz, and R. K. McMullan. The structure and symmetry of crystalline solid solutions: A general revision. *Science*, 241:1475, 1988.
- [87] T. Watanabe and H. Hoshina. Monte Carlo simulation of structure evolution in binary alloys. *J. Japan Inst. Metals*, 59:902, 1995.

- [88] J. D. Weeks and G. H. Gilmer. Dynamics of crystal growth. *Adv. Chem. Phys.*, 40:157, 1979.
- [89] I. Weissbuch, M. Lahav, and L. Leiserowitz. Centrosymmetric crystals as host matrices for second-order optical nonlinear effects. *Chem. Mater.*, 1:114, 1989.
- [90] I. Weissbuch, R. Popovitz-Biro, M. Lahav, and L. Leiserowitz. Understanding and control of nucleation, growth, habit, dissolution and structure of two- and three-dimensional crystals using 'tailor-made' auxiliaries. *Acta Crystallogr. Sec. B*, 51:115, 1995.
- [91] T. Wüst, C. Gervais, and J. Hulliger. How symmetrical molecules can induce polarity: On the paradox of dilution. *Cryst. Growth Des.*, in press.
- [92] T. Wüst and J. Hulliger. Growth-induced polarity formation in solid solutions of organic molecules: Markov mean-field model and Monte Carlo simulations. *J. Chem. Phys.*, in press.
- [93] B. Xing and H. Umezawa. Mean-field solution for random mixtures  $A_xB_{1-x}$  of an Ising site model. *Phys. Rev. B*, 46:14563, 1992.

# Curriculum Vitae

## Thomas Wüst

### ADDRESS

Sulgenauweg 16  
CH-3007 Bern, Switzerland  
Email: thomas.wuest@iac.unibe.ch

### PERSONAL DETAILS

Gender: Male  
Date of birth: 15th of July, 1972  
Place of birth: Locarno, Switzerland  
Citizenship: Oberriet-Montlingen (St. Gallen), Switzerland

### EDUCATION

- 07/2002 - 02/2005 PhD thesis at the University of Berne, Switzerland, Department of Chemistry and Biochemistry. Subject: Theoretical investigation of growth-induced polarity formation in molecular crystals. Project leader and supervisor: Prof. Dr. J. Hulliger.
- 04/2000 - 06/2002 PhD student at the Swiss Federal Institute of Technology (ETH) Zurich, Switzerland, Laboratory of Physical Chemistry. Work on computational quantum chemistry. Project leader: Prof. Dr. J. Hulliger; supervisor: PD Dr. H. P. Lüthi.
- 10/1993 - 03/1999 Study of physics at the Swiss Federal Institute of Technology (ETH) Zurich, Switzerland. Diploma thesis in Astronomy. Title: Simulation of a convection zone. *Dipl. Phys. ETH.*
- 1987 - 1992 Kantonsschule Schaffhausen, Switzerland.
- 1985 - 1987 Secondary school in Schaffhausen, Switzerland.
- 1979 - 1985 Primary school in Schaffhausen, Switzerland.